Poly(N-isopropylacrylamide) and its copolymers: a review on recent advances in the areas of sensing and biosensing

Das, A.; Babu, A.; Chakraborty, S.; Guyse, J.F.R. van; Hoogenboom, R.; Maji, S.

ADVANCED FUNCTIONAL MATERIALS
www.afm-journal.de

Poly(*N*-isopropylacrylamide) and Its Copolymers: A Review on Recent Advances in the Areas of Sensing and Biosensing

Anubhab Das, Anashwara Babu, Sourav Chakraborty, Joachim F. R. Van Guyse, Richard Hoogenboom,* and Samarendra Maji**

Stimuli-responsive polymers have received increasing attention for various applications due to their ability to adapt physical and chemical properties in response to external environmental stimuli. In this regard, poly(*N*-isopropylacrylamide) (PNIPAM) is the most extensively studied stimuli-responsive polymer and, consequently has been prominently featured in (bio)-sensor development, adaptive coating technology, drug delivery, wound healing, tissue regeneration, artificial actuator design, sensor technology, responsive coatings, and soft robotics. This success can be mainly attributed to the accessible and versatile nature of the PNIPAM platform, thus allowing the synthesis of a wide variety of copolymer architectures, topologies and compositions. Within this review, the structural and compositional features of PNIPAM-based materials in sensor and biosensor applications are discussed with a focus on the literature from 2016 until now. The reader is provided with the current state of the art regarding PNIPAM-based sensor development and their molecular design. Finally, the challenges ahead in the successful implementation of PNIPAM-based sensors are highlighted, as well as the opportunities in the rational design of improved PNIPAM-based sensors. Altogether, this review provides comprehensive insights into the exciting and rapidly expanding field of PNIPAM-based sensing systems, which will benefit the chemical, pharmaceutical, textile, and biotech industries is believed.

1. Introduction

All organisms share an adaptive nature, i.e., they can adapt to changes in both external and internal environments. More particularly, this adaptive behavior typically involves a physicochemical change in/of the organism in response to a particular stimulus. Some examples are given in (**Figure 1**). In this context, a prominent example is that of the Mimosa pudica plant, which changes its leaf orientation in response to stimuli such as light, pressure, and temperature.[1] Another example from the plant kingdom is the carnivorous Venus flytrap, which relies on motion activation to close its trap to catch prey.[2] Likewise, adaptable features are ubiquitous in the animal kingdom. For instance, the Desert Horn Viper changes the look of its skin when it is hunting,[3] or Octopi, which can heavily mimic the shape and color to match their surroundings or even take on the appearance of other species.[4] In addition, various biological processes occur in response to external stimuli, for instance

A. Das, A. Babu, S. Maji
Department of Chemistry, Faculty of Engineering & Technology
SRM Institute of Science and Technology
Kattankulathur, Tamil Nadu 603203, India
E-mail: samarenr@srmist.edu.in
S. Chakraborty
Department of Chemistry, Scottish Church College
1 & 3, Urquhart Square, Manicktala, Azad Hind Bag, Kolkata, West Bengal 700006, India

J. F. R. Van Guyse
Leiden Academic Centre for Drug Research
Einsteinweg 55, Leiden 2333 CC, The Netherlands
E-mail: j.f.r.van.guyse@lacdr.leidenuniv.nl
R. Hoogenboom
Supramolecular Chemistry Group, Centre of Macromolecular Chemistry (CMaC)
Department of Organic and Macromolecular Chemistry
Ghent University
Krijgslaan 281-S4, Ghent B-9000, Belgium
E-mail: richard.hoogenboom@ugent.be

The ORCID identification number(s) for the author(s) of this article can be found under https://doi.org/10.1002/adfm.202402432

DOI: 10.1002/adfm.202402432

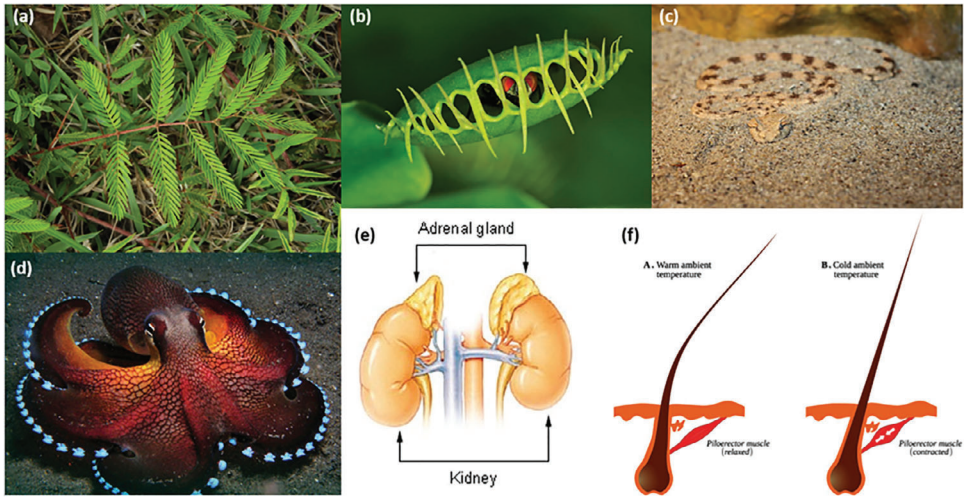

Figure 1. Biological examples of stimuli-responsive systems: a) Mimosa pudica, b) Venus's flytrap, c) Sand viper, d) Octopus, e) Adrenalin hormone, f) Hairs.

when the human body experiences stressful conditions, nerves connected to the adrenal glands trigger the release of the adrenaline hormone,[5] or in response to cold temperatures, hairs on the body rise to trap warm air, thus providing insulation, a process called piloerection.[6] Inspired by these and other natural phenomena, scientists have developed materials capable of mimicking such adaptive responses, so-called "smart" materials. These "smart" materials have been engineered to appropriately alter their properties in response to external physicochemical impulses. This engineered adaptive behavior is highly desirable, as materials can be "programmed" to fit the needs of specific applications and situations without human intervention or computerized control, such as earthquake-proofed buildings and bridges in Japan. In polymer science, adaptive or programmable features are highly desirable, as polymers nowadays are required to fulfill highly specialized roles to tackle the challenges in the realization of a circular economy, sustainable society, and advanced/ personalized healthcare.

To address these challenges, considerable effort has been devoted to the development of "smart" or responsive polymers, whereby physicochemical parameters such as solubility, volume, and/or conformation undergo controlled changes in response to external stimuli such as temperature,[7–11] pH,[12–14] light radiation,[15,16] electric fields,[17,18] bioactive molecules,[19,20] magnetic fields,[21] presence of specific ions and mechanical force.[22] Therefore, using this property, external stimuli can influence the nature of polymers in such a way that they can perform a wide range of functions in areas such as drug delivery systems, bioseparation, sensing, bio-sensing, biomimetic actuators and immobilized biocatalysis.

The first instance of the thermal phase transition behavior of PNIPAM, one of the most studied responsive polymers was reported in 1967 by Scarpa et al.[23] Ever since, numerous articles have appeared on smart or stimuli-responsive polymers, covering their structure, synthesis, and application. Various polymer structures and stimuli-responsive behaviors have been investigated, some representative examples of which are given in **Table 1**, and structures are mentioned in **Figure 2**.

Given the limitless structural diversity of polymers, smart polymers with varying sizes, topologies, and compositions have been synthesized and shown promising behavior in several domains. The field has particularly flourished since the advent of controlled or "living" polymerization mechanisms such as nitroxide-mediated polymerization (NMP),[24] atom transfer radical polymerization (ATRP),[25] reversible addition–fragmentation chain-transfer polymerization (RAFT),[26] ring-opening (metathesis) polymerization[27,28] as well as efficient post-polymerization modification strategies, most notably through the contributions of click chemistry.[29] With these tools, stimuli-responsive polymers have been designed with a myriad of topologies/morphologies, such as linear polymers (homopolymers, di/ter/multi-block copolymers, and organic/inorganic hybrid polymers) and non-linear polymers (star polymers, (hyper)-branched polymers) as illustrated in **Figure 3**.[30]

Furthermore, by carefully controlling the polymer structure, self-assembly can be induced, thus forming higher-order structures such as micelles, polymersomes, nanoparticles, or capsules. Alternatively, stimuli-responsive polymers can be grafted to a surface, generating "smart" surfaces in the form of single/mixed polymer brushes, films, porous membranes, or layer-by-layer (LBL) membranes.[31,32] Finally, 3D responsive polymer-based networks (i.e., hydrogels and hydrogel particles, capsules, micelles) have also been generated using physical and/or chemical crosslinkers.[33]

While various stimuli can induce a response from a suitably designed polymer, the application of temperature as a stimulus, or thermoresponsive behavior, has been the most widely investigated, owing to its vital roles in nature and the noticeable changes in polymer solubility, volume, and conformation that may be controlled across a large temperature range. Generally, two categories of thermoresponsive polymers can be distinguished, whereby the polymer displays either Lower Critical Solution Temperature (LCST) or Upper Critical Solution Temperature (UCST) phase behavior, which relates to the occurrence of

Table 1. Representative examples of responsive polymers.

Types of stimulus	Polymers
Temperature-responsive	Poly(*N*-vinylcaprolactam),[34] poly(2-ethyl-2-oxazoline),[35] poly(vinyl methyl ether),[35] poly(2-*iso*propyl-2-oxazoline),[36] poly((2-dimethylamino) ethyl methacrylate),[37] poly(propylene oxide)[34] and poly(*N*-acryloylpiperidine)[38]
pH responsive	Poly(acrylic acid), poly(2-ethyl acrylic acid), poly(*N*,*N*-dimethyl aminoethyl methacrylate),[39] poly(vinyl imidazole),[40] Polyaspertate,[41] polylysine,[42] and polyhistidine[43]
Light responsive	Poly(ethylene oxide-methacrylate) with pyrene pendant,[16] nitrobenzyl and dithiodipropionic acid modified polyetherimide,[44] poly-*N*-isopropylacrylamide-spiropyran,[45] poly[*N*-isopropylacrylamide-*b*-sodium 2-(acrylamido)−2-methylpropane sulfonate-spiropyran][46]
Electric responsive	Hyaluronic acid/polyvinyl alcohol (HA/PVA) hydrogels[47]
Glucose responsive	Poly[(2-dimethylamino) ethyl methacrylate-*co*-3- acrylamidephenylboronic acid][48]
Magnetresponsive	Poly(*N*-isopropylacrylamide) hydrogel containing iron oxide nanoparticles[49]
Mechanoresponsive	Crosslinked polyarylamide based nanofibers[50]

phase separation in a solvent (e.g., water) as a function of temperature.

The terms LCST and UCST describe the minimum or maximum temperature of the binodal (or the coexistence curve) of the phase diagram, respectively, as depicted in **Figure** 4a,b,[51] i.e., with the decrease of temperature polymer becomes immiscible in solution.

Within this review, the most recent developments on the extensively utilized LCST-type polymer PNIPAM will be covered in depth. PNIPAM is the most extensively studied LCST-type

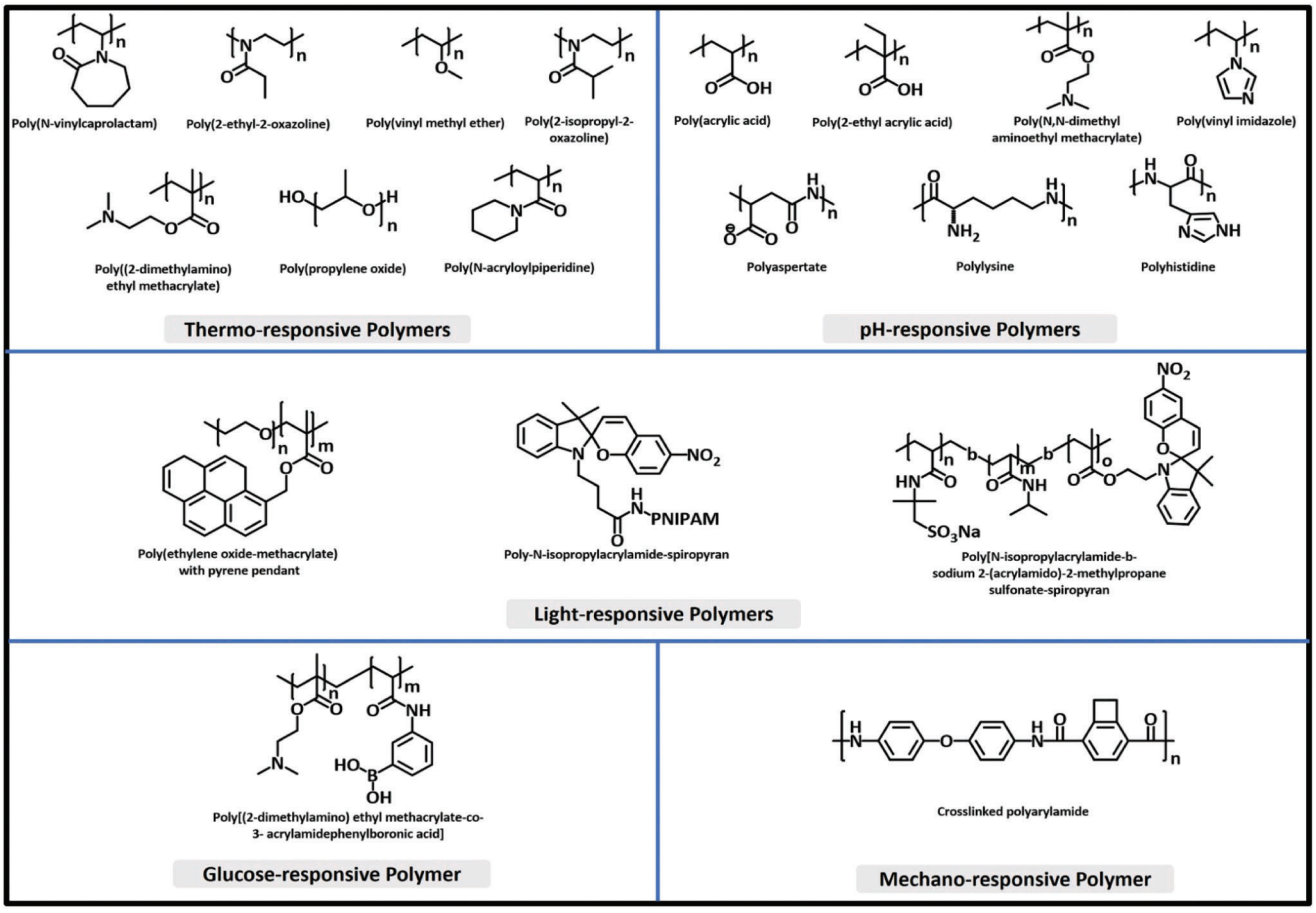

Figure 2. Chemical structures of illustrative examples of responsive polymers.

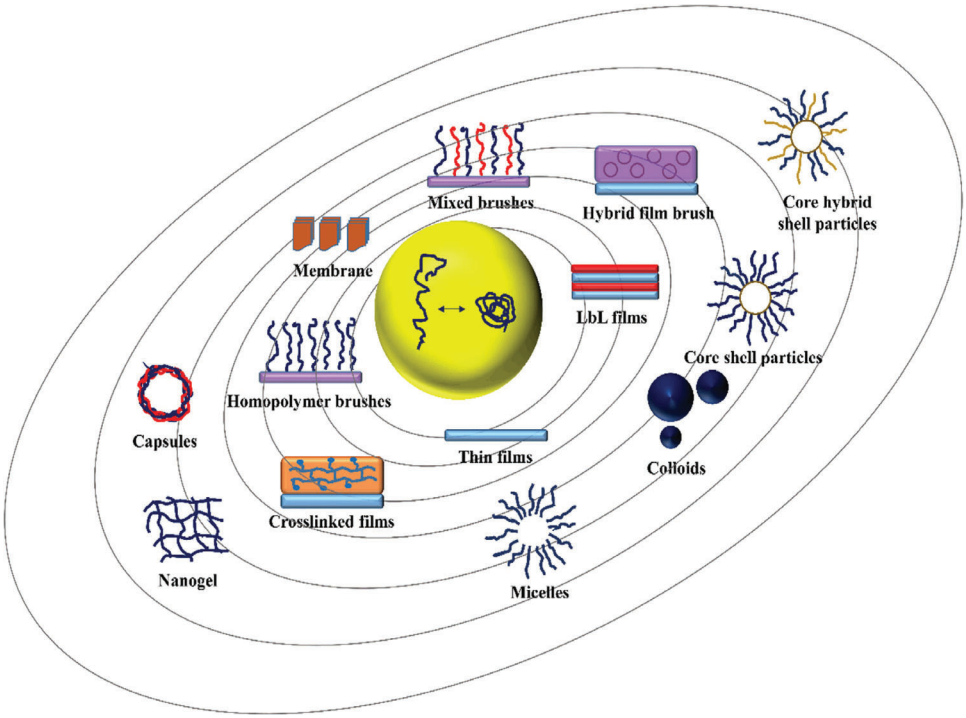

Figure 3. Stimuli-responsive polymer with different topological/morphological features. Reproduced with permission.[30] Copyright 2021, Elsevier Ltd.

polymer and has garnered considerable interest from various fields concerning its altering hydrophilicity in response to temperature variations.[52,53]

The LCST-behavior or temperature-induced phase separation occurs as the result of a phase transition, whereby the polymer chains transition from a hydrated random coil to a dehydrated or hydrophobic globular state. From the perspective of the solvent, water, in most cases, acts as a good solvent at low temperatures whereby favorable solvent-polymer interactions promote an expanded coil conformation. As temperature increases, the solvent becomes poorer and the polymer chains contract, passing through a Θ-point around the binodal, where the solvent

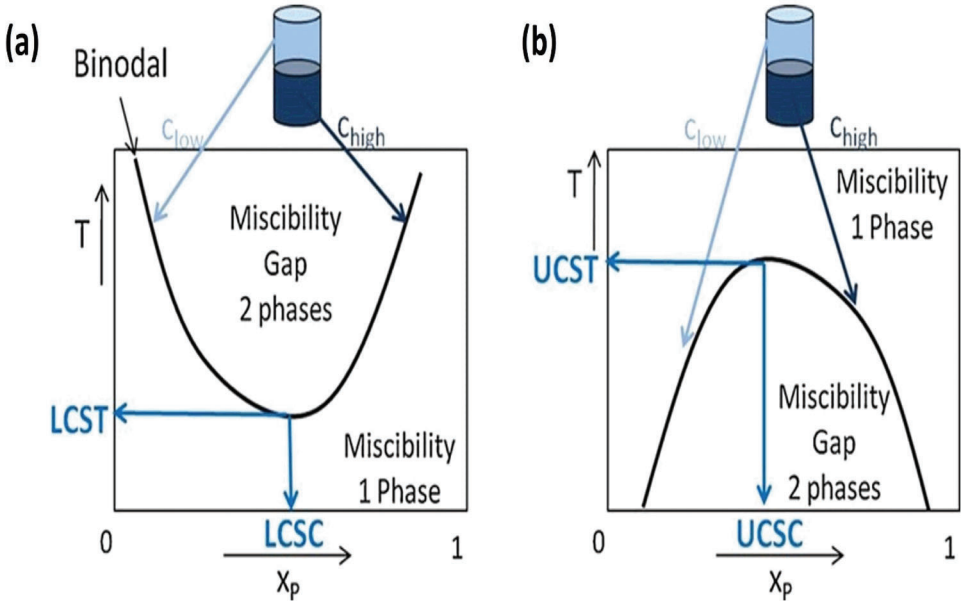

Figure 4. Schematic phase diagram of a) LCST type, b) UCST type aqueous polymer solutions. Reproduced with permission.[51] Copyright 2011, Elsevier Ltd.

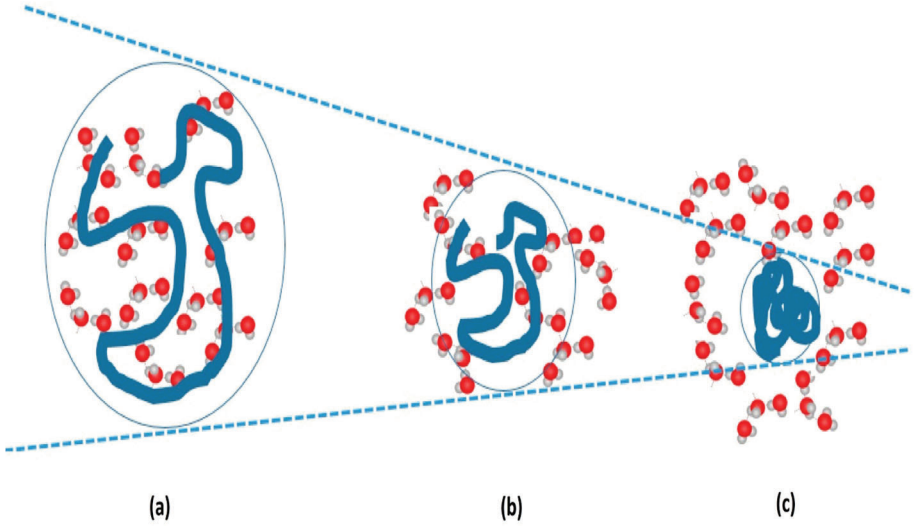

Figure 5. Schematic representation of the different hydration states of aqueous thermoresponsive polymer solutions: a) Expanded coil found between UCST and LCST Θ-points where solvent defined as "good", b) Θ-point (upper and lower), still one phase and polymer minimally perturbed by solvent, c) Fully contracted globule, two phases, and solvent now excluded and described as "poor.".[55]

minimally perturbs the polymer chain. Beyond the Θ-point, the polymer chains fully contract and adopt a globular state and the phase transition is complete, as shown in **Figure 5**. These globules can further aggregate and form mesoglobules (**Figure 6**), a process that is often referred to as macroscopic phase separation between a high polymer concentration phase and a low polymer concentration phase. It should be emphasized, however, that it is difficult to discern between phase transition and phase separation, as these processes are dynamic and occur nearly simultaneously. For PNIPAM specifically, the contribution of each process is still a matter of debate.[54-56]

The phase transition and phase separation of polymers are directly correlated with the chemical structure of the polymer. The hydrophilic amide (—CONH—), hydrophobic isopropyl ($—CH(CH_3)_2$), and a ($—CH_2—CH=$) backbone are the different structural properties of PNIPAM that contribute to the phase change, with each having a unique contribution.[57] In general, this phase transition (**Figure 7**) is reversible in nature and in this case, the hydrophilic/hydrophobic states of the polymer can be switched by varying the temperature below or above the LCST value (32 °C for PNIPAM). The sudden change from hydrophilic to hydrophobic behavior of the same polymer depends on hydrogen bonds present between the polymer and the surrounding water molecules at low temperatures. At low temperatures, the hydrogen bonds between water and the hydrophilic amide groups of PNIPAM cause the hydration and solubilization of the polymer chains, thus forming a one-phase system. With the increase in temperature, these hydrogen bonds become weak, and hydrophobic interactions lead to the phase transition, driven by the entropic release of the hydrating water molecules into the bulk water. From molecular dynamics studies, it was found that both the water coordination around the hydrophobic side chain and the solvent-accessible surface displayed a stronger decrease with the temperature. As a result, the translational entropy of water molecules increased. This entropic effect linked to hydrophobic hydration leads to the release of water from the hydration shell to the bulk water.[58,59]

This can be seen in other examples of LCST polymers such as the following listed poly((meth)acrylamide)s: poly(*N*,*N*-diethylacrylamide),[34] poly(2-carboxyisopropylacrylamide),[60] poly(*N*-(L)-(1-hydroxymethyl) propylmeth-acrylamide,[61] poly(*N*-acryloyl-N'-propilpiperazine),[40] poly(*N*-ethylacrylamide),[35] poly(*N*-methyl-N-ethylacrylamide),[35] poly(*N*-n-propylacrylamide),[35] poly(*N*-ethylmethacrylamide),[38]

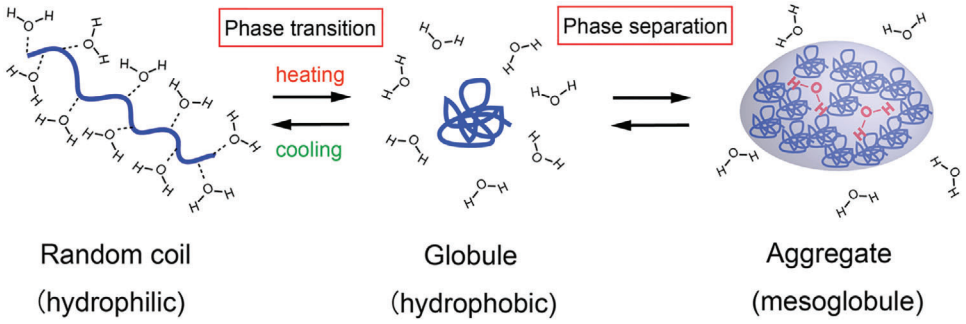

Figure 6. LCST-type behavior of a polymer and its schematic solution state. Reproduced with permission.[56] Copyright 2017, American Chemical Society.

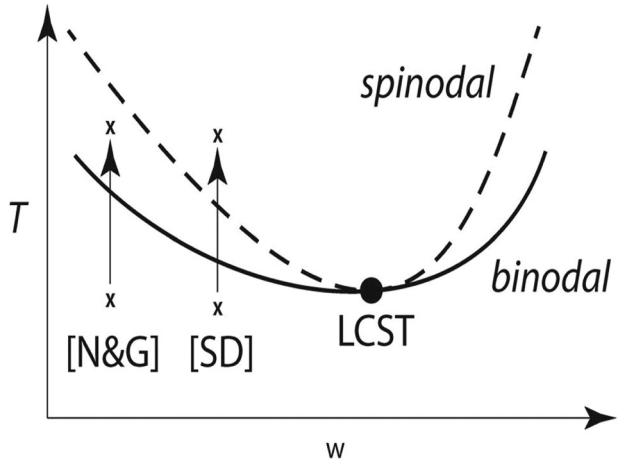

Figure 7. Phase diagram of PNIPAM where coexistence curve was represented as a full line, the spinodal as dashed line and the LCST was pointed by a filled circle. Due to demixing via nucleation and growth [N&G] temperature was quenched from the homogenous, one-phase region into the metastable region between the binodal and the spinodal. The temperature quench into the unstable region within the spinodal curve gave rise to spinodal decomposition [SD]. Reproduced with permission.[54] Copyright 2015, Wiley-VCH.

poly(*N*-methyl-*N*-isopropylacrylamide),[38] poly(*N*-isopropylmethacrylamide),[38] poly(*N*-n-propyl-methacrylamide),[38] poly(*N*-methyl-*N*-isopropylacrylamide),[38] poly(*N*-cyclopropylacrylamide),[38] poly(*N*-cyclopropymethacrylamide),[38] poly(*N*,*N*-bis(2- methoxyethyl) acrylamide),[35] poly(*N*-(3--methoxypropyl) acrylamide),[35] poly(ethoxypropylacrylamide),[35] and poly(aminomethoxypropylacrylamide).[62]

Although there is a large variety of thermoresponsive poly(acrylamide)s, PNIPAM remains of particular interest due to its ability to phase separate or demix from aqueous solutions in between room temperature and body temperature.[63–65] For LCST-type polymers, and most prominently PNIPAM, the phase transition and separation have been exploited to facilitate drug delivery, actuation, and catalysis, all of which rely directly on the adaptation of the polymer to its environment. In addition, the adaptive response can also be regarded as a measurable/observable output, thus enabling the detection or quantification of physicochemical or biological events. Since sensors are tools that enable the generation of information or data of our surroundings, they are key in driving the generation of knowledge and the technological advancement of society.

Given their usefulness, the development of lightweight, portable sensors with intrinsic responsivity, thus requiring no human or computerized intervention nor an energy source, is of tremendous interest. Hence, polymers are ideal materials for the development of sensors, as they enable miniaturization, a high degree of tunability, and multi-responsivity. While the advantages of polymeric sensors are clear, still some challenges remain, such as the handling of complex samples (e.g., blood), online/in vivo monitoring, measurable output, solid-state materials, complex structural relationships, recycling/reuse with recoverability. In addition, a high degree of tunability also means that finding the right structure for the application can be challenging thus being both labor-intensive on the synthesis and material testing fronts. To facilitate the development of suitable polymer-based sensors, the polymer design is typically fine-tuned to match the application, whereby general considerations will be outlined below.

While PNIPAM possesses intrinsic responsivity to temperature in aqueous environments and to the ionic strength of aqueous solutions, it lacks responsivity to other stimuli as well as the ability to report its phase transition behavior at low concentrations or with low limit of detection (LOD). Hence, other functional moieties are incorporated in the PNIPAM structure mostly by statistical copolymerization or chain-end functionalization. The incorporation of reporter molecules, such as fluorescent dyes,[66–71] or Fluorescence Resonance Energy Transfer (FRET) pairs,[72] can facilitate the quantification and read-out of the response or provide a simple colorimetric signal. In this respect, the phase transition behavior of PNIPAM plays an important role in photophysical processes such as FRET, and Aggregation Induced Enhanced Emission (AIEE), which benefit from the intra- and inter-chain aggregation to increase the response and sensitivity. In addition to reporter moieties, several sensing moieties have been prominently incorporated in the PNIPAM structure, such as phenyl boronic acids,[73–80] crown ethers,[81–85] and pH-responsive groups,[86] to enable responsivity to and sensing of pH, glucose, ions and other biomolecules. The physicochemical changes of these sensing moieties upon exposure to their stimuli often directly affect the hydration of the PNIPAM-based structure, thus affecting the phase transition behavior.

The incorporation of such moieties can be performed by modifying the chain-end of PNIPAM, or by the incorporation of functional or reactive comonomers, thus enabling the incorporation of these groups in the polymer chain. In this fashion, it is possible to modify not only the specific composition, such as the comonomer ratio, but also the distribution of these groups along the polymer chain, changing them from statistical to block-copolymers. By modulating the compositional features of the PNIPAM-based structures non-covalent interactions driving self-assembly can be controlled, e.g., the formation of micelles from block-copolymers,[87–89] double hydrophilic block copolymer (DHBC).[90] Such compartmentalization in supramolecular structures can again be exploited for increased sensitivity or enhanced detection sensitivity, water dispersibility, biocompatibility, facile incorporation into devices, and the ability of further functionalization for targeted imaging and detection. In addition to linear polymers, a variety of polymer architectures are accessible such as brush copolymers,[91,92] cyclic, and comb-copolymers.

Besides the direct chemical modulation of the PNIPAM structure, also the direct processing of PNIPAM-based materials can be performed to increase the sensitivity of PNIPAM or enable the monitoring of macroscopic properties as a read-out. Electrospinning (ES) is a unique and simple technique to prepare various functional and composite nanofibers called electrospun nanofibers featuring typical diameters of a few hundreds of nanometers. The small diameters of nanofibers provide a high surface area-to-volume ratio, which makes them ideal for sensing applications. It also presents advantages like low cost, flexible morphology tuning, and high-throughput continuous production. Compared to continuous thin films, electrospun nanofibers possess 1–2 orders of magnitude more surface area that facilitates high sensitivity and rapid responses to external signals[93]

such as pH, temperature, and metal ions.[94–98] Imprinted polymers prepared from the gel are another vast area of sensing for biomolecules[99,100] and organic molecules.[101] Various types of gels (hydrogel, microgel, and nanogel) with high mechanical and reusable properties were made via crosslinking with excellent sensing properties.[102–117]

Composites offer another attractive alternative for developing PNIPAM-based sensors, as often the functionality of the composite is greater than the sum of its components. Components like carbon nanotubes (CNTs), graphene, gold nanoparticles (AuNPs), quantum dots, and electrospun nanofibers have been used for preparing composites. Their properties were improved by immobilizing the thermoresponsive PNIPAM. CNTs are extensively used because of their high conductivity and desirable dispersibility. Two types of CNTs have been used: single-walled carbon nanotubes (SWCNTs) and multi-walled carbon nanotubes (MWCNTs). SWCNTs are 1D conductors with all electrons moving in an atomic layer having surface atoms. Whereas MWCNTs consist of a complex structure with each carbon layer having different chirality and electronic properties. They possess a large specific surface area, small diameter, and high surface energy. Moreover, MWCNTs have great electrical conductivity, electrocatalytic activity, and adsorption performance, which is utilized to accelerate signal transmission, improve sensing capability, and sensor sensitivity. CNTs coated with PNIPAM have acceptable biocompatibility, excellent water dispersibility, and solubility. Therefore, they are used as an ideal electrode material and widely utilized in electrochemical sensors.[118] Graphene is an allotrope of carbon consisting of a single layer of atoms arranged in a 2D honeycomb lattice. Graphene quantum dots (GQDs), nanometer-sized graphene derivatives, show very interesting optoelectronic properties due to quantum confinement and edge effects. Their tunable luminescent properties depend on their size, as well as the surrounding pH and the presence of metal ions, making them great candidates for a multi-sensing platform. Graphene oxide (GO) has a 2D, graphene-like structure with oxygen-containing functional groups such as epoxide, OH, and COOH. Due to this structure, GO contains good hydrophobicity, moderate conductivity, high chemical stability, and excellent electrochemical properties, and can act as a support for the deposition of inorganic nanocatalysts or polymers. GO is specially used in the sensing field to facilitate or mediate the charge/electron transfer between the electroactive species and the electrode surface. Surface properties and functionalities of GO can be explored by anchoring NPs and polymers via chemical and physical interactions, such as electrostatic, cycloaddition, hydrophobic, and π-π stacking interactions.[119] AuNPs have attracted immense attention because of their extraordinary electrical properties, optical properties excellent size/shape control, biocompatibility, and novel plasmonic and catalytic properties. Therefore, the immobilization of PNIPAM on AuNPs improves the accessibility of their unique optical properties and can be used as excellent optical sensors.[120–122] Recently, quantum dots (QDs) have been used as optical labels for biosensing events due to their size-controlled fluorescence properties, high quantum yield, and stability against photobleaching over organic fluorophores. Carbon dots (CDs) are one of the most popular QD among them. They are a class of 3D nanostructured materials that have the sp^2 carbon hybridization and represent nanocrystalline graphite. They show various merits like excellent photostability, small size, biocompatibility, highly tunable photoluminescence (PL) property, up-conversion PL property, electrochemiluminescence, and chemical inertness. These characteristics make it an excellent material for sensing. Immobilization of PNIPAM onto CDs generated hybrid materials with both the properties of CD and PNIPAM whereby chemical signals could be converted into optical signals.[123–126]

Given the widespread research, development, and application of PNIPAM-based sensors in the last decades, an up-to-date account of PNIPAM-based sensor development will be presented in this review, starting from 2016. More specifically, this review will focus on the most recent developments in both physicochemical and biosensors (**Figure 8**), which will be complemented by a brief discussion of the structural features of the polymer. Finally, a summary and outlook into the development and application of sensors will be presented, with a particular focus on the remaining challenges in the successful application of PNIPAM-based platforms.

2. PNIPAM-Based Physiochemical Sensors

2.1. Temperature Sensors

As PNIPAM possesses intrinsic thermoresponsive behavior in aqueous solutions, its concomitant use as a temperature sensor has been the most widely explored. Although widely explored, one limitation is the often-limited temperature sensing window and resolution of PNIPAM sensors. The development of sensors with milli-degree temperature resolution enables the monitoring of several cellular processes, including gene expression,[127,128] tumor metabolism,[129] and pathogenesis of diseases.[130] In other cases, changes in intracellular temperature can affect various critical cellular functions, such as mass transport, energy conversion, signal transduction, cell metabolism, division, and cell death. So intracellular temperature monitoring could provide information regarding the underlying causes of diseases and, offer diagnostic and therapeutic methods for clinical applications.[131–134] Furthermore, the utilization of body temperature in the diagnosis of diseases or normal biological processes, such as the menstrual cycle,[135] has prompted the exploration of compact and wearable sensors. Temperature sensors are also applicable for many non-biological processes like oil mining,[136] radiators in vehicles,[137] glass industries,[138] chemical industries,[139] and in integrated circuits.[140]

2.1.1. Composite-Based Temperature Sensors

To address some of these issues, PNIPAM-based polymers have been combined with photonic materials as they provide an easy-to-understand read-out. A recent example of a photonic sensor can be found in the work of Huang et al., who synthesized PNIPAM dip-coated silica nanofibers by the electrostatic interaction of an amino group of modified PNIPAM with the acidic silanol groups on the surface of the nanofibers (**Figure 9**).[141] From the phase transition of PNIPAM from a hydrated to a dehydrated state, the authors could monitor the surface refractive index (sRI) of the fibers as a function of temperature. Initially, the fibers displayed a sRI close to that of water (T < LCST). However, as the

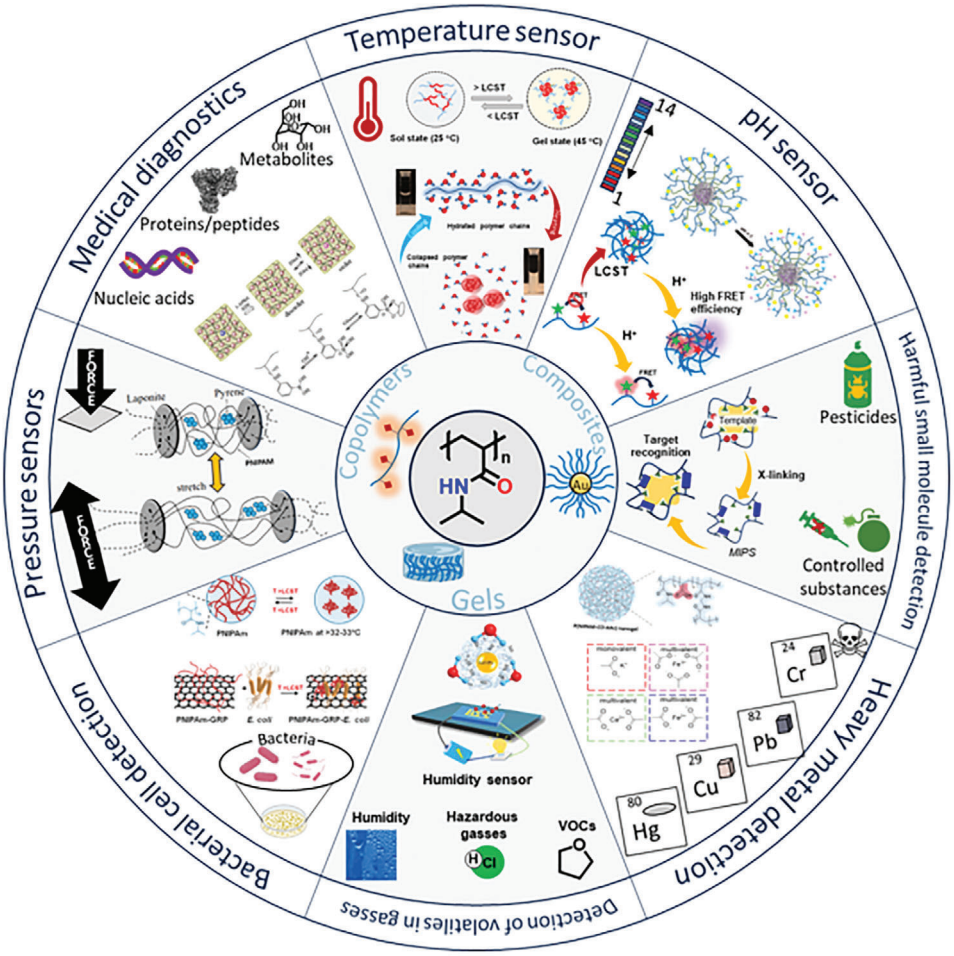

Figure 8. Schematic representation of the PNIPAM-based physicochemical and biosensors.

temperature rose a dehydrated polymer film formed on the fiber surface, resulting in a large shift in sRI. In this fashion, a temperature resolution up to millidegrees could be reached in the range of body temperature 35–42 °C, while also improving the sensitivity by 2 orders of magnitude (18.74 nm $°C^{-1}$) compared to typical radiation-based thermometry.

Besides sRI, other characteristics of the sensor can be monitored as well. For example, Oh et al. developed a skin-attachable thermal sensor, which utilized electrical resistance as a measurable output to monitor temperature. For this purpose, they developed an octopus-mimicking microstructure adhesive that was modified with polydimethylsiloxane (PDMS), followed by deposition of an Au film.[142] Then a PEDOT:PSS/CNT composite spin-coated with PNIPAM was added on top of the adhesive film to fabricate the sensor (**Figure 10**) with PDMS as the insulating layer and PEDOT:PSS/CNT as the conducting layer. As the temperature rises, the volume of PNIPAM shrinks, resulting in a dense percolation network of PEDOT:PSS/CNT and, as a result, a reduction in electrical resistance. With the decrease of temperature, the opposite phenomenon occurs, i.e., the volume of PNIPAM increases, thus loosening the percolation network of PEDOT:PSS/CNT which causes increases in the electrical resistance. This system showed a high thermal sensitivity of 2.6% $°C^{-1}$ between 25 °C and 40 °C with a LOD of 0.5 °C.

Also, Rullyani et al. explored the use of PNIPAM in an electrical sensor recently. They fabricated an organic thin-film transistor (OTFT) that served as a temperature sensor with a detection range of 30–45 °C.[143] This transistor was synthesized by spin-coating a solution of carboxylic acid terminated PNIPAM on an indium tin oxide (ITO) coated glass substrate, whereby the PNIPAM functioned as the gate dielectric. Next, a metal-insulator-metal (MIM) structure of Au/pentacene/Au was deposited on the PNIPAM layer, whereby the pentacene functioned as a semiconductor (**Figure 11**). The capacitance of the ITO/ PNIPAM/Au system depended on the PNIPAM thickness. The thickness of PNIPAM film reduced with increasing temperature due to its phase transition, which in turn increased the conductance. So, the temperature measurement was done by measuring the value of the resistive current between the drain and source (I_{DS}), *i.e.*, both Au constructs which increased from an initial value of −5.7 µA at 30 °C to a final value of −9.8 µA at 45 °C.

Another approach for developing thermal (bio)sensors with high sensitivity, is the combination of stimuli-responsive polymers with inorganic NPs. These NPs can be used as an excellent probe for sensing due to their unique optical properties

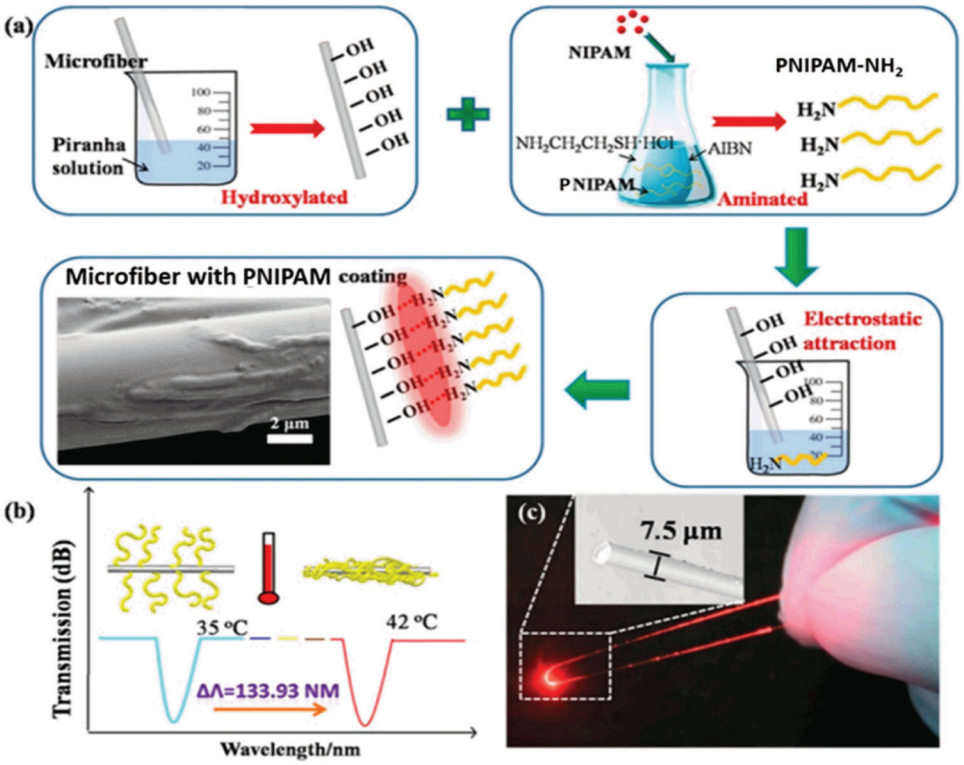

Figure 9. a) Synthesis of PNIPAM coated nanofibers and their temperature sensing mechanism, b) the effect of the morphological change in the interferometric fringe of the transmission spectrum, c) the image of the microfiber biosensor needle. Reproduced with permission.[141] Copyright 2017, American Chemical Society.

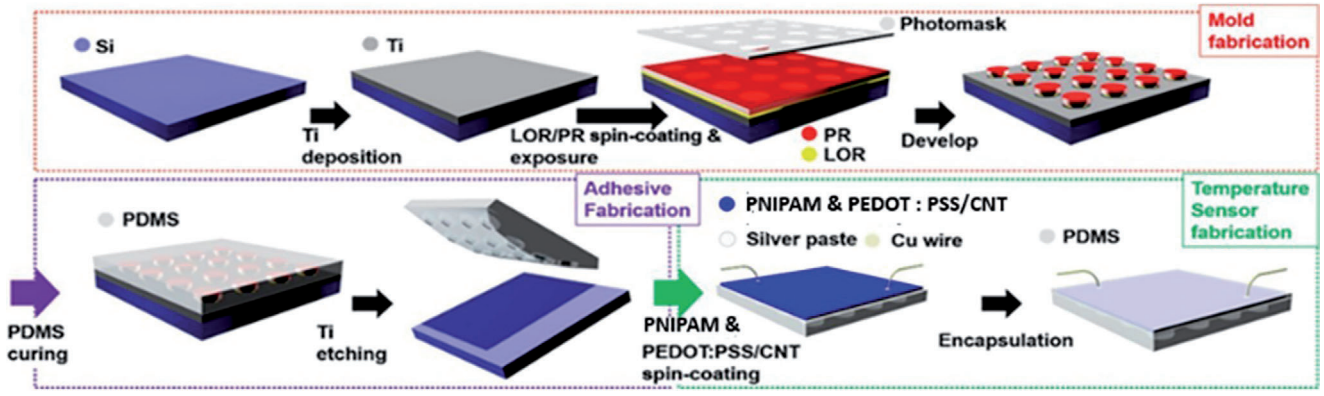

Figure 10. Fabrication of temperature sensor by preparing composite. Reproduced with permission.[142] Copyright 2018, American Chemical Society.

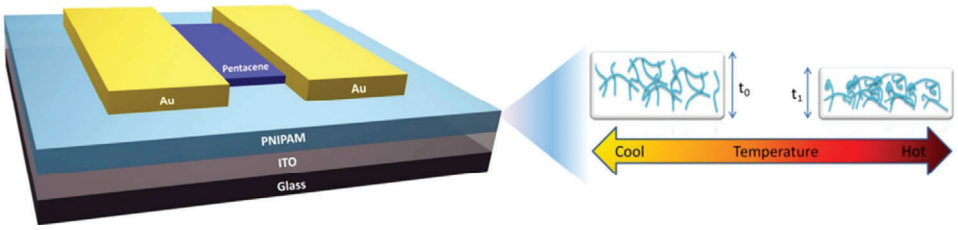

Figure 11. Fabrication of system with temperature sensing organic thin-film transistor. Reproduced with permission.[143] Copyright 2020, Elsevier Ltd.

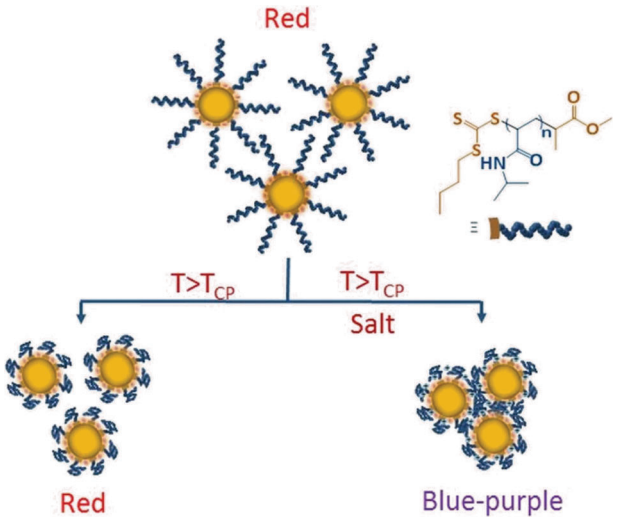

Figure 12. Temperature sensing of the system by color-changing in the presence of fixed salt concentration. Reproduced with permission.[145] Copyright 2016, Royal Society of Chemistry.

due to quantum effects, such as bright emission without photobleaching, and strong localized surface plasmon resonance (SPR). AuNPs, in particular, have already demonstrated invaluable for sensing, imaging, and drug delivery.[144] By applying a smart polymer coating, AuNPs can sense external stimuli, including temperature, pH, and light irradiation. When the AuNP surface is decorated with stimuli-responsive polymers, a given stimuli can induce optical property changes in the AuNP. In one example, Maji et al. designed a colorimetric temperature sensor by coating AuNPs with a thermoresponsive PNIPAM shell.[145] The polymer was prepared by RAFT polymerization using methyl 2-(((butylthio)carbonothioyl)thio)propanoate (MBTTC) as a chain transfer agent (CTA), and the AuNPs were functionalized via a "grafting to" approach, which comprised the exchange of the weakly bound citrate for the polymer-bound trithiocarbonate group. The authors showed that the sensing mechanism of the AuNPs depended on the interparticle association which was controlled by temperature and salt concentration. At a fixed salt concentration (100×10^{-3} M NaCl), heating of the AuNPs led to the shift from a red solution (30 °C) to a purple-blue solution (45 °C), whereby the shift was attributed to interparticle association and dissociation (**Figure 12**). Moreover, the process was shown to be reversible, and the system exhibited temperature sensing in the range of 28–42 °C for NaCl and 30–44 °C for NaSCN. Furthermore, the authors also hypothesized that the sensitivity of the smart sensor may change as the polymer chain length increases. Similarly, Lei and co-workers also explored the use PNIPAM decorated AuNPs for temperature sensing.[146] They prepared PNIPAM via RAFT and aminolyzed the trithiocarbonate end-group to a thiol to facilitate the "grafting to" the AuNPs. With the increase of temperature, the aggregation of NPs occurred due to the collapse of PNIPAM accompanied by a color change to purple in the presence of 50×10^{-3} M NaCl due to red-shifting of the plasmon peak of PNIPAM–AuNPs (**Figure 13**). Here, salt was added to screen the electrostatic interactions and temperatures in the range of 25–50 °C could be detected.

A similar "grafting to" approach was utilized by Liu et al., who conjugated thiolated PNIPAM to AuNPs of various shapes, viz. nanospheres (AuNSs), gold nanorods (AuNRs), and gold nanobipyramids (AuNBPs) to understand the effects of plasmonic resonance modes on sensing performances.[147]

Their systems displayed a red-shift of the absorbance peak in the temperature range of 25–34 °C, which was attributed to an increasing refractive index because of polymer dehydration from the hydrophilic–hydrophobic phase transition. In the temperature range of 34–50 °C, a linear decrease in the longitudinal resonance peak intensity occurred due to a chemical damping effect caused by the PNIPAM chains collapsing on the particle surfaces. To avoid NP aggregation, the authors did not employ salt in this experiment, instead relied on different shapes of NP, thus enabling the first observation of, a linear correlation between the resonance peak shift and the temperature. The researchers then applied three well-known machine learning techniques to the obtained absorption data, namely random forest regression (RF), gradient boosting regression (GB), and adaptive boosting regression (AB), to estimate the temperature from the absorbance of NP solution.[148]

In addition to solutions of PNIPAM-coated AuNPs, Choe et al. explored the embedding of AuNPs in PNIPAM-based microgels.[149] More specifically, PNIPAM microgels were prepared with acrylamide (AAm) using *N,N'*-methylenebisacrylamide (MBAM) as a crosslinker and a plasmonic microgel was prepared by mixing microgels with AuNP solution. Due to the thermally induced aggregation of PNIPAM chains, the AuNPs on the PNIPAM microgels displayed loosely packed structures at 24 °C and densely packed assemblies at 50 °C, resulting in uncoupled and coupled plasmon modes at 24 °C and 50 °C, respectively. Therefore, large color changes could be thermally induced by switching from uncouple to couple plasmonic mode of the AuNPs (**Figure 14**). The authors also demonstrated smart colorimetric array patches with varying color transition temperatures, which displayed a wide temperature-detection range (29–40 °C) and high resolution (0.2 °C).

2.1.2. Hydrogel-Based Temperature Sensors

Besides composites, PNIPAM-based hydrogels can be used as another wearable temperature sensing device, as demonstrated by Feng et al., relying on ionic hydrogels. They designed their system to display excellent conductivity, mechanical tolerance, and rapid recoverability.[150] Their hydrogel was prepared from a multi-component mixture containing polyvinylalcohol (PVA), polyacrylic acid (PAA), and AAm monomers to which graphene oxide (GO) and Fe^{3+} were added, followed by the addition of NIPAM, and MBAM as a crosslinker. With PNIPAM-AAm hydrogel PVA–GO, PVA–GO/PAA–Fe^{3+}, and PNIPAM–AAm/Fe^{3+} conductive hydrogels were synthesized by a two-step polymerization method (**Figure 15a**) where first chain growth polymerization of AAm was completed followed by hydrogel formation with NIPAM. The hydrogels were subsequently utilized as ionic strain sensors that displayed temperature-dependent conductivity which depended on the free ion's mobility and their shuttle distance. At low temperatures, the mobility of free ions in

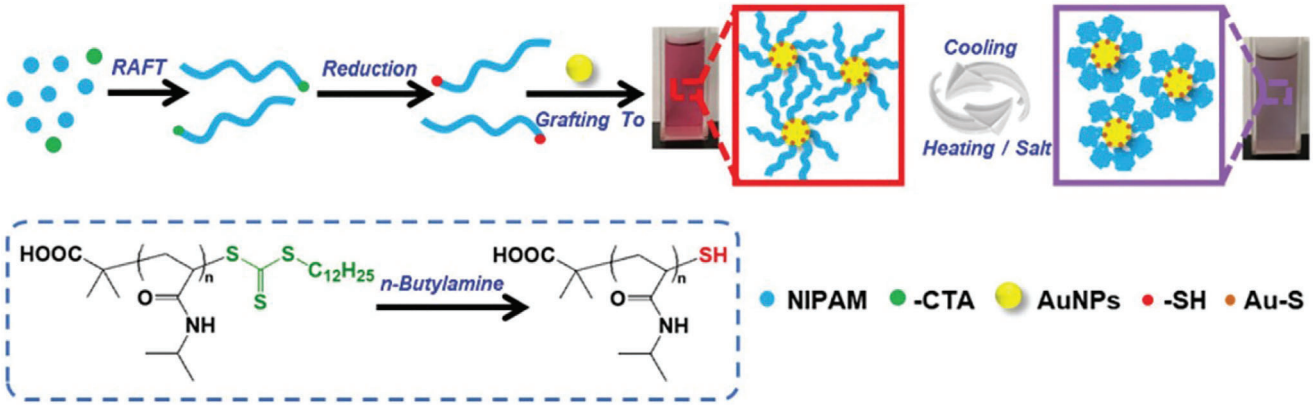

Figure 13. Preparation of PNIPAM-AuNPs hybrid with temperature response. Reproduced with permission.[146] Copyright 2021, Royal Society of Chemistry.

thermosensitive hydrogels was low thus exhibiting poor conductivity. Nevertheless, with increasing temperature ionic mobility was enhanced, causing increasing conductivity of hydrogels (Figure 15b). Besides temperature sensors, this material can also be used as a wearable strain sensor. Liu et al. explored the use of double network (DN) hydrogels and applied their mechanical properties for the development of a temperature sensor.[151]

A DN hydrogel has properties like fracture toughness, fracture tensile stress, and fracture tensile strain. In this report, DN hydrogels were prepared from chemically reduced GO and

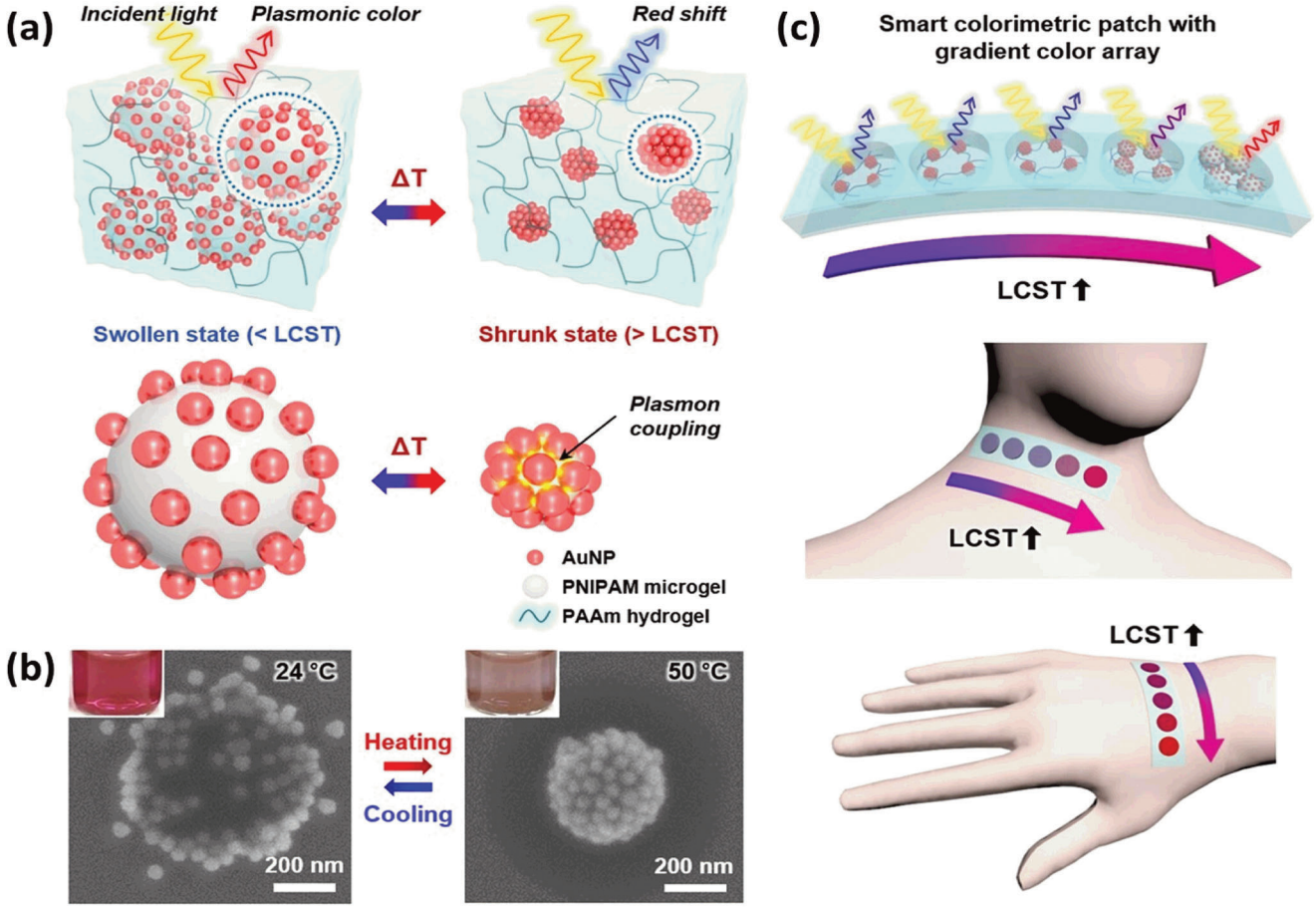

Figure 14. Demonstration of wearable sensor by Choe et al.[149] a) Effect of temperature on the microgel, b) SEM images of the microgel under the swollen state at 24 °C (left) and under the shrunken state at 50 °C (right), c) representation of the sensor array patches attached to human skin at different positions (neck and hand).

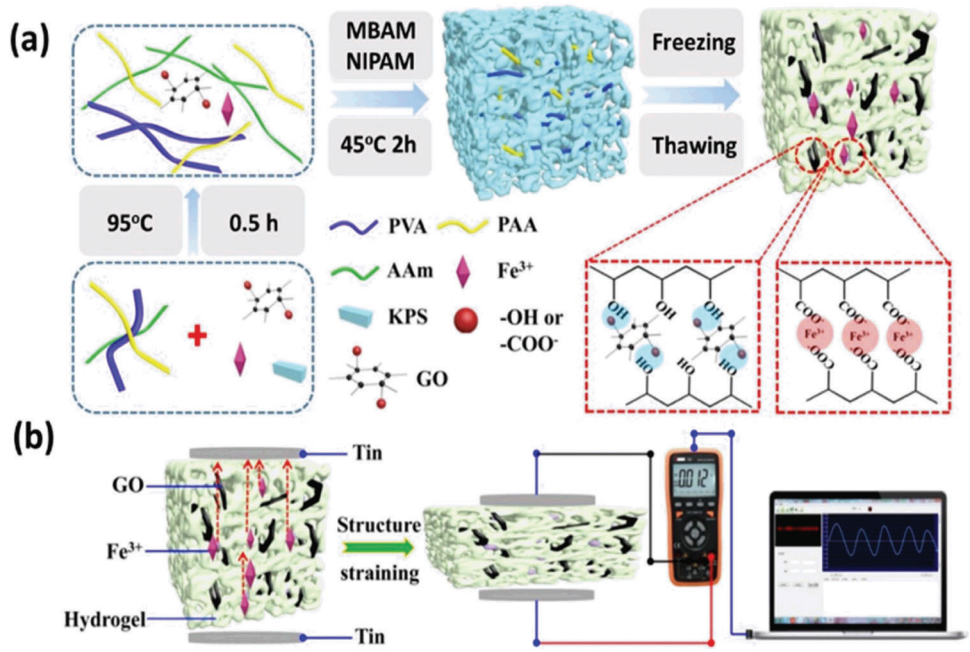

Figure 15. a) Synthesis of conductive hydrogel using two-step polymerization, b) Temperature sensing mechanism reported by Feng et al. Reproduced with permission.[150] Copyright 2019, American Chemical Society.

carboxymethyl chitosan (CMC), which were combined with NIPAM monomer and MBAM crosslinker (**Figure 16**). GO was reduced to reduced GO by CMC via the amidation reaction, which improved the conductivity of the fabricated hydrogels. The increase in temperature caused the deswelling of the continuous layer structure of GO and the tight DN structure of PNIPAM improved the continuous electronic transmission and resulted in decreased resistance.

The authors observed a reproducible change in resistance in the range of 25–60 °C. In addition to temperature sensing, it can also measure strain, as mentioned in the pressure sensing section.

A temperature-alerting hydrogel was developed by Wang and co-workers by utilizing an electrically conductive hydrogel, whereby the sensor relied on the shrinking and swelling of the hydrogel.[152] Here a PNIPAM hydrogel was prepared with crosslinker double bond end-capped Pluronic F127 (F127DA) and electrically conductive polyaniline (PANI) was synthesized with phytic acid as a crosslinker. By mechanically interlocking these two hydrogels, temperature changes could be detected from hydrogel shrinking. At 20 °C, the F-PNIPAM/PANI hydrogel tightly contacted the two copper electrodes, which closed an electrical circuit. When the temperature increased to 50 °C, a thermally induced chain collapse of PNIPAM occurred, and as a consequence the hydrogel shrank, resulting in a loss of contact between the electrodes and disconnection of the circuit with varying resistance. The authors also demonstrated that the hydrogel in this configuration could be used to detect and quantify strain.

Similarly, Zhan et al. also explored the incorporation of PNIPAM-based conducting hydrogels in electrical circuits. Their hydrogel was a composite of PNIPAM/carboxymethyl chitosan (CMCS)/MWCNT/PANI, which featured highly porous structures.[153] In the first step, the PNIPAM/CMCS/ MWCNT hydrogel was synthesized by a one-pot sol-gel synthesis, which was followed by the incorporation of an aniline monomer through noncovalent interactions between the active functional groups of the CMCS and MWCNT chains and the hydrogen atoms of the aniline monomers. Finally, the polymerization of the aniline monomer was initiated by ammonium persulfate (APS) in the presence of HCl. The hydrogel was designed in such a way that the conductivity of the hydrogel gradually reduced with increasing temperature in the range of 20 °C to 50 °C due to changes in the swelling state and microstructure of the hydrogel (**Figure 17**). Besides measuring temperature, their system was also capable of measuring pressure and pH, which we describe separately in the pressure and pH sensing section.

Stop-flow lithography is another method for creating unique thermal hydrogel sensors. This technique was applied by Wang et al. to synthesize a Y-shaped double-layered hydrogel.[154] This Y-shaped hydrogel was synthesized in a PDMS microfluidic channel to generate an angle between the hydrogel layers. The two-layered structure features a PNIPAM poor and rich side, thus providing a distinct thermal response for each layer. Upon heating, a stronger deformation of the PNIPAM-rich side occurs, resulting in a bent structure (**Figure 18**). Therefore, the bending angle can be utilized to accurately measure the temperature within the range of 16–55 °C.

Another hydrogel thermosensor was developed by Zhang et al., who modified PNIPAM hydrogel by grafting it onto individual nanodiamond (NDs) to form a shell. Then magnetic Ni nanoparticles (Ni MNPs) were added to the hydrogel.[155] (**Figure 19**). With the increase in temperature, the hydrogel collapsed, which caused a sharp decrease in the distance between the NDs and MNPs, and a large change in the magnetic field was observed via optically detected magnetic resonance (ODMR). Umar et al. made creative use of optical hydrogels where

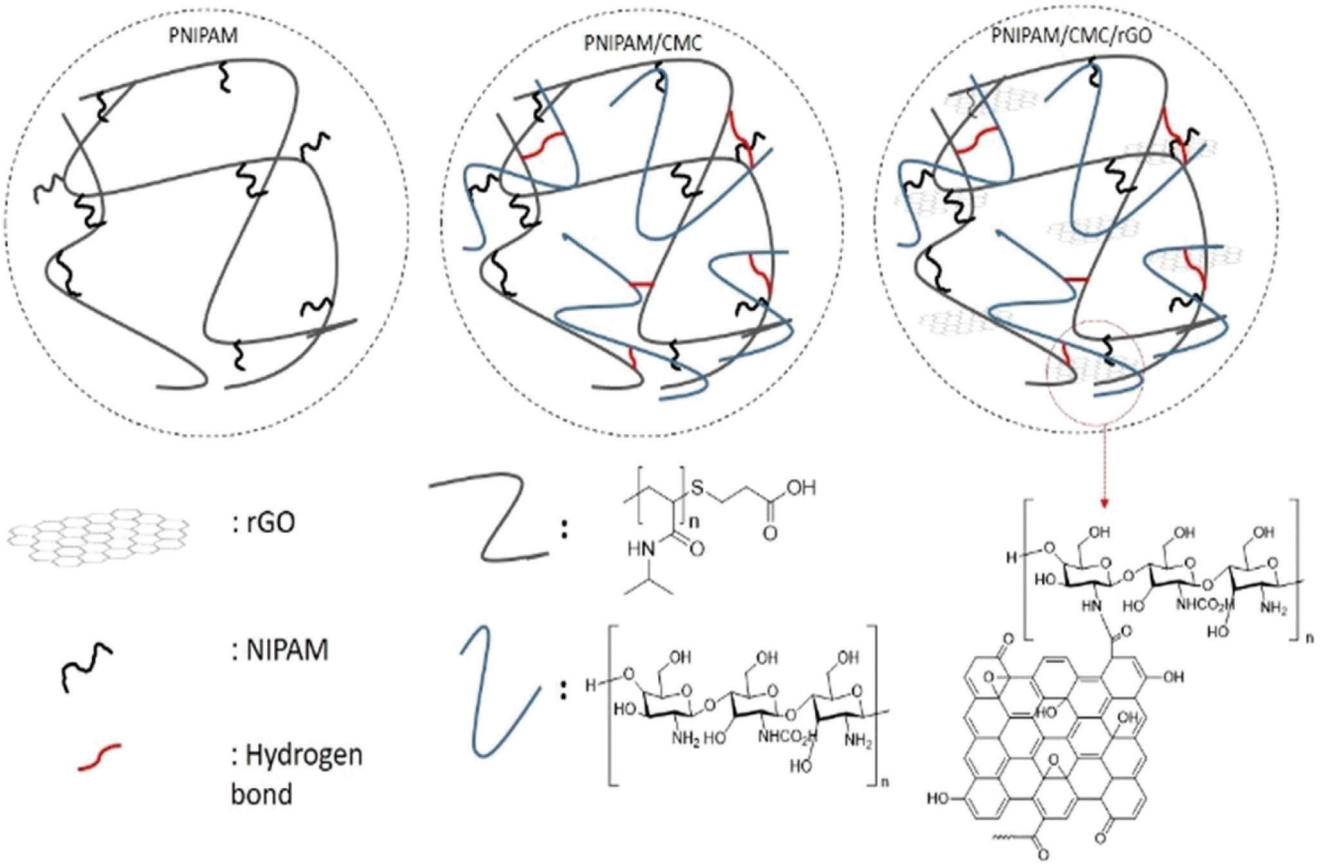

Figure 16. Schematic representation of three hydrogels prepared by Liu et al., where the rightmost depicts the functional hydrogel thermosensor.[151]

they fabricated MIM optical cavities with insulating nanolayers of thermoresponsive copolymer.[156] For their purpose, a poly(*N*-isopropylacrylamide-*r*-glycidyl methacrylate) [P(NIPAM-*r*-GMA)] was produced by free-radical polymerization with two photosensitive crosslinker bis(2-nitrobenzyl)methylenebis(4,1-phenylene)- dicarbamate (BL) and bis(2-nitrobenzyl)hexane-1,6-diyldicarbamate (HL).

The MIM cavities were prepared by sandwiching the insulator between two Ag nanolayers based on a Fabry–Perot etalon. Upon increasing temperature, the PNIPAM part in the hydrogel layer collapsed, causing a decrease in wavelength. In this fashion, the device could detect temperatures in the range of 19–30 °C of locally laser-heated protein particles and a chicken breast tissue sample. In addition, they demonstrated that the same phenomena may be exploited to detect alcohol concentration in food and biological samples.

A photonic sensor formed by a hydrogel was designed by Kye et al., where they introduced a photonic gel using 2-hydroxyethyl methacrylate (HEMA) as a hydrogel building block, and 4-acryloyl morpholine (ACMO) and NIPAM as thermoresponsive monomers (**Figure 20**).[157] ACMO unit has higher LCST (around 88 °C) and the opal-templated photonic gel shows a periodic modulation of the refractive indices within the gel, and an appropriate periodic distance results in a specific color due to the Bragg diffraction from the periodic inverse opal (IO) structure. The temperature in the range of 10–80 °C can be detected using this gel.

Another technique that can be used to monitor the temperature-dependent coil-to-globule transition of PNIPAM is particle image velocimetry (PIV). This technique relies on an experimental method that uses microscale particles as minimally invasive tracers to measure the velocity of a fluid flow.

Barbieri and co-workers explored the use of PNIPAM hydrogels to develop PIV-based thermosensors.[158] An interpenetrated polymer network (IPN) was designed with the NIPAM monomer followed by the addition of alginate to a PNIPAM solution and coated with chitosan after adding Nile red (NR)-alginate solution into PNIPAM hydrogel (**Figure 21**). Chitosan was added to adjust the particle permeability. Upon increase of temperature due to coil to globule transition, the polarity of PNIPAM decreased which caused the enhancement of fluorescence intensity of the polarity-sensitive dye up to 20 times compared to the original emission. The fabricated composites detected temperatures in the range of 29–41 °C.

Another PIV-based system was reported by Cellini et al.[159] For this purpose, they synthesized a copolymer of PNIPAM which incorporated a polarity-sensitive fluorescent dye, viz. 4-(2-acryloyloxyethylamino)−7-nitro2,1,3-benzoxadiazole (NBD-AE). The copolymer was then incorporated into a commercial PDMS matrix to enable PIV. Their system displayed a temperature-dependent increase in fluorescence as a result of the reduction of the micro-environmental polarity around fluorescent units from the PNIPAM chain. In addition, their

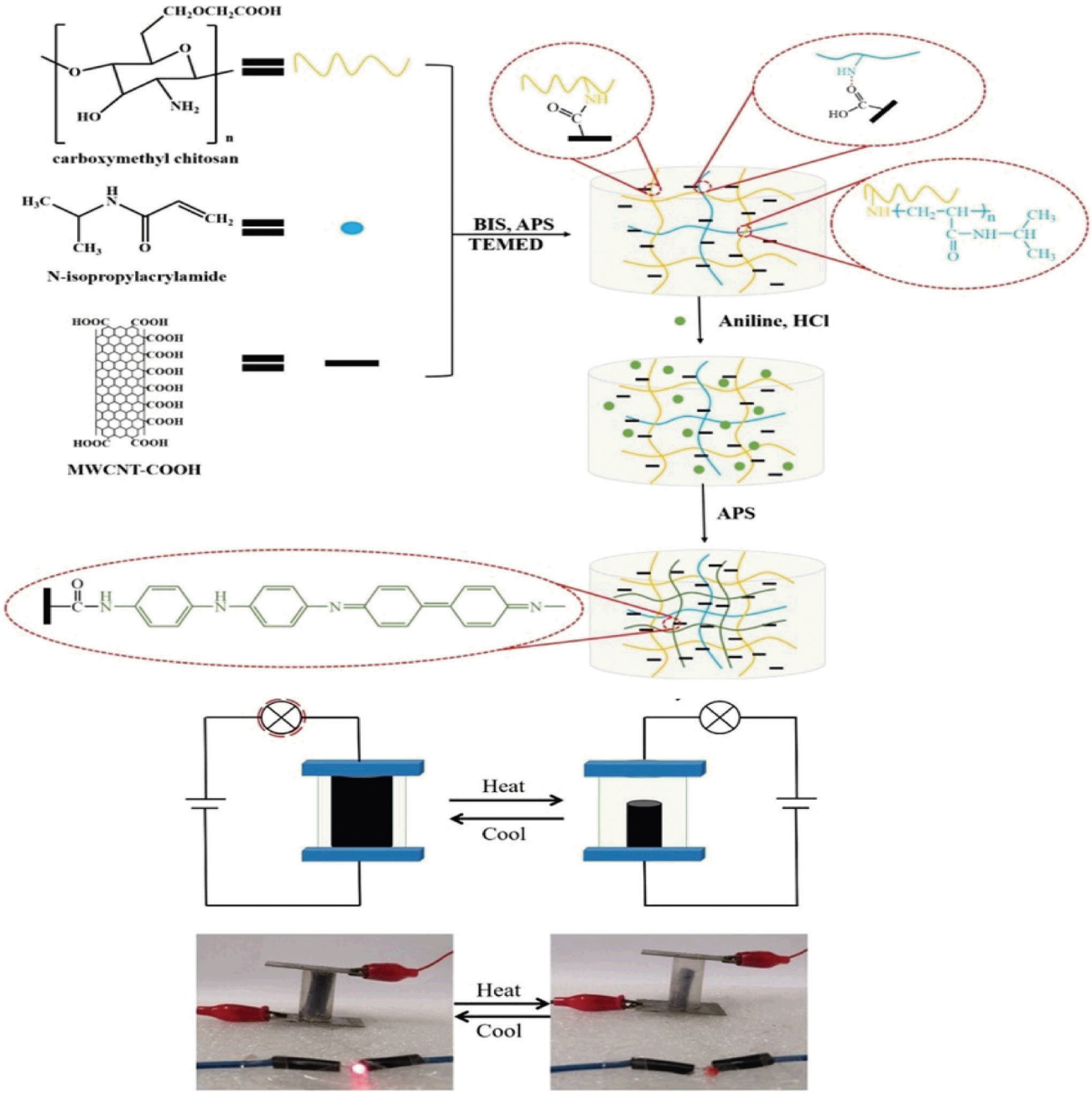

Figure 17. Synthesis of PNIPAM-based conducting hydrogels placed in an electrical circuit to allow a temperature alerting mechanism. Reproduced with permission.[153] Copyright 2021, Wiley-VCH.

system allowed for the observation of the fluorescence emission in the range of 14–50 °C temperature within the device by using an optical microscope. A nanogel thermometer capable of monitoring temperature inside living cells was developed by Uchiyama et al.[160] For this, they designed a cationic structure with low toxicity using a new cationic radical initiator, 2,2′-azobis-[2-(1,3-dimethyl-4,5-dihydro-1H-imidazol-3-ium-2-yl)]propane triflate (ADIP), which helped to show excellent ability to enter living mammalian cells in a short incubation period. With this radical initiator, a nanogel was produced by copolymerization of NIPAM, an MBAM crosslinker, and a DBThD-AA (oxygen atom of the 2,1,3-benzoxadiazole moiety in DBD-AA (*N*-{2-[(7-*N*,*N*-dimethylaminosulfonyl)−2,1,3-benzoxadiazol-4-yl](methyl) amino}ethyl-*N*-methylacrylamide) was replaced with a sulfur) as the environment-sensitive fluorescent unit (**Figure 22**). This nanogel displayed increasing fluorescence intensity as a function of temperature due to the lowering of the polarity in the immediate environment of the dye. Therefore, this nanogel could quantify temperature with a sensitivity of 0.02–0.84 °C in the range of 20–40 °C. The authors demonstrated the use of this nanogel for intracellular thermal imaging in HeLa (human epithelial carcinoma) cells.

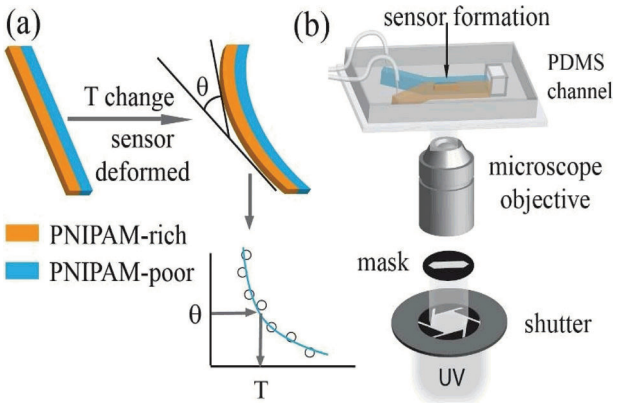

Figure 18. a) Schematic illustration of bilayer hydrogel and its deformation upon heating, b) Fabrication of PDMS microfluidic channel. Reproduced with permission.[154] Copyright 2019, American Chemical Society.

2.1.3. Copolymer-Based Temperature Sensors

In addition to gels, PNIPAM (co)polymers can be processed by electrospinning to obtain nanofibers, which are ideal for sensing applications due to their porous nature and high surface area. In this fashion, the interaction between the sensor and analytes can be maximized and the response occurs with a minimal time lag.

A recent example of such a system can be found in the work of Chen et al., who developed an ES nanofiber thermo-sensor from a P(NIPAM-*co*-NMA-*co*-RhBN2AM) polymer prepared through free radical polymerization.[161] At a fixed Hg^{2+} concentration (10^{-3} M) with the increase in temperature, the diameter of the fiber decreased resulting in aggregated and dense Rh-chelated Hg^{2+} moieties which resulted in the enhancement of fluorescence intensity (**Figure 23**). With the increase of temperature from 27 °C to 55 °C the wavelength of photoluminescent spectra ($\lambda_{PL,\,max}$) also increased. Besides temperature, this ES nanofiber could also detect changes in Hg^{2+} concentration and pH.

Block-copolymers also present a useful architecture for the synthesis of highly sensitive PNIPAM-based sensors. Such a system was recently reported by Qiao et al.[162] Whereby a block-copolymer of NIPAM and 4-vinylphenyl boronic acid (VPBA) was prepared via RAFT polymerization. In this configuration, the VPBA-block serves as the chemical anchor for curcumin via boronate ester formation, thus allowing its immobilization on a PNIPAM-VPBA framework (PNIPAM-VPBA-C) (**Figure 24**). In a subsequent step, Fluo-4 AM (FAM) was added to PNIPAM-VPBA-C unit to prepare PNIPAM-VPBA-C-FAM. The obtained block-copolymer composite relied on the donor–acceptor intramolecular charge transfer between curcumin and the fluorescent dye as a reporter event, leading to increasing fluorescence properties upon the temperature-induced collapse of PNIPAM. In this fashion, the temperature in the range of 30–42 °C could be measured in HeLa cells. Additionally, the authors demonstrated that this system could detect Ca^{2+} concentration down to 5.7×10^{-6} M.

An alternative strategy to boost thermal resolution focuses on lanthanide-based compounds, which allow for luminescence nanothermometry through a forbidden 4f–4f transition. One major downside of this approach is the relatively weak absorbance associated with the 4f–4f transition. In order to augment the performance of lanthanide-based materials, conjugation of PNIPAM has been shown to be a promising approach to develop highly sensitive nanothermometers. Such a nanothermometer was developed by Zhang et al., who synthesized a copolymer via the free radical copolymerization of NIPAM, (3-acrylamidopropyl) trimethylammonium (APTMA), and polymerizable Ir(III) and Eu(III) complexes.[163] The different components functioned as a thermo-responsive unit, a water-soluble endocytosis-promoting unit, a responsive phosphorescent luminophore, and a forbidden 4f–4f transition monitoring unit, respectively. When the polymer was heated from 20 °C to 42 °C, the PNIPAM chain became hydrophobic, thus decreasing the polarity around the Ir(III) complexes, which consequently enhanced their radiative transition (**Figure 25**). However, due to the forbidden 4f–4f transition, the luminescence intensity from the Eu(III) complexes remained unchanged. This result indicated that this system can image the temperature inside HeLa cells and zebrafish larvae using ratiometric and phosphorescence lifetime imaging microscopy.

Another nanothermometer based on a trivalent lanthanide (Ln^{III} = Tb and/or Eu) complex was reported by Sobrinho et al.[164] In their example, the lanthanide was incorporated by postpolymerization modification, through its chelation to a coordinating comonomer, viz. 4-(allyloxy)dipicolinic acid (dpal). The authors copolymerized this monomer with NIPAM as a thermoresponsive unit, MBAM as a crosslinker to obtain copolymeric NPs via emulsion polymerization. When these lanthanide-containing NPs were subjected to increasing temperatures, the coil to globule transition of PNIPAM caused the expulsion of water molecules from the NP interior (**Figure 26**). In the dehydrated interior, the water molecules in the first Ln(III) coordination sphere were replaced by weak chemical interactions with carbonyl groups available in the polymer chains, which in turn decreased the non-radiative pathways that lead to the emission quenching. In this fashion, the temperature in the range of 30–50 °C could be detected in a reversible manner, which was demonstrated for five consecutive cycles. Alternative to heavy metals, organic dyes can also be incorporated in the thermoresponsive polymer structure, whereby properties such as absorption intensity, wavelength, fluorescence lifetime, solvatochromism, and other characteristics can be monitored to report temperature changes. Gong et al. exploited these features to develop a polymer capable of detecting temperatures in the range of 37–42 °C inside living cells. Towards this end, a copolymer of P(NIPAM-*co*-BODIPY-AA) was prepared via RAFT polymerization, whereby the BODIPY-AA (5-thiol allyl-3-phenylamino-8-phenyl-4,4-difluoro-4-bora3a,4a-diaza-s-indacene) provides polarity-dependent fluorescence.[165] Upon heating, the polarity of the polymer decreased, resulting in the formation of hydrophobic aggregates, which increased the fluorescence of the dye (**Figure 27**).

In addition to the direct use of dyes and assessing their solvatochromic effects, the distance between dye pairs can be monitored by Förster resonance energy transfer (FRET). This process relies on the energy transfer of an excited donor dye to a suitable acceptor dye, which results in fluorescence of the acceptor dye. FRET is therefore a very sensitive technique that enables the probing of inter- and intramolecular distances. In addition, the FRET process is capable of providing multicolor fluorescence by

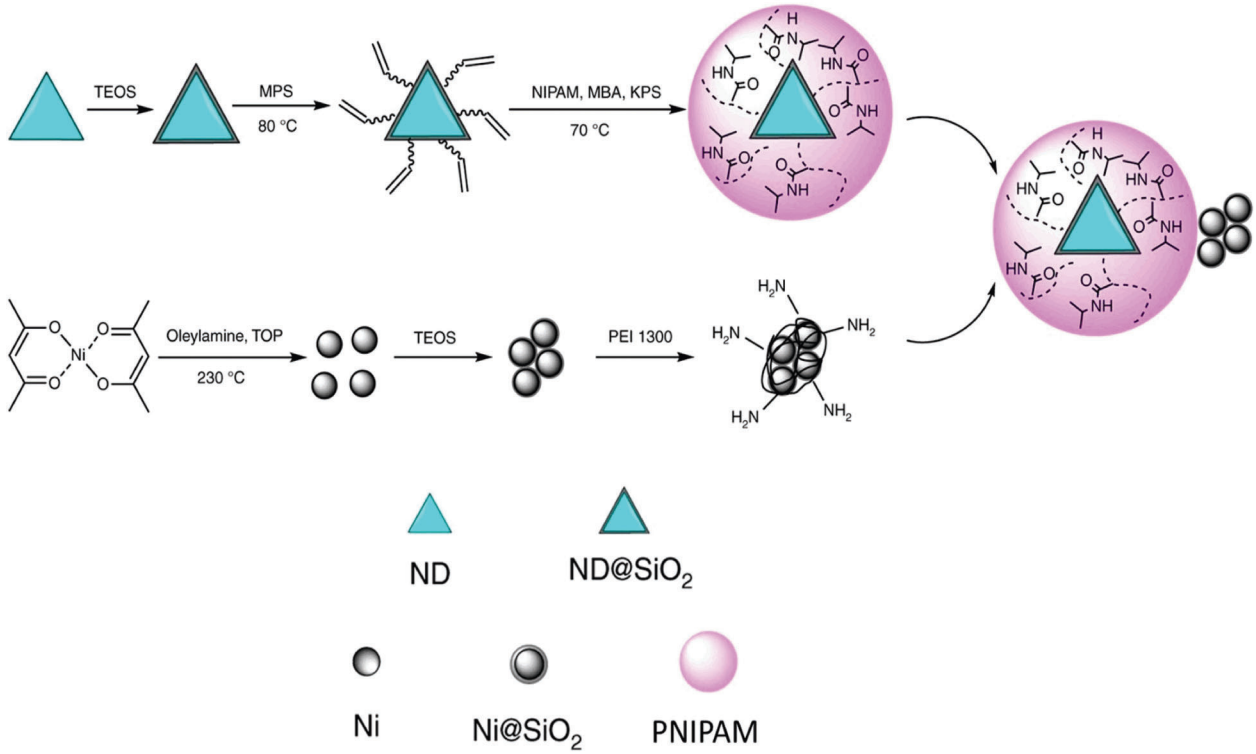

Figure 19. Synthesis of the hydrogel layer outside ND and followed by addition of Ni MNPs.[155]

selecting suitable acceptor and donor dye pairs. Hence, the FRET process is an attractive photophysical phenomenon for the development of thermometers with high sensitivity.

A recent example can be found in the work of Lee et al., who introduced the FRET donor nitrobenzoxadiazole (NBD) and FRET acceptor spiropyran (SP) dyes in a P(NIPAM-NBD) nanogel via emulsion copolymerization followed by the formation of P(NIPAM-NBD-SP) nanogels with adding SP-COOH to P(NIPAM-NBD).[166] Upon UV radiation ring-closed weakly fluorescent SP moiety changes into the ring-opened coral-red merocyanine (MC) moieties, resulting in light-pink fluorescent nanogels. With the increase of temperature, the distance between donor and acceptor moieties decreases which causes enhanced FRET with coral-red fluorescence (**Figure 28**).

Another FRET-based temperature sensor was reported by Kong et al.[167] They synthesized a PNIPAM copolymer via RAFT, which contained rhodamine 6G as the acceptor dye, while a 1,8-naphthalimide moiety featuring a piperazine was chosen as the donor dye. Their system exploited the thermoresponsive behavior of PNIPAM to modulate the distance between the 1,8-naphthalimide and rhodamine 6G moieties as a function of temperature. As the temperature increased, the distance between

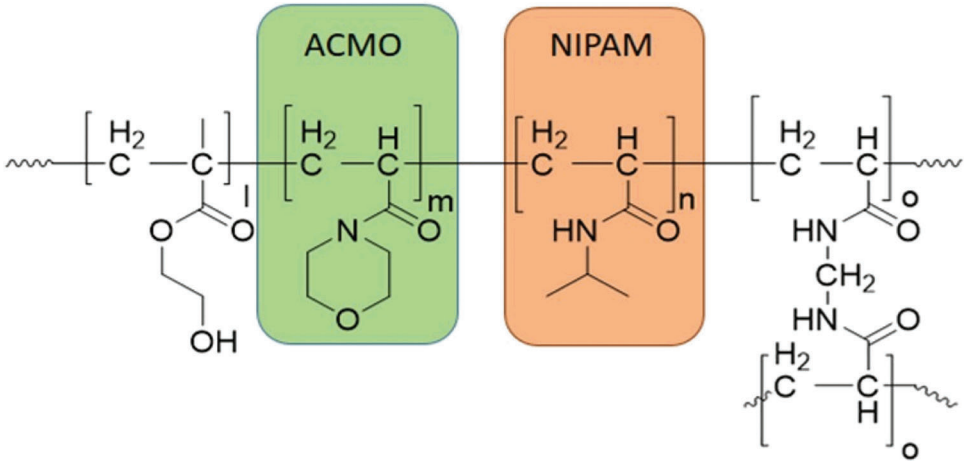

Figure 20. The structure of the hydrogel gel utilized by Kye et al. with *N,N'*-methylenebis(acrylamide) (MBAM) as cross-linker.[157]

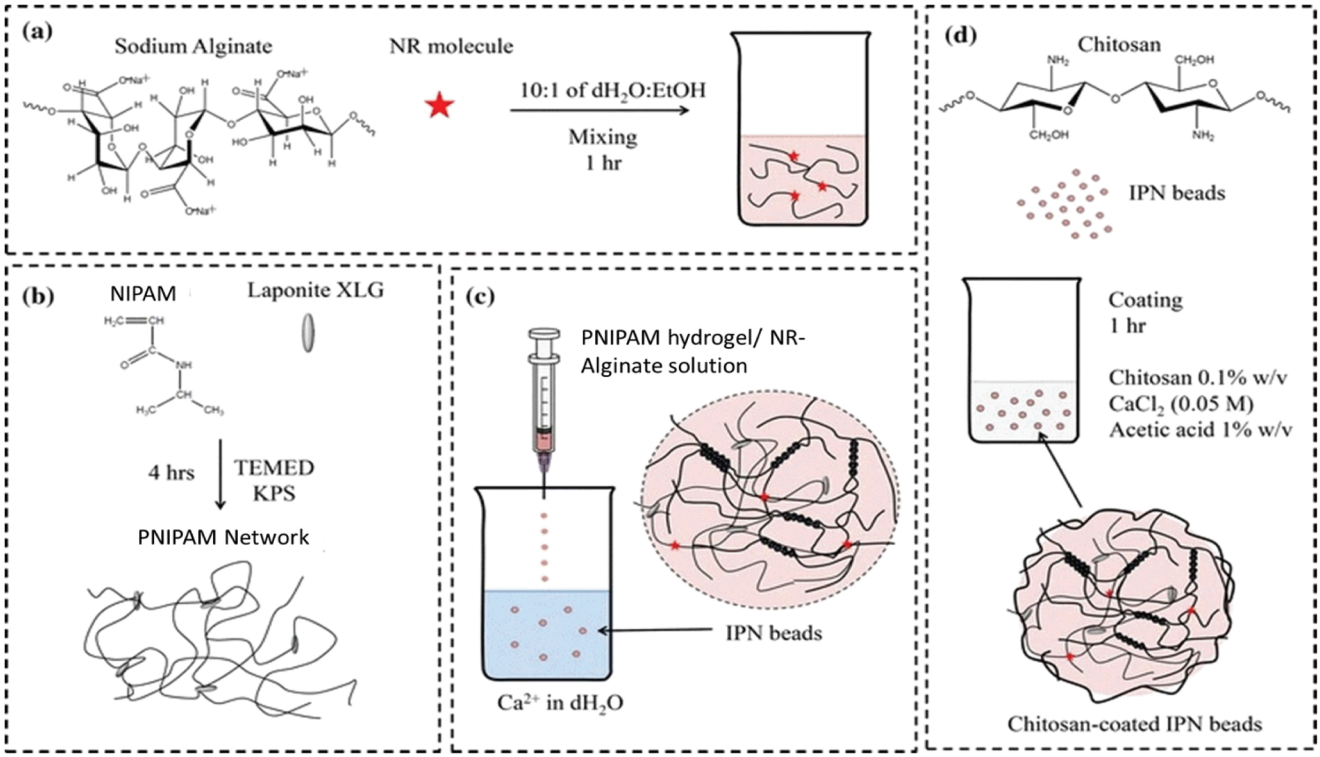

Figure 21. Preparation of the IPN reported by Barbieri et al. where, a) Formation of NR/alginate solution, b) Polymerization of NIPAM, c) Synthesis of IPN beads by ionic cross-linking, d) Coating of the IPN beads with chitosan by dipping. Reproduced with permission.[158] Copyright 2017, Springer Nature.

donor and acceptor dyes decreased, resulting in increased FRET efficiency. Besides temperature sensing, the authors also demonstrated the utility of their system as a Fe^{3+} and pH sensor which will be discussed in the respective sections. Finally, temperature sensors can also be prepared by incorporating polarity-sensitive monomers into the polymeric chain.

In this context, Uchiyama et al. designed the fluorescent 8-methoxy-2-oxo-2H-benzo[g]chromen-4-yl)methyl acrylate (MBC-AE) monomer and formed a P(NIPAM-*co*-MBC-AE) copolymer via free radical polymerization, which displayed enhanced fluorescence in polar environments. Upon heating, the fluorescence intensity gradually decreased allowing facile read-out of the temperature. Unfortunately, the ester in the MBC-AE units was found to be susceptible to hydrolysis under neutral and basic conditions, hampering its reversibility, as the polar sensitivity was lost once the dye was cleaved from the polymer.[168] To address these shortcomings, they synthesized the MBC-AA monomer, whereby the amide provides higher hydrolytic stability, and performed a random copolymerization with NIPAM to yield P(NIPAM-*co*-MBC-AA).[169] The newly obtained copolymer exhibited stronger fluorescence at longer wavelengths in polar solvents, whilst the polarity-dependent fluorescence behavior could be maintained. This was demonstrated by its excellent reproducibility over various cycles, allowing the reproducible monitoring of temperature between 30 and 40 °C.

As a result, a variety of PNIPAM-based temperature sensors can be designed using composites, nanomaterials, and PNIPAM copolymers. The structural design is suitable not only for the design of temperature sensors, but also for multi-functional chemosensors. The majority of the covered examples feature a robust temperature response in the range of 20 °C to 50 °C, and with proper design, materials can be developed to monitor biological processes inside cells. Although robust temperature sensors have been reported, in many examples the sensitivity of the sensors is not demonstrated which is an important feature of the sensors. From the covered examples it is clear that the incorporation of fluorescent dyes or other optically active moieties allows for the development of sensors with high sensitivity down to a few hundredths of a degree Celsius with a response time of about 160 s.

2.2. pH Sensors

pH plays an important role in many fields of science and engineering and is an important indicator of physiological and metabolic processes. Therefore, quantitative pH measurements are a useful tool in cellular analysis or diagnostics, i.e., the monitoring of the pH of wound fluid can provide information on the healing process, as well as septic conditions.[170] pH-responsive polymers are a group of stimuli-responsive polymers which undergo structural changes and properties such as surface activity, chain conformation, solubility, and configuration in response to solution pH.[171] Polymer-based pH sensors are attractive due to their low cost of production and high sensitivity in relatively small volumes. In the case of PNIPAM, the most

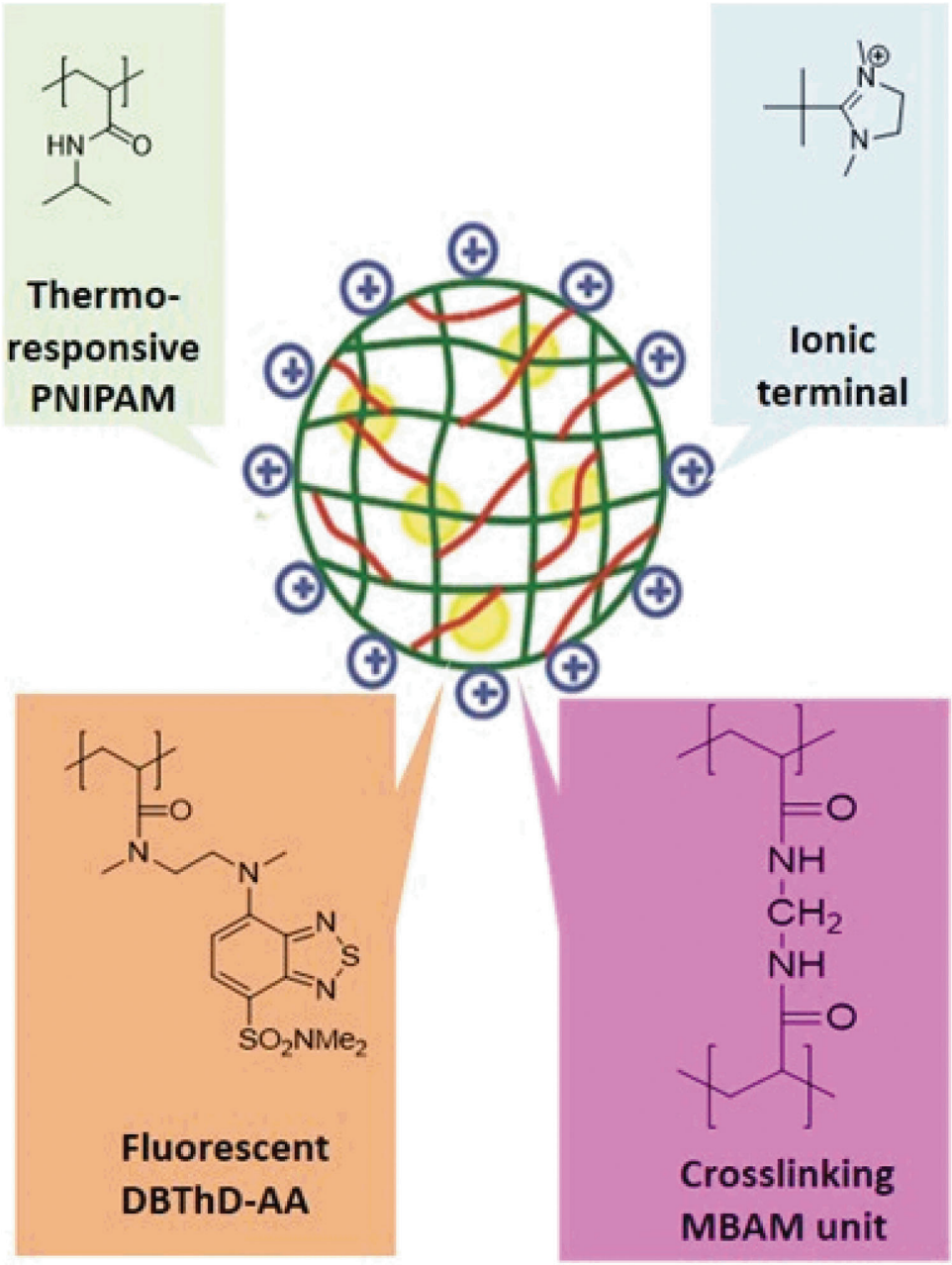

Figure 22. Structure of nanogel produced by Uchiyama et al. for intracellular temperature monitoring. Reproduced with permission.[160] Copyright 2018, Wiley-VCH.

common method to prepare a pH sensor is by incorporating acrylic acid as a comonomer, as it features an ionizable —COOH group. Several hydrogels containing acrylic acid have been prepared to detect pH, relying on the differential swelling behavior as a function of the COOH protonation degree.[172,173] Besides such macroscopic hydrogels, similar microgels have been incorporated into etalons-based pH sensors.[110,111] In addition, a fluorescence dye can be combined with acrylic acid to facilitate easy interpretation of the colorimetric sensor output.[174] Also, pH-responsive fluorescent dyes, such as *N*-{2-[(7-N,N-dimethylaminosulfonyl)−2,1,3-benzoxadiazol-4-yl]- (methyl)amino}ethyl-*N*-methylacrylamide (DBD-AA),[175] dicyano-methylene-4H-pyran,[71] benzaxazole,[94,176] rhodamine unit,[177] PNME (combination of 2-(6-(4-(2-hydroxyethyl)piperazin-1-yl)−1,3-dioxo-1H-benzo-[de] isoquinolin-2(3H)-yl)ethyl methacrylate with NIPAM),[69] CPMA ((Z)−4-(1-cyano-2-(4-(dimethylamino) phenyl)vinyl)phenylmethylacrylate)[178] can be incorporated to facilitate the read-out without the need for acrylic acid. Also, in the context of dye-functionalized polymers, the AIEE (aggregation-induced enhanced emission) phenomenon can be exploited for pH detection.[179]

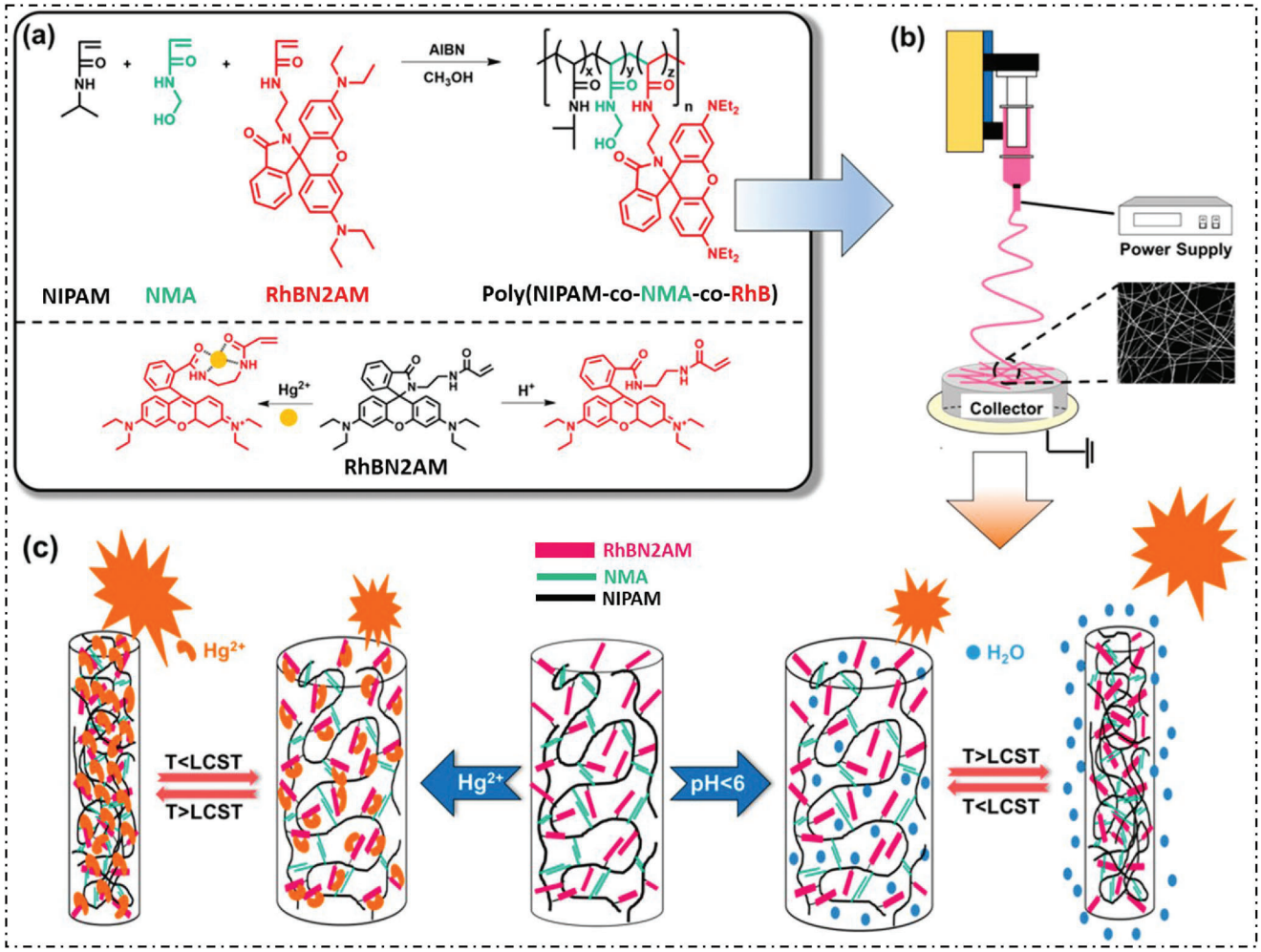

Figure 23. a) Synthesis of P(NIPAM-*co*-NMA-*co*-RhBN2AM) for multifunctional detection, b) Development of ES nanofiber, c) Schematic representation of detection for temperature, pH and Hg^{2+}.[161]

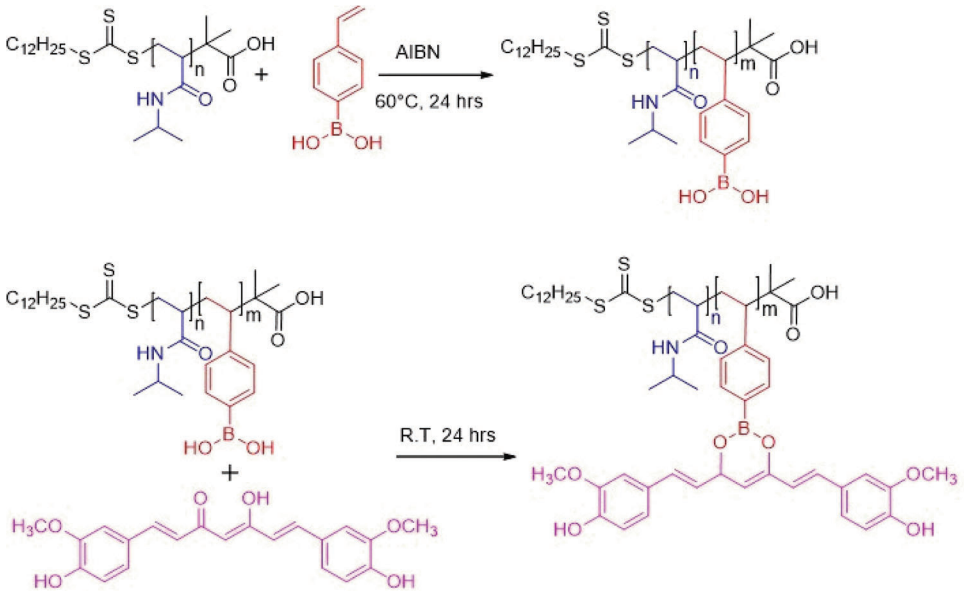

Figure 24. Synthesis of block copolymer where first VPBA was incorporated and then curcumin was added to prepare PNIPAM-VPBA-C.[162]

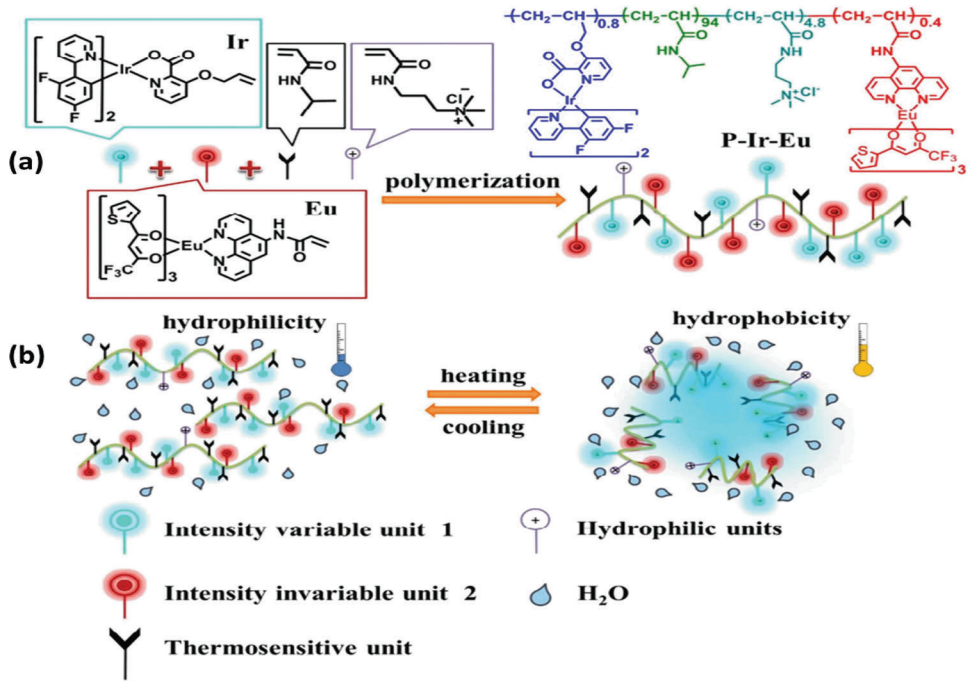

Figure 25. a) Preparation of polymer P-Ir-Eu, b) Representation of the effect of temperature on polymeric structure. Reproduced with permission.[163] Copyright 2018, American Chemical Society.

Moreover, NPs have been incorporated to prepare pH sensors.[180] Silver nanoclusters (AgNCs) are extensively featured due to their easy preparation and bright fluorescence. Lu et al. explored their use to develop a pH sensor with a temperature-responsive copolymer ligand (CPL).[181] The copolymer PNIPAM-*co*-5-(2-methacryloylethyloxymethyl)-8-quinolinol (MQ) was synthesized via free radical copolymerization (**Figure 29**). Then modification with AgNCs was performed to prepare CPL-AgNCs. At pH less than 3, no fluorescence was observed while with further increase of pH, the fluorescence intensity was found to be increased. Here, introduction of PNIPAM made the polymer water-soluble. The system exhibited a pH detection range 3.04–5.25.

As mentioned previously,[153] the swelling and deswelling characteristics of PNIPAM/CMCS/MWCNT/PANI hydrogels enabled temperature monitoring through the related changes in conductivity. The same system could also be used to monitor pH, as the conductivity of the hydrogel increases with decreasing pH due to the protonation of PANI. In this fashion, the pH could be monitored in between 2 and 12.

Moreover, the FRET-based thermosensor of Kong et al. could be used to monitor pH.[167] The spirolactam rings present in the R6GEM units of the copolymer undergo ring-opening in acidic conditions, which results in characteristic absorption and emission bands (**Figure 30**). Through the temperature-induced aggregation of PNIPAM chains the distance between rhodamine

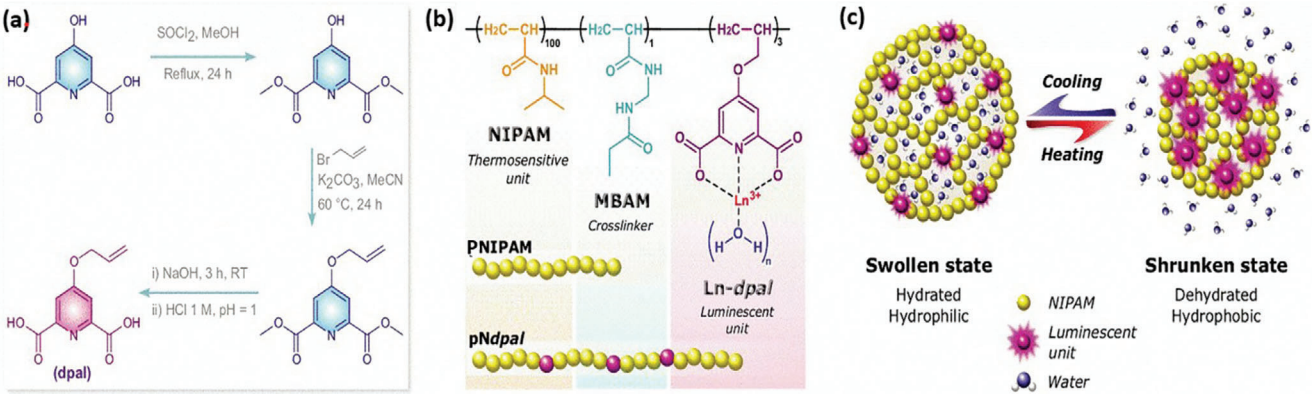

Figure 26. a) Synthetic route of the dpal monomer for trivalent lanthanide chelation, b) Chemical composition of the synthesized polymeric NPs, c) Schematic representation of the thermally induced collapse of PNIPAM-based NPs and associated luminescence. Reproduced with permission.[164] Copyright 2020, Royal Society of Chemistry.

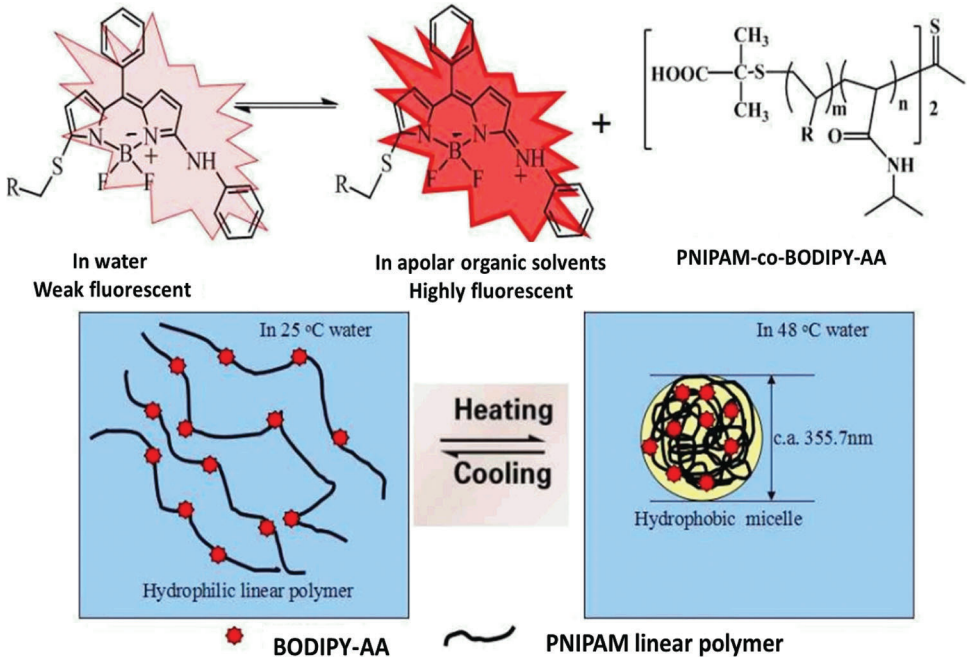

Figure 27. Reported temperature sensing mechanism of P(NIPAM-*co*-BODIPY-AA). Reproduced with permission.[165] Copyright 2017, Elsevier Ltd.

6G and 1,8-naphthalimide moieties decreased, resulting in enhanced FRET, thus allowing more accurate monitoring of pH between 2–7. Another example is a rhodamine-based pH sensor made from electrospun PNIPAM nanofiber.[161] As reported earlier, without mercury ions H^+ also induced the RhBN2AM to transform from its non-fluorescent spirocyclic form into its opened cyclic form resulting in enhanced fluorescence. Here also a pH in the range 2–7 could be detected. Similar to the previous example, heating caused the condensation of the PNIPAM chain and reduction of rhodamine-rhodamine distance which

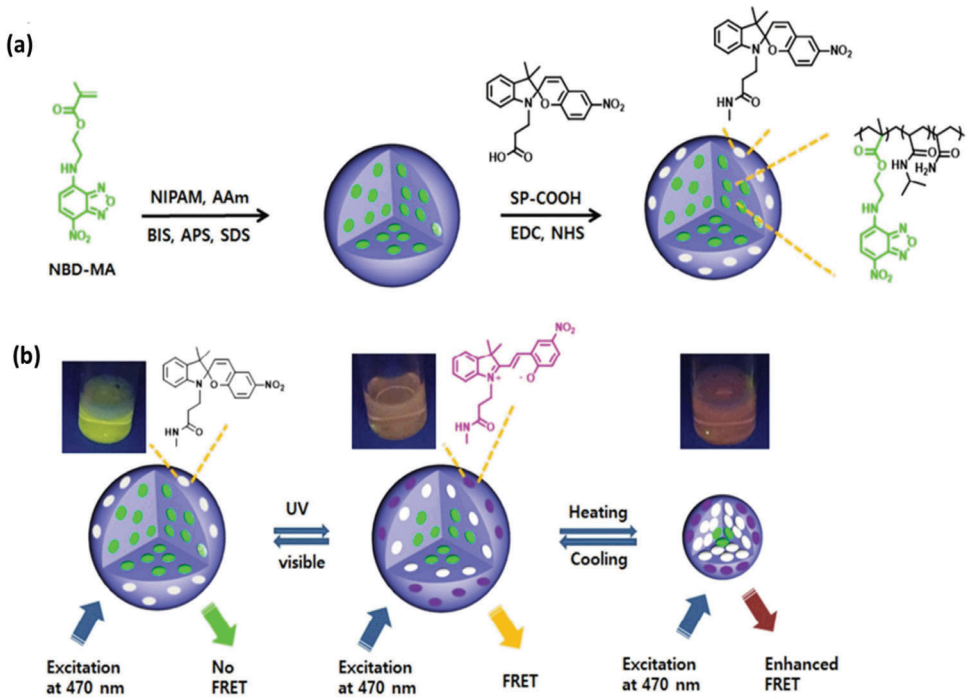

Figure 28. a) Preparation of nanogel, b) Temperature sensing mechanism using FRET mechanism. Reproduced with permission.[166] Copyright 2017, Elsevier Ltd.

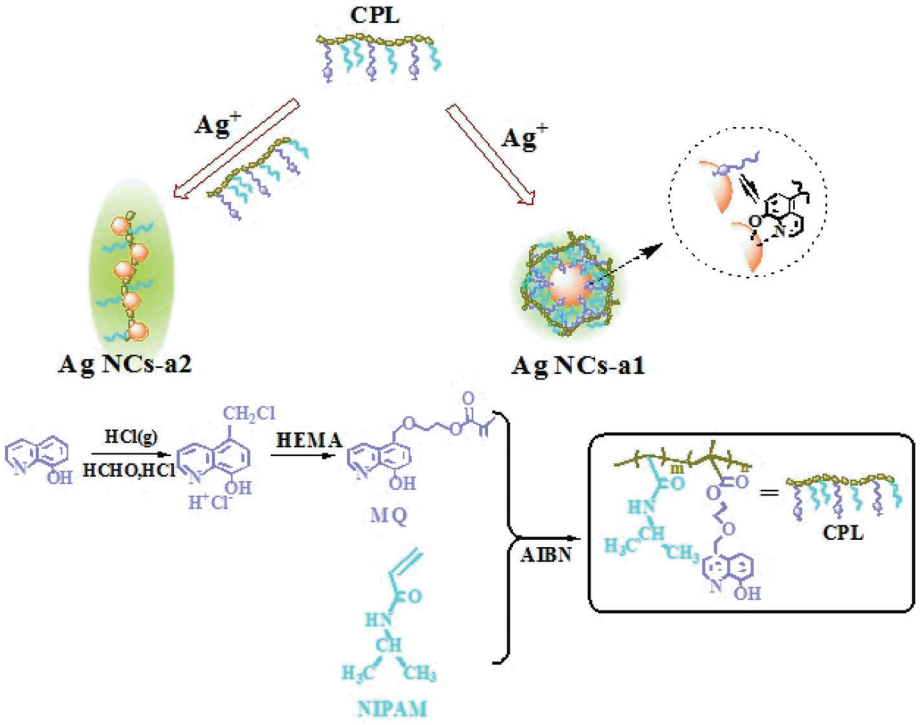

Figure 29. Synthesis of CPL-AgNCs. Reproduced with permission.[181] Copyright 2017, Elsevier Ltd.

increased the PL intensity of emission maxima, thus providing easy readout.

The polymer PNIPAM is thermoresponsive, consequently, PNIPAM cannot serve as a pH sensor on its own. Usually, other pH responsive units are added in order to facilitate pH readout. These pH-responsive moieties allow pH measurements in both basic and acidic ranges, making it a useful tool for proton detection with a response time of ≈12 s. Since protonation is simply diffusion-limited, quicker responses for pH is expected relative to temperature. Temperature changes, however, can have an impact on pH sensitivity, affecting the chemical equilibrium of the system, absorbing additional heat and producing protons, which lower pH in the solution as a function of increasing temperature. Therefore sensors that rely on the temperature-induced phase transition/separation behavior of PNIPAM in their sensing mechanism could have limitations with accuracy of the pH measurement.

2.3. Analyte Sensing

An analyte is a component or a chemical species that is of interest in an analytical procedure. Analyte sensing can be utilized for, e.g., disease monitoring, drug discovery, and detection of pollutants. Analytes such as metal ions and salts are discussed in this part.

2.3.1. Metal Ion Sensing

Heavy metal ions have recently received a lot of attention since they are a significant health hazard. Because of their poor biodegradation and long-term persistence in the environment, they have the propensity to bioaccumulate, presenting an increasing risk to organisms higher up the food chain. Mercury is one of the most notorious pollutants among the heavy metal

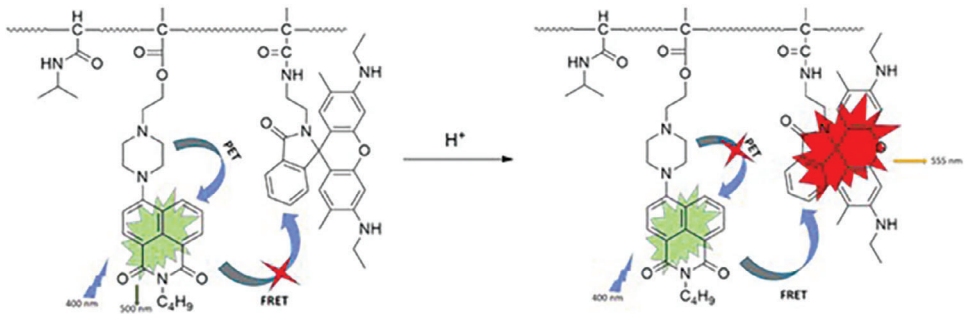

Figure 30. Change of absorption and emission property in presence of H^+.[167]

ions and is especially known for its effective bioaccumulation which can cause permanent damage in the central nervous and endocrine systems.[182,183] Another well-known heavy metal is lead, which is commonly found in industrial wastewater because of its extensive use in facilities such as waste incinerators, smelteries, battery manufacturing plants, and printed circuit board factories.[184] It accumulates in the human body through water or food intake and can cause neurotoxicity, kidney dysfunction, and several immunological effects, and is particularly harmful to children concerning intellectual development.[185,186] Besides these well-known heavy metals, several others, (such as copper, zinc, and iron) are known to play important physiological roles, though overexposure or excess of these heavy metals can lead to several diseases and disorders. Therefore, governmental agencies around the world have tried to limit environmental exposure to these metals by defining safe limits for drinking water and food contaminants.[187] Hence selective detection of metal ions is of paramount importance for assessing water pollution, eliminating environmental hazards and their occurrence in biological systems. Most common detection techniques, viz. atomic absorption spectroscopy (AAS), inductively coupled plasma spectroscopy, and various electrochemical methods typically require large, expensive instruments and associated infrastructure.[188–192] Alternatively, fluorescent sensors based on acridine-based dyes can also detect heavy metal ions, though the poor water solubility of these dyes makes them unsuitable for detecting ions in water.[193–196] Therefore, there exists a need for an economic, light-weight, water-soluble sensor that allows easy detection, quantification, and interpretation of its output. Polymer-based sensors are ideally suited for this purpose as their chemical structure can be adjusted to modulate sensitivity, selectivity, in addition to presenting small, biocompatible, yet inexpensive materials for sensor development. Also, for metal ion sensing, the coil to globule phase transition has been exploited for developing sensors. Therefore, it is no surprise that PNIPAM has been prominently featured in such applications, though for these applications the incorporation of sensing moieties in the polymer structure is typically required. Alternatively, PNIPAM has also been incorporated in composite materials to facilitate detection. A major advantage of these systems is that they can be used repeatedly with minimal loss of function due to the reversible phase transition behavior. Some of the systems that will be outlined below rely on copolymer structures of metal-sensing monomers such as rhodamine derivatives, naphthylamide derivatives, thiourea, CdSe/ZnS QDs which simultaneously detect metal (e.g., Hg) and exhibited fluorescence deviation in presence of metal ions.

Rhodamine-based chemosensors are widely used due to their excellent photophysical properties, viz. high fluorescence quantum yield, a broad range of absorption and emission wavelengths, and large absorption coefficients. Unfortunately, rhodamine derivatives typically display poor water solubility, and therefore conjugation to PNIPAM has been explored to facilitate their application in the sensing of metal ions in aqueous and biological media. Deng et al. utilized this strategy to develop a Hg^{2+} sensor, and incorporated a *N*-tripodal rhodamine 6G (RD) dye via aminolysis of a poly(*N*-isopropylacrylamide-*co*-*N*-acryloxysuccinimide [poly(NIPAM-*co*-NASI)] to prepare poly(NIPAM-*co*-RD) copolymer.[197] In presence of Hg^{2+}, ring-opening of the rhodamine units occurs, whereby the solution changed from colorless to pink, in addition to an enhancement in fluorescence properties (**Figure 31**). After exposure to Hg^{2+}, the sensing property of their system could be recovered by treatment with sulfide ions in heating conditions as heating condition polymer collapsed and Hg^{2+} was separated from polymer chain. The polymer selectively sensed Hg^{2+} in mineral water and tap water in the presence of cations such as K^+, Na^+, Ca^{2+}, Ba^{2+}, Cd^{2+}, Co^{2+}, Cu^{2+}, Fe^{2+}, Mn^{2+}, Ni^{2+}, Pb^{2+}, Zn^{2+}, Al^{3+}, Fe^{3+}, Cr^{3+} with a LOD as low as 2.25×10^{-8} M.

Another rhodamine-based Hg^{2+} sensor was reported by Chen et al.[161] (in the temperature sensing section we elaborated the synthesis). The moiety is primarily present in the non-fluorescent, less colored spirocyclic form in absence of Hg^{2+}. Upon exposure to Hg^{2+} the spirolactam ring-opens resulting in bright pink fluorescence (**Figure 32**). Above the LCST, the thermally induced aggregation of PNIPAM decreases the rhodamine–rhodamine distance, thus enhancing fluorescence and sensitivity. The fiber can sense 10^{-3} M Hg^{2+}.

Another type of Hg^{2+} sensing mechanism was explored by Liang et al.[198] They prepared composite nanofibers via electrospinning blends of poly(*N*-isopropylacrylamide)-*co*-(*N*-methylolacrylamide)-*co*-(acrylic acid) [poly(NIPAM-*co*-NMA-*co*-AA)], the fluorescent probe 1-benzoyl-3-[2-(2-allyl-1,3-dioxo-2,3-dihydro-1Hbenzo[de] isoquinolin-6-ylamino)-ethyl]-thiourea (BNPTU), and magnetite NPs on a single-capillary spinneret. The incorporated 1,8-naphthalimide-based dye served as a colorimetric indicator to selectively detect Hg^{2+}, relying on the transformation of the BNPTU thiourea moiety to an imidazoline moiety. This transformation causes a significant reduction in electron delocalization within the fluorophore resulting in a bathochromic shift from green to blue emission (**Figure 33**). The "off" state of the sensor was exhibited at a higher temperature when PNIPAM was collapsed, which blocked the absorption of incident light by the BNPTU moiety with Hg^{2+} resulting in a decrease of PL intensity. This system exhibited sensitivity up to 10^{-3} M with sensitivity over other heavy metal ions including Co^{2+}, Ni^{2+}, Pb^{2+}, Zn^{2+}, Mg^{2+}, Cu^{2+}, Fe^{2+}, and Cd^{2+}. Zhu et al. developed a multicomponent system for detecting both Hg^{2+} and Cu^{2+} ions.[199]

The first component consisted of an azobenzene (AZO)-terminated PNIPAM-*b*-(PS-co-MQ) block-copolymer, which was synthesized by RAFT polymerization. These polymers were then complexed with previously prepared CdSe/ZnS QDs, which resulted in self-assembled structures presenting the AZO moiety on their surface. In a subsequent step, the AZO moieties were complexed via host-guest chemistry with β-cyclodextrin (β-CD). This water-soluble composite displayed the characteristic fluorescence peaks of both CDs and CdSe/ZnS QDs in the absence of metal ions. With the addition of Hg^{2+} and Cu^{2+} efficient charge transfer between the metal ions, QDs and CDs takes place, resulting in fluorescence quenching (**Figure 34**). The system exhibited LODs down to 1.6×10^{-6} and 2.74×10^{-6} M for Hg^{2+}, Cu^{2+}, respectively.

In addition to Hg^{2+}, Pb^{2+} is a hazardous metal. To enable its efficient detection macrocyclic ligands such as crown ethers have been used. Crown ethers, in particular, display the ability to chelate cations (metal ions and organic molecules), as long as they fit inside the crown ether cavity. This size discrimination in the formation of "host-guest" complexes can therefore be exploited to capture and detect ions of

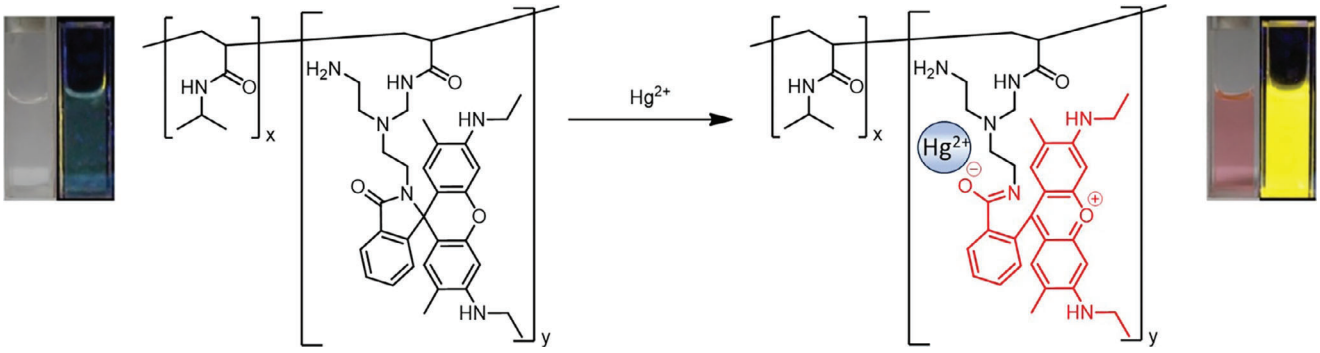

Figure 31. Rhodamine-based NIPAM copolymer for detecting Hg^{2+} and its associated color change in presence of Hg^{2+}. Reproduced with permission.[197] Copyright 2016, Elsevier Ltd.

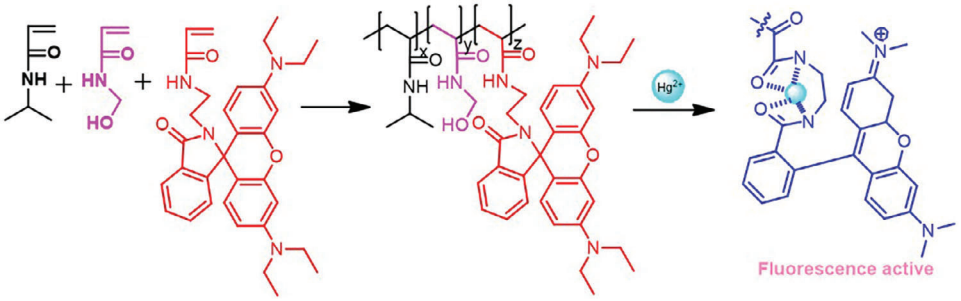

Figure 32. Metal sensing mechanism.[161]

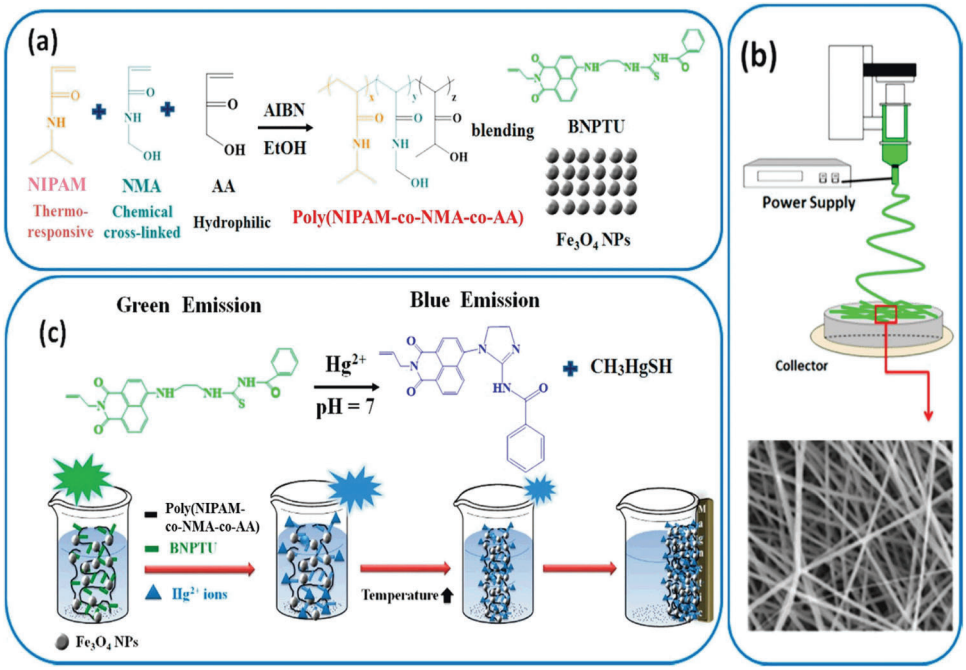

Figure 33. a) Chemical synthesis of composite nanofibers for the detection of heavy metal ions, b) Schematic representation of electrospinning process of the composite, c) Sensing mechanism of the obtained composite nanofibers.[198]

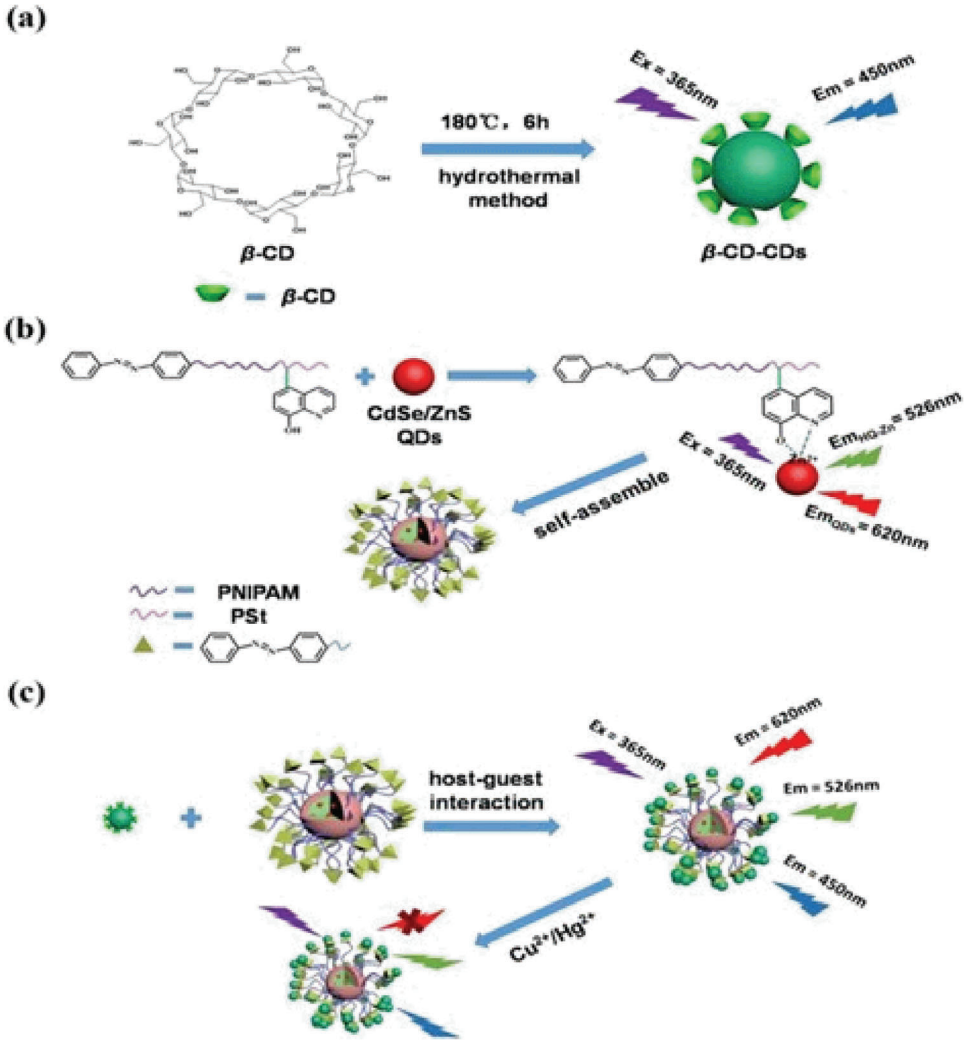

Figure 34. Synthesis and sensing mechanism of NIPAM-based NP composite developed by Zhu et al. for Hg^{2+}, Cu^{2+} sensing. a) Preparation of β-CDs, b) Self-assembly of PNIPAM-*b*-(PS-*co*-MQ) with CdSe/ZnS QDs, c) Host–guest interaction with β-CDs of the self-assembled structures and their fluorescent emission in absence and presence of Hg^{2+} or Cu^{2+}. Reproduced with permission.[199] Copyright 2019, Elsevier Ltd.

interest. Lin et al. utilized this strategy to develop a Pb^{2+} detecting microchip based on a poly(*N*-isopropylacrylamide-*co*-benzo-18-crown-6-acrylamide) [P(NIPAM-*co*-B18C6Am)] microgel.[200] This microgel was synthesized via photo-initiated free radical copolymerization of NIPAM with B18C6Am. This process took place inside the glass-capillary microchannels of a microfluidic chip to form uniform cylinder-shaped microgels.

By putting a cylinder-shaped P(NIPAM-*co*-B18C6Am) microgel inside capillary microchannels, a crescent-moon-shaped micro-space for flowing fluids was formed between the microgel and capillary. Upon recognizing Pb^{2+}, the microgel isothermally swells, thus decreasing the free space in the channel and the flow rate drops correspondingly (**Figure 35**). The microgel's reusability was tested at high temperatures because the microgel shrank, reducing the distance between B18C6Am/Pb^{2+} complexes. As a result, electronic repulsion increased, resulting in Pb^{2+} decomplexation. Pb^{2+} could be detected down to 10^{-9} M concentrations by using an online flowmeter and monitoring the flow rate.

In their next report about Pb^{2+} sensing, the same nanogel was synthesized and immobilized on a commercialized polycarbonate membrane.[201] Upon addition of Pb^{2+}, the volume of the nanogel increased, thus allowing [Pb^{2+}] monitoring through easy detectable transmembrane flux changes. The pore size of the PNIPAM-nanogels reduced as the gels swelled, resulting in decreased trans-membrane flow and a LOD of 10^{-10} M (**Figure 36**). In another study, a similar device was made by using a poly(*N*-isopropylacrylamide-*co*-acryloylamidobenzo-12-crown-4) (PNB) nanogel chamber and a bottom semipermeable membrane with a top indicator tube.[202] Pb^{2+}-exposure induced hydrophobic to hydrophilic transitions, thus increasing the osmotic pressure, which increased the liquid level in the indicator tube (**Figure 37**). This device detected Pb^{2+} in water with a LOD of 10^{-10} M.

Their group also exploited the crown ether-PNIPAM combination in several other configurations exploiting hollow microgel P(NIPAM-B18C6Am),[203] hydrogel grating membrane P(NIPAM-*co*-B18C6Am),[83] nanogel P(NIPAM-B18C6Am),[204]

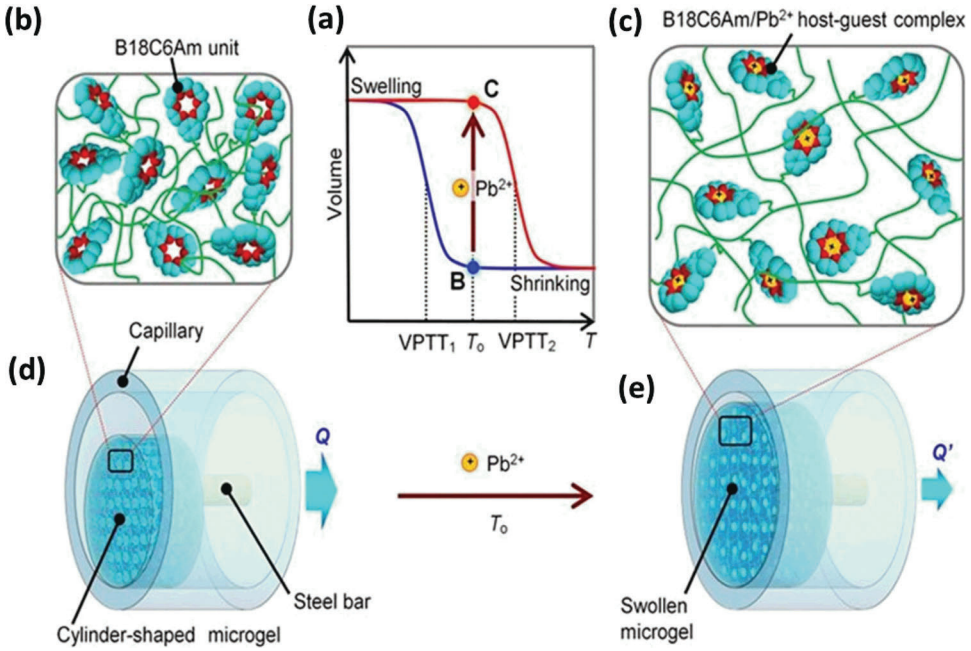

Figure 35. a–c) Swelling of (NIPAM-*co*-B18C6Am) hydrogel after recognizing Pb^{2+}, d,e) Change of the shape of microgel inside the capillary.[200]

and calcium alginate membrane encapsulated with P(NIPAM-B18C6Am) nanogel.[205]

Copper is one of the most important transition metals in the body. In absence of Hg^{2+}, rhodamine can be utilized to sense Cu^{2+}, which also operates via a similar mechanism, viz. ring-opening of the spirolactam in presence of Cu^{2+} resulting in strong fluorescence. This property was utilized by Wu and co-workers, who developed electrospun nanofibers containing rhodamine for Cu^{2+} sensing.[98] These electrospun nanofibers were made from random copolymer

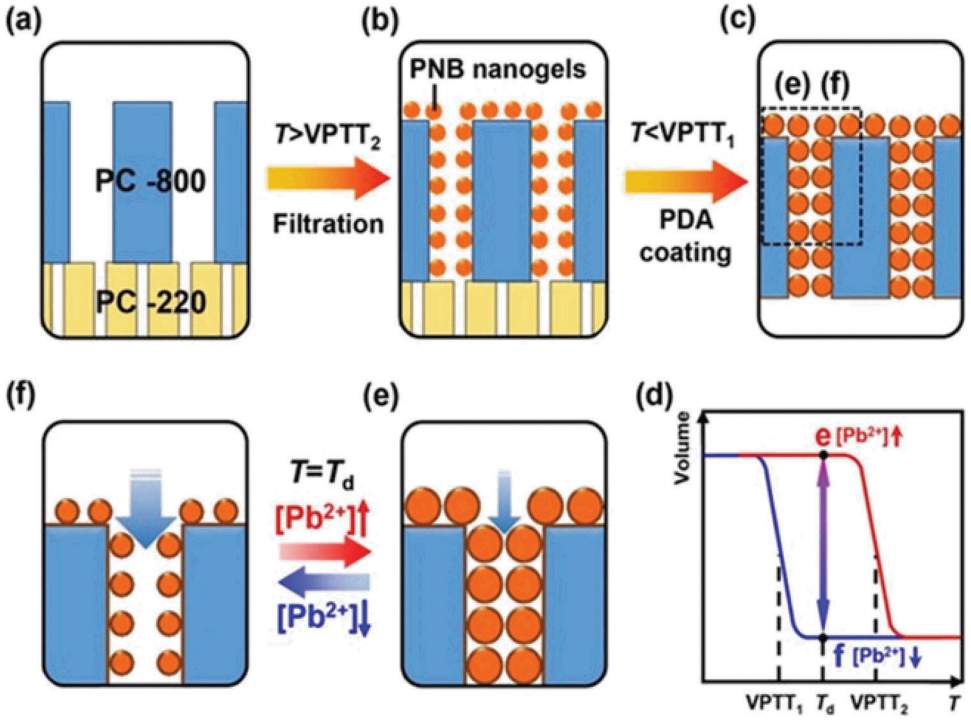

Figure 36. a–c) Preparation of membrane with nanogel, d-f) Pb^{2+}-Responsive swelling and shrinking of nanogel. Reproduced with permission.[201] Copyright 2018, American Chemical Society.

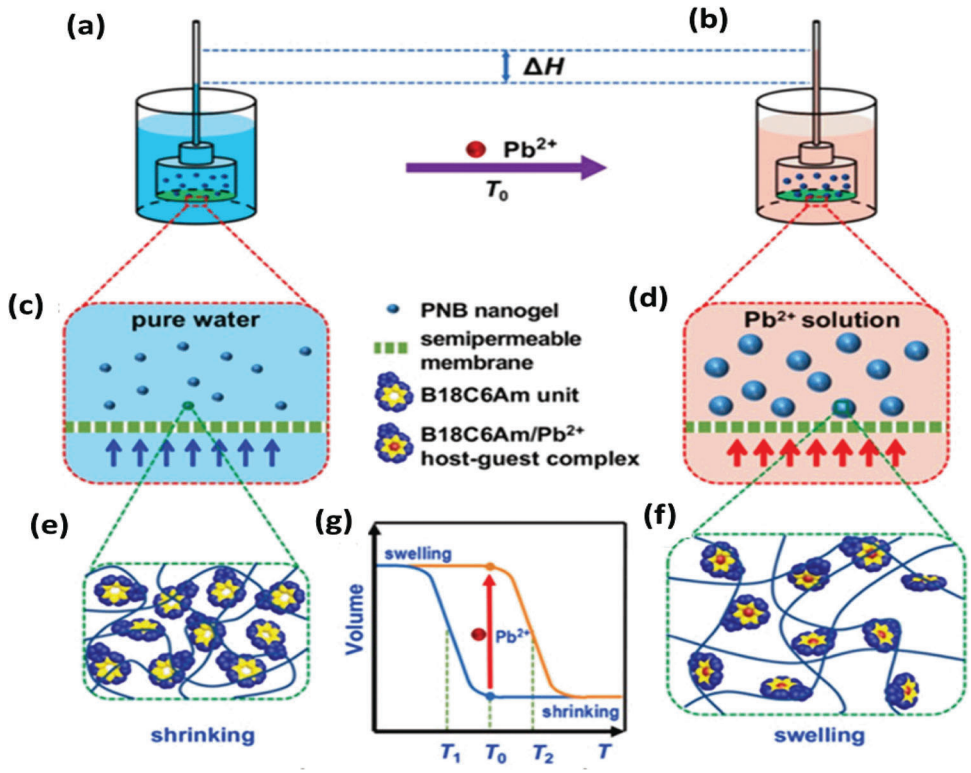

Figure 37. Fabrication of device with Pb-response. a,c,e) Without Pb^{2+} shrinking nanogel, b,d,f) In presence of Pb^{2+} swelling of nanogel occurs with higher osmotic pressure causing increase of height (ΔH). Reproduced with permission.[202] Copyright 2020, Elsevier Ltd.

P(NIPAM-*co*-NMA-*co*-RHPMA) (PNNR) where NMA is *N*-hydroxymethyl acrylamide and RHPMA is 4-rhodamine hydrazonomethyl-3-hydroxy-phenyl methacrylate (**Figure 38**). When heat is applied, the polymer collapses and the rhodamine moieties get compacted in the nanofibers, which results in the suppression of the fluorescence due to aggregation-induced quenching showing "off" state and hence proving regeneration of sensor. The sensor showed highly selective and sensitive recognition over Ca^{2+}, Cd^{2+}, Co^{2+}, Fe^{3+}, Hg^{2+}, K^{+}, Mg^{2+}, Mn^{2+}, Pb^{2+}, and Zn^{2+} with a LOD down to 1×10^{-6} M.

Wang and co-workers designed a PNIPAM nanosphere for detecting Cu^{2+}.[206] First, a negatively charged ligand anilino diacetate (phenyl-IDA) was prepared and added to NIPAM and MBAM cross-linker to synthesize PNIPAM NPs using emulsion polymerization. Finally, the NPs were immobilized in a polyacrylamide gel. The negatively charged ligand made the NPs swell and exhibited fluorescence. Nevertheless, in the presence of paramagnetic Cu(II) the negative charge gets neutralized, causing the particle to shrink which resulted in fluorescence quenching (**Figure 39**).

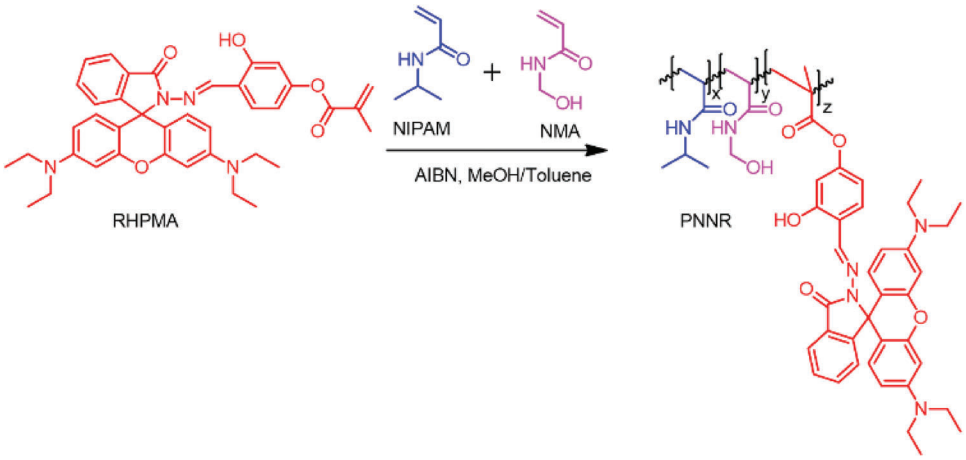

Figure 38. Synthesis of PNNR.[98]

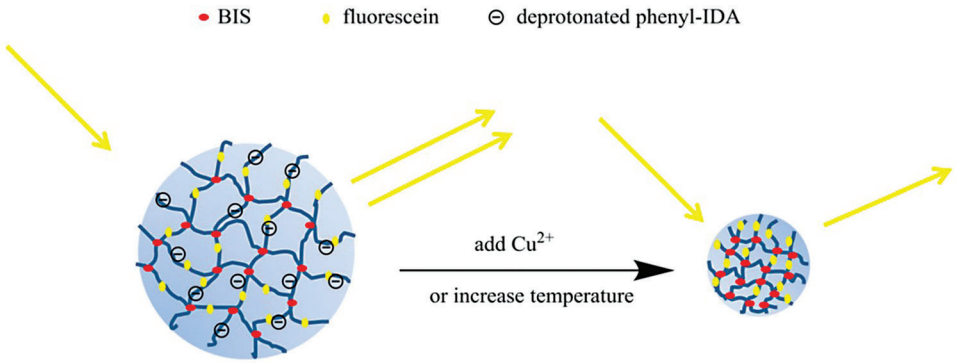

Figure 39. Cu^{2+} responsive mechanism of NPs reported by Wang et al.[206]

Qiao et al. developed a PNIPAM-based sensor for the detection of Cu^{2+} in serum.[207] To facilitate the detection in serum, the authors grafted PNIPAM via living/controlled radical polymerization method to AuNPs via a droplet microfluidic system. The PNIPAM improved the stability of the NPs by preventing aggregation. However, in presence of Cu^{2+}, the lone pair electron of amide groups in the PNIPAM polymer chains bind to Cu^{2+} ions, thus causing aggregation of PNIPAM@AuNPs through Cu–N coordination bonds (**Figure 40**). This aggregation caused a bathochromic shift in the UV–vis absorption spectrum of the PNIPAM@AuNPs from blue to red. The detection range was calculated to be in the range 5.0–750.0 × 10^{-6} M with a LOD of 2.5 × 10^{-6} M.

Utilizing aggregation-induced emission (AIE), a Cu^{2+} sensor was fabricated by Nhien et al.[208] Here the AIEgenic tetraphenylethylene-dipicolylamine (TPEDPA) monomer was incorporated in the PNIPAM chain using free radical polymerization and two different polymers were prepared with different molar ratios (P1:- *x*:*y* = 60:1and P2:- 175:1). The fluorescence of the TPE unit was quenched by photoinduced electron transfer (PET) phenomena in presence of Cu^{2+} ions, thus halting the cyan emission (**Figure 41**).

At high-temperatures, aggregation of PNIPAM occurred, thus causing enhanced rotation and vibration of phenyl rings on TPE moieties. This, in turn, led to remove the restrictions to intramolecular rotation (RIR), thus reducing fluorescence intensity. The two copolymers (P1 and P2) exhibited LODs 57 × 10^{-9} and 72 × 10^{-9} M respectively. The reusability of the polymer was facilitated by treatment with a disodium ethylenediaminetetraacetate (EDTA) solution.

Han et al. investigated the use of rhodamine dyes for the detection of Al^{3+} and Fe^{3+} in a DHBC system. The block-copolymer was synthesized from a polyethylene glycol (PEG) macroinitiator, whereby a second copolymer block of NIPAM with rhodamine

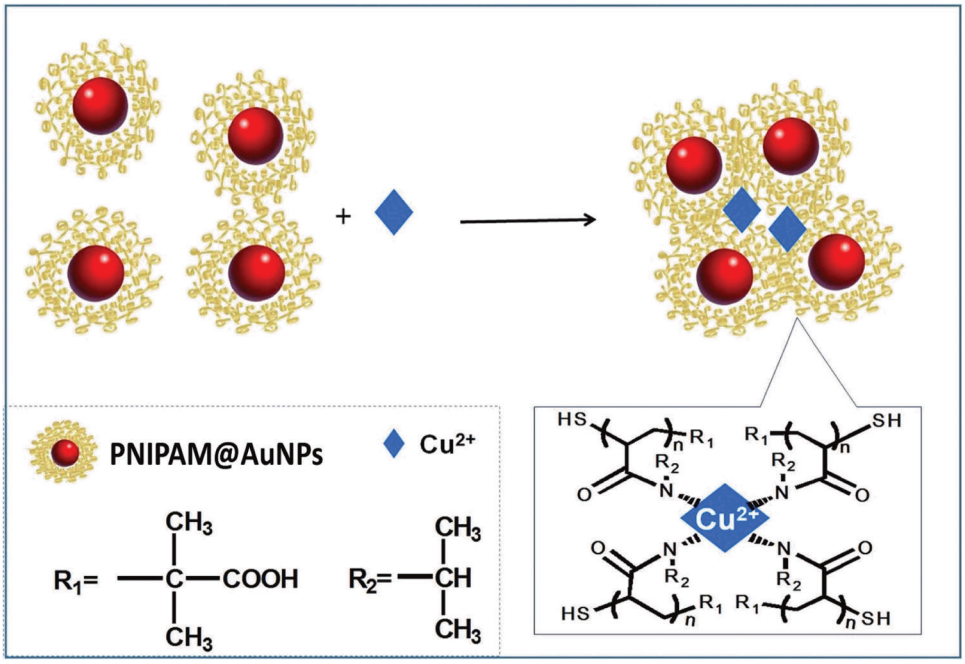

Figure 40. Binding of PNIPAM with Cu^{2+}. Reproduced with permission.[207] Copyright 2017, American Chemical Society.

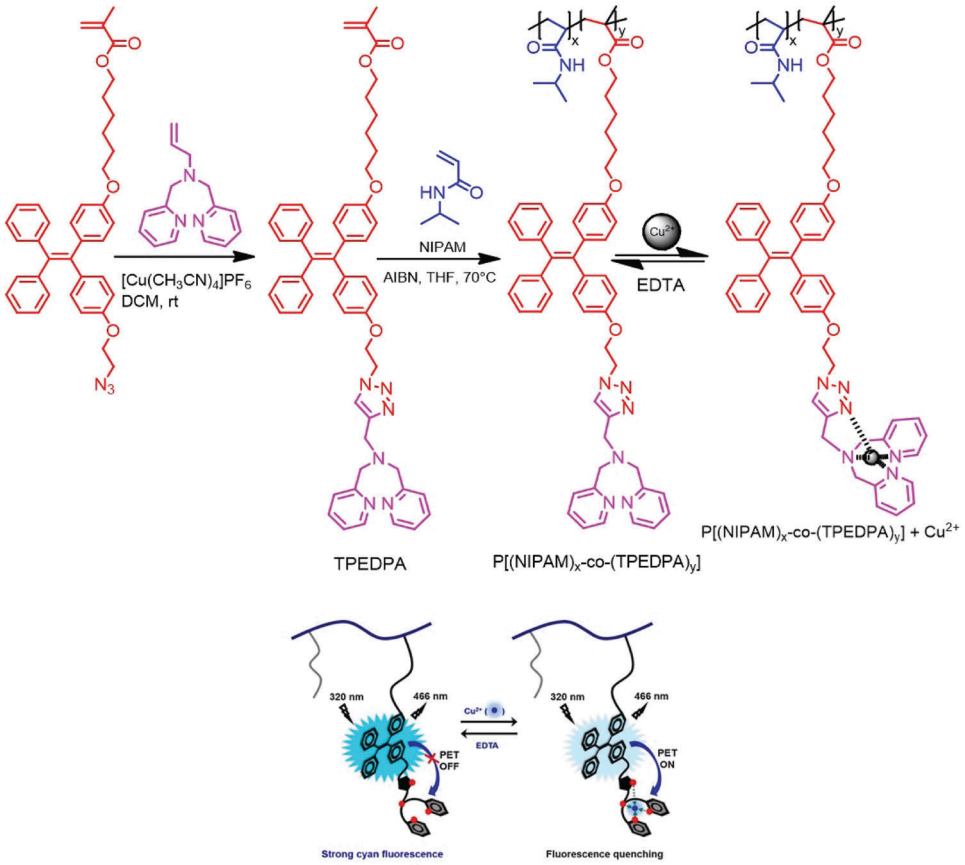

Figure 41. Synthesis of polymer and in presence of Cu strong cyan fluorescence was quenched. Reproduced with permission.[208] Copyright 2021, Elsevier Ltd.

6G methacrylic acid (Rh6GEMa) was prepared in a subsequent step to yield (PEG_{113}-*b*-P(NIPAM-*co*-$Rh6GEMa)_{67}$).[209] In addition, they also prepared a double hydrophilic polymer with another metal recognizing scaffold, viz. 2,4-methacryloyl benzaldehyde oxime (BDMa), in a similar fashion, to obtain (PEG_{113}-*b*-P(NIPAM-*co*-$BDMa)_{60}$). Here, BDMa was chelated with Al^{3+} through the interactions with the oxygen atom of the carbonyl, imine nitrogen, and the phenolic hydroxyl group to form a rigid complex that exhibited blue fluorescence. On the other hand, the rhodamine motif featuring the amide group of the ethylenediamine moiety and the cyclic amide of the spirolactam ring could coordinate Fe^{3+}, which resulted in visible yellow fluorescence (**Figure 42**). At elevated temperatures, the hydrophobic association of the PNIPAM block facilitated micellization and the aggregation of the metal ion sensing moieties in the hydrophobic core of the micelle, which increased fluorescence and consequently LODs. In this fashion, the developed system could reach LODs of $\approx 5.95 \times 10^{-9}$ to $\approx 4.02 \times 10^{-9}$ M for Al^{3+} and $\approx 30.30 \times 10^{-9}$ to $\approx 23.84 \times 10^{-9}$ M for Fe^{3+}.

Detection of the hexavalent Cr(VI) ion is of particular importance in air and water, due to its genotoxicity and carcinogenicity. For drinking water, in particular, governmental agencies allow only low levels of hexavalent Cr(VI) ions, e.g., California allows only 10 ppb.[210] While challenging, Shen et al. developed a PNIPAM-based sensor capable of detecting hexavalent Cr(VI) ions down to a limit of 1 ppb in water. Towards this end, they designed a novel thermo-responsive photoluminescent silver cluster/P(NIPAM-*co*-AAc) microgel nanocomposite, which relies on the excellent photoluminescent properties of Ag nanoclusters for accurate detection.[211] The submicron hydrogel particles were synthesized via one-step precipitation copolymerization followed by the formation of Ag clusters/P(NIPAM-*co*-AAc) hydrogel composites by irradiation reduction. The PL intensity of the nanocomposites was effectively quenched by Cr(VI) due to the electron transfer from the electron-rich Ag nanoclusters to electron-deficient Cr(VI). Again, free coordination of the metals to polymer bound —COOH and —NHCO groups reduced the distance between Cr(VI) and Ag nanoclusters, thus resulting in quenching of PL of the nanocomposite. Upon heating, the conformation of hydrogel changed resulting in aggregation and reducing the distance between Ag nanoclusters, and consequently the PL intensity (**Figure 43**).

Another hazardous metal-oxide ion is MnO_4^-, which is of particular concern due to its carcinogenic properties and extensive use in both laboratory and industrial fields. The World Health Organization (WHO) has fixed the guideline value for manganese in drinking water from 500 to 400 µg L^{-1}.[212] Zhu et al., however, developed a very sensitive MnO_4^- sensor, capable of detecting MnO_4^- anions up to 25×10^{-9} M with a linear concentration range of 0–50×10^{-6} M, well below the limits set for drinking

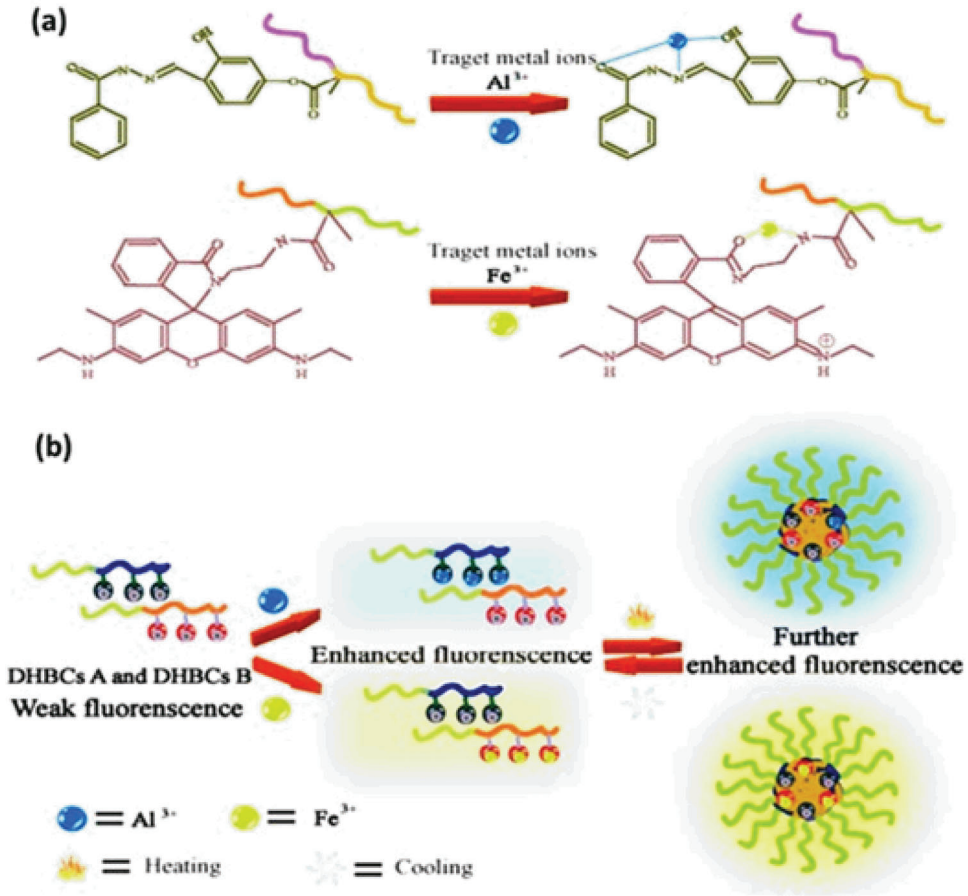

Figure 42. a) Metal ion responsive mechanism, b) Sensor mechanism of the polymer. Reproduced with permission.[209] Copyright 2018, Royal Society of Chemistry.

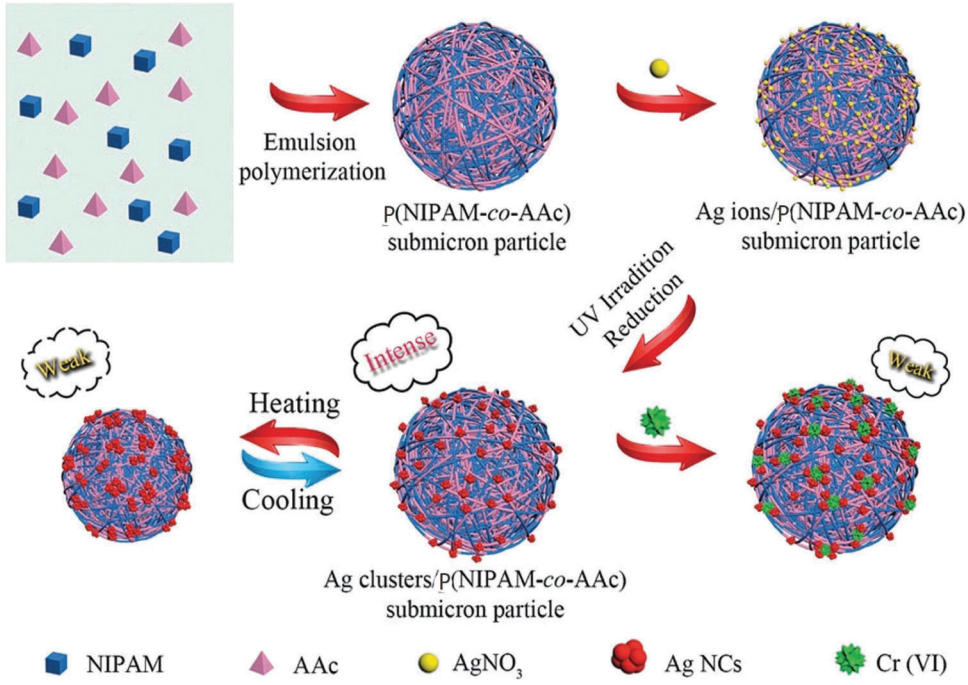

Figure 43. Synthesis of nanocomposite which exhibited detection of Cr(VI). Reproduced with permission.[211] Copyright 2018, Royal Society of Chemistry.

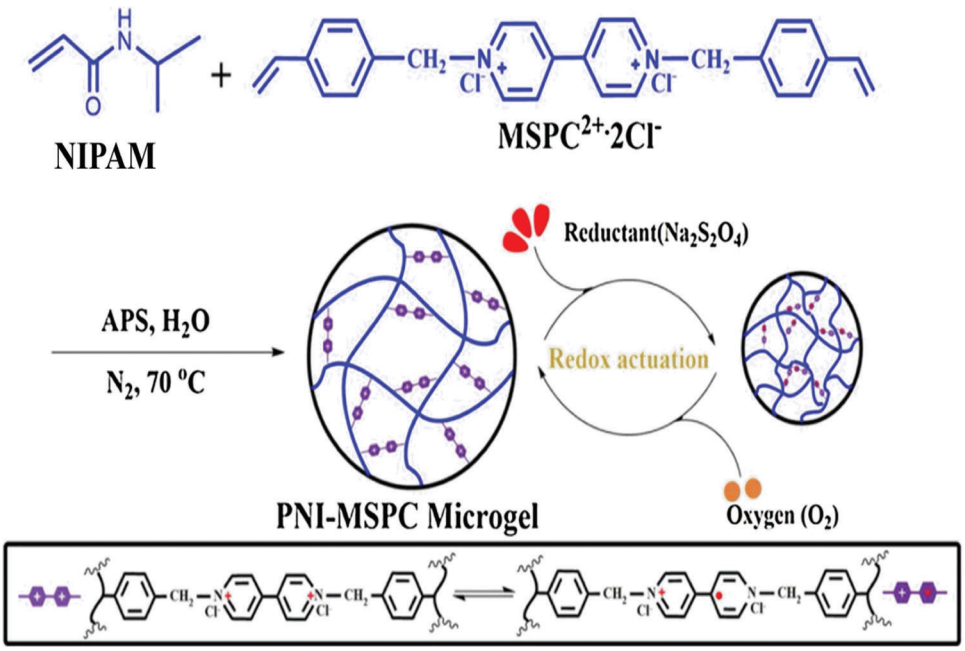

Figure 44. Synthesis of microgel with fluorescence properties. Reproduced with permission.[213] Copyright 2019, Elsevier Ltd.

water.[213] Their system consisted of a fluorescent microgel PNI-MSPC, which was prepared by surfactant-free emulsion polymerization (SFEP) of NIPAM and a dichlorinated crosslinker, viz. 1,1′-di[4-(vinyl) benzyl]−4,4′-pyridinium salt ($MSPC^{2+}.2Cl^{-}$), which served as fluorophore and ion sensing receptor (**Figure 44**). In the presence of MnO_4^- in aqueous solvent, significant fluorescence quenching for PNI-MSPC microgel was observed. At high temperatures, the microgel shrunk, as observed from decrease in the hydrodynamic diameter, which went paired with a blue shift of the fluorescent spectrum. As a result, the detection sensitivity was greater at low temperatures (below LCST).

A final metal ion of interest is the calcium (II) ion (Ca^{2+}), although not toxic, this metal ion plays a significant role in biological processes. The variation of Ca^{2+} concentration plays a vital role in signal transduction, which is related to Alzheimer's disease. This fact made detection of Ca^{2+} so important. The fluorescence method also was used to detect Ca^{2+}. As reported previously[162] the modified homopolymer of PNIPAM detected Ca^{2+}. Due to Ca^{2+} entry through transduction channels, fluorescence intensity was increased.

Again, using SPR process small multivalent cations (e.g., Ca^{2+}, Fe^{2+}, and Fe^{3+}) were distinguishably measurable over monovalent cations (e.g., Na^+ and K^+) with nanogel P(NIPAM-*co*-AAc) nanogels.[214] The nanogel was prepared with radical polymerization and the Ca^{2+}, Fe^{2+}, and Fe^{3+} ions formed MPB-like structures by interacting with carboxylates in the nanogel networks (**Figure 45**), while Na^+ and K^+ cannot form such MPB-like structures due to the charge valence of the metal ions. A high SPR value was observed for bi or tri-valence cations than monovalence cations.

PNIPAM based chemosensors towards metal ions are generally very sensitive and specific. Nevertheless, most covered examples are single-use sensors due to the irreversible nature of the sensing mechanism. While some examples cover regeneration steps to enable reuse, others employ the thermoresponsive behavior of PNIPAM to enable reuse, facilitating repeated and accurate readout by simply applying mild heat. Besides reuse, these chemosensors display often sufficiently high selectivity towards single analyte in the presence of background analytes, which ensures a broad applicability. In addition, the sensor offers a quick readout and a LOD in the nM range, which makes it appropriate for disease diagnosis, and environmental protection. Analyte-sensitive sensors should typically provide for accurate and dependable readout and have a wide tolerance to various media. A possible application of the sensor is when it detects Cu(II) ions in serum, a complicated medium.

2.3.2. Salt Sensing

As PNIPAM contains both hydrophilic (amide) and hydrophobic (isopropyl) groups, it has been used as a model system to understand the complex ionic interactions between salts[215] and proteins in aqueous solutions. These interactions have been extensively studied and are known as the Hofmeister series, first determined by Franz Hofmeister who studied the salt effect on hen egg protein solubility in water,[216] where he qualitatively ranked ions by their ability to precipitate/solubilize proteins or macromolecules in aqueous solution.[217]

Ions on the left side of chloride and sodium in **Figure 46** are known as kosmotropes ("order-makers") and those on the right side are known as chaotropes ("disorder-makers"). The ions on the left side of the series with high charge density form hydrate complexes by breaking hydrogen bonding to the amide oxygen and nitrogen of PNIPAM, which decreases the number of water molecules that are available to form hydrogen bonds with the polymer, thus decreasing its hydration. Again, due to the addition of ions to the solution the surface tension

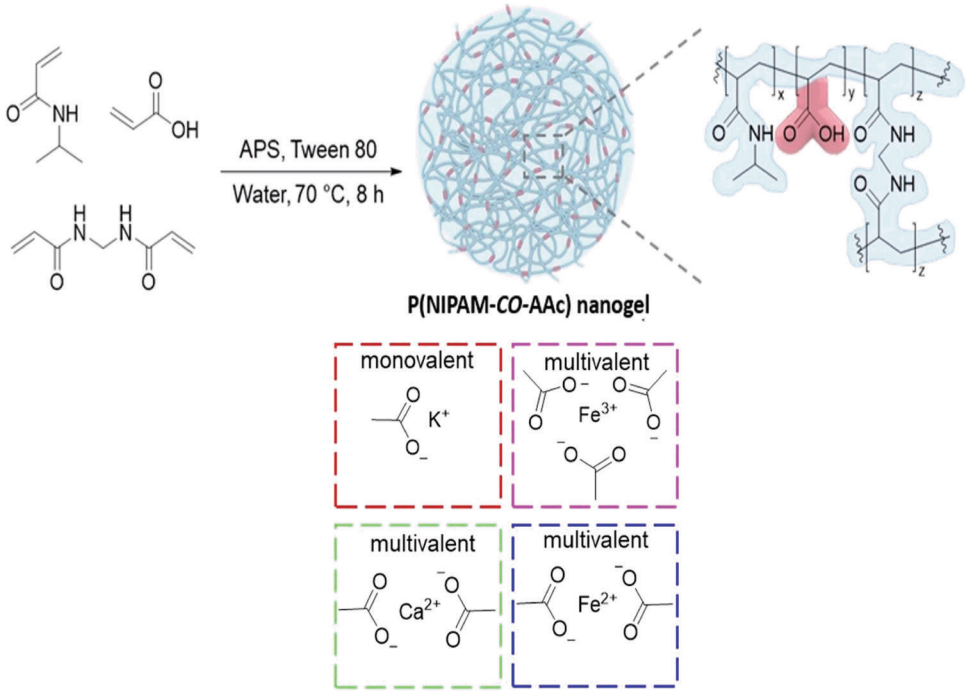

Figure 45. Synthesis of nanogel with the formation of complex. Reproduced with permission.[214] Copyright 2020, American Chemical Society.

of the water/polymer hydrophobic interfaces increases. As a result, the free energy increases to form cavities to accommodate the hydrophobic isopropyl groups and the polymer backbone. This effect is known as the salting-out effect, which decreases polymer solubility via the formation of aggregates followed by phase separation. The ions on the right side of the series form weakly hydrated ions of low charge density which increase the solubility of the polymer and is known as salting in effect.

For salt sensing, AuNPs decorated with PNIPAM have been demonstrated to be excellent tools, due to their colorimetric output. Yusa et al. were the first who reported the effect of salt on PNIPAM-coated AuNPs.[218] In this configuration, the concentration and identity of the salt have a significant impact on the

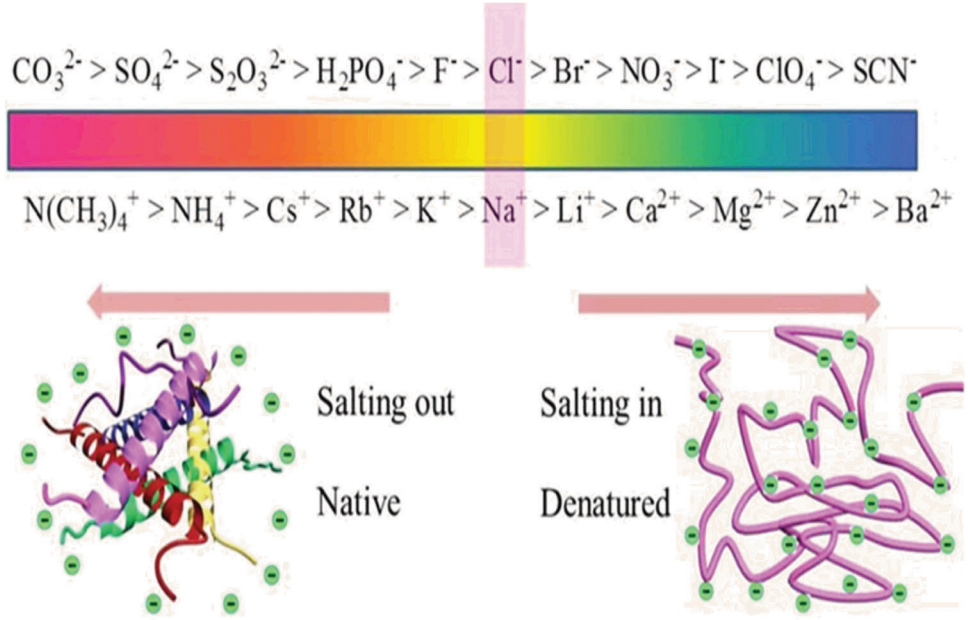

Figure 46. Hofmeister series of anions and cations and their salting in and salting out influence on protein or macromolecules in aqueous medium.[217]

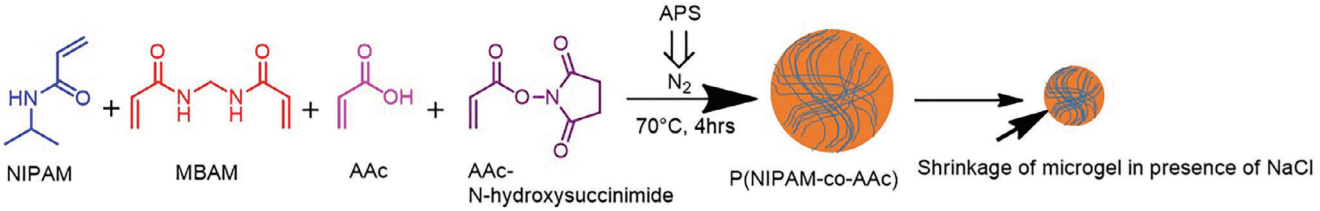

Figure 47. Synthesis of microgel which got shrink in presence of NaCl.[222]

LCST behavior of PNIPAM and consequently on the colorimetric output of the AuNPs. This observation has been well-described by Maji et al.[145] (the structure was defined at the temperature sensing portion). They showed that different salt concentrations facilitated a shift in absorbance at elevated temperatures due to AuNP aggregation, which in turn induced electronic coupling of the SPR. In their study, they also demonstrated that the temperature sensitivity increased in the presence of NaSCN, compared to NaCl, due to charge screening and Hofmeister effects. In a separate publication, the authors demonstrated that the sensitivity of the system can be enhanced by increasing polymer chain length.[219] In addition to AuNPs, other PNIPAM-decorated colloidal particles have been used for salt sensing. Humphreys et al. prepared colloidal silica particles with PNIPAM brushes via a "grafting to" method from surface-initiated activators regenerated by electron transfer-atom transfer radical polymerization (SI-ARGET ATRP).[220] These hybrid particles are electrostatically stabilized in pure water at high temperatures. Whereas, the brush layer is collapsed due to the electrostatic repulsive overlap between the diffuse double layers. This repulsive overlap occurs at a longer range than the attractive hydrophobic polymer brush layer interactions. With the addition of salt, the Debye length was reduced and consequently, the influential range of the particle surface potential decreased. This lower surface potential value is unable to extend beyond the thickness of the collapsed polymer brush (above the LCST) and the attractive polymer-polymer interactions between particles effect in particle aggregation. The authors confirmed the effect of the Hofmeister series in the presence of 1×10^{-3}, 10×10^{-3}, and 500×10^{-3} M solutions of KCl, KNO_3, or KSCN.

Carvalho et al. fabricated an etalon device where they check the validity of the Hofmeister series.[221] The device consisted of a P(NIPAM-AAc) prepared by free radical precipitation polymerization, which was placed between two Au layers. The microgel P(NIPAM-AAc) changed in thickness in response to salt, which induced the variation of distance between two Au layers. The variation of interlayer distance resulted in a reflectivity change. Here taking NaCl, CH_3COONa, KCl, $MgCl_2$, $CaCl_2$, $MgSO_4$, $NaSO_4$, $(NH_4)_2SO_4$ salts they verify the series. A blue shift of the reflection spectra was obtained in the presence of all salts due to cation screening of the negatively charged carboxylic groups, causing the anionic microgels to shrink.

Mugo and Dhanjai exploited the influence of salt on the phase transition of PNIPAM to measure NaCl in sweat.[222] Usually, chloride levels in sweat are typically $\approx 17–55 \times 10^{-3}$ M, with $\geq 60 \times 10^{-3}$ M being a possible indicator for cystic fibrosis.[223] The sensor consisted of porous films from nanoporous carbon nanotube-cellulose nanocrystals (CNC/CNT) which were entrained with PNIPAM based microgels.[222] The sensor was prepared by first preparing P(NIPAM-*co*-AAc-*co*-NSA). Next, a suspension of the microgel was deposited onto a prepared CNC/CNT nanoporous film. Subsequently, aniline (ANI) and phenylboronic acid (PBA) were added, followed by the addition of a lactate solution to induce polymerization, yielding the lactate imprinted PANI/PBA-PNIPAM @CNC/CNT sensor (**Figure 47**). With the increase of salt concentration, the microgel shrunk due to PNIPAM-induced water dislodgement from the microgel network, which resulted in increased sensor capacitance. The sensor exhibited a linear detection range of $(1–25) \times 10^{-3}$ M and a LOD of 0.10×10^{-3} M of NaCl in sweat. It also detected the biomarker lactate in sweat.

The Hofmeister series commonly serves as the basis for salt recognition using responsive polymers. Scientists used the influence of salt content on the phase transition of PNIPAM to develop a salt sensor. Still, one drawback of the Hofmeister series salt sensor is its limited selectivity towards a specific salt. It has been noted that it tends to follow the Hofmeister series rather than being selective, which complicates the analysis of complex mixtures or enable salt detection in complex media. Similar to the metal-ion sensing, moieties that have selective interactions with the analytes of interest could possibly address this shortcoming.

2.4. Organic Molecule Sensing

Besides metal ions and salt sensing, the detection of specific classes of organic molecules or functional groups plays a huge role in modern society ranging from the detection of hazardous substances, such as toxins,[224] explosives,[225] and contaminants in food,[226] pharmaceuticals,[227] and various other consumer and industrial products, to the detection of molecules present in the body such as metabolites, performance-enhancing drugs, alcohol and various illegal substances. Analytical methods such as GC-MS and LC-MS are available for the detection of organic compounds, just like they are for metal ions. Nevertheless, this associated equipment requires suitable infrastructure for its operation. In addition, samples from complex media, e.g., blood can require substantial sample preparation prior to the analysis, further complicating its implementation and application for non-experts. Therefore, the development of lightweight, portable sensors with straightforward interpretation is of particular interest for these applications. Moreover, for this purpose, various PNIPAM based systems have been developed, which will be outlined below according to the analyte of interest.

Alcohols are quite important in various fields, including chemical, biological, pharmaceutical, medical, material, and food industries. They take part in a variety of metabolic processes directly or indirectly. They are metabolized predominantly by the liver.[228] Their concentration detects the quality of the

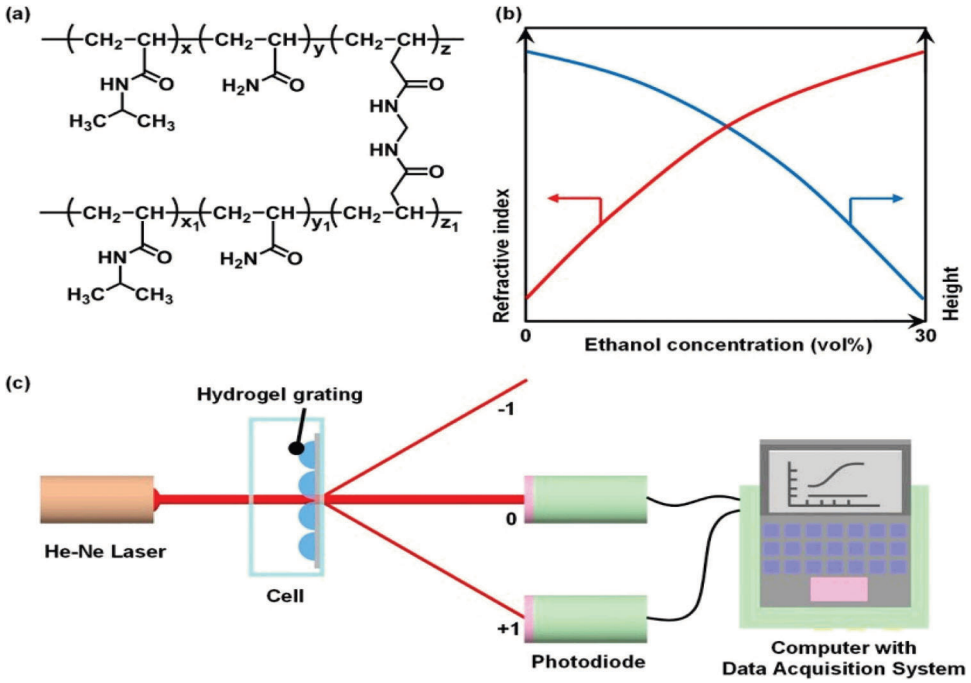

Figure 48. a) Structure of hydrogel grating, b) Change of the refractive index and height with ethanol concentration, c) Design of the ethanol detecting system.[231] Copyright 2019, American Chemical Society.

materials, e.g., during the biological fermentation process for ethanol production, the efficiency and yield are controlled by the tolerance capability of the yeast to the ethanol concentration.[229] Generally, PNIPAM-based phase separation occurs in an aqueous solvent, but in aqueous ethanol solutions, ethanol competes with water to form stable PNIPAM clathrate hydrate structures and, generally, PNIPAM shrinks when the ethanol concentration exceeds the critical responsive concentration (C_c) due to the broken hydrogen bonds, also known as co-nonsolvency. Zou et al. fabricated an ethanol detecting device based on the combination of microfluidics and membranes.[230] First, a PNIPAM nanogel was synthesized by precipitation polymerization and the ethanol responsive membrane was prepared from it via a vapor-induced phase separation (VIPS) process. PDMS modules were prepared by soft-lithography techniques using SU-8 2035 and a microfluidic membrane device was made with an ethanol responsive membrane via a "stamp-like" method by using a PDMS prepolymer as the adhesive. Below the LCST, the PNIPAM chain is swollen in water due to the hydrogen bonds formed between water molecules and amide groups. Whereas, in the presence of ethanol, both water and ethanol compete to solvate PNIPAM, which results in the formation of stable water clathrate hydrate structures. Consequently, the PNIPAM chains collapse when the concentration of ethanol exceeds the C_c. When the ethanol concentration (C_E) is lower than C_c, the permeation flux across the ethanol-responsive membrane decreases due to the high resistance for permeation of the swollen nanogel, while at high ethanol concentration the collapse of the chains and dehydration of the nanogel allows for a higher permeation flux. The authors could quantify the ethanol concentration between 3 vol% to 13 vol% by measuring the permeation flux in the device.

The same group also explored a system with a grated hydrogel membrane for the detection of ethanol.[231] The hydrogel grating was produced by sandwiching a solution of NIPAM, AAm, and a MBAM cross-linker between a glass substrate and PDMS stamp and subsequent exposure to UV irradiation. In the next step, the PDMS film was removed, thus obtaining the grated hydrogel (**Figure 48**). In their earlier work mentioned above, the ethanol causes the polymer chains to collapse; however, this time, the authors measure the change in diffraction efficiency (DE) to identify the changes in the height and refractive index of the hydrogel gratings. This system, therefore, enables facile ethanol detection via a straightforward optical approach, which enabled the detection of ethanol concentrations of 0–30 vol%.

Planar MIM optical cavities also have the ability to sense alcohols, as described in the temperature-sensing section.[156] In the described example, the thickness of the PNIPAM microgel drops in the presence of alcohol up to a 20% concentration, causing a decrease in transition wavelength.

Hydroquinone (HQ), a phenolic compound, is used in the preparation of rubber antioxidants, stabilizers, and antioxidants. However, it is extremely harmful to both the environment and mankind. HQ can be sensed using unique optical, electronic, and catalytic properties of carbon nanotubes, and graphene. Zhou and co-workers designed an electrode that consisted of a composite film for electrochemical "on/off" detection of dihydroxybenzenes, such as HQ.[232] A [poly(*N*-isopropylacrylamide)$_{101}$-*b*-poly(2-acrylamidoethyl benzoate)$_{37}$] PNIPAM$_{101}$-*b*-PAAEB$_{37}$ copolymer was prepared and GO solution was added to yield a suspension solution of PNIPAM$_{101}$-*b*-PAAEB$_{37}$/GO. Similarly, a PNIPAM$_{101}$-b-PAAEB$_{37}$/SMWCNs solution was synthesized by adding short multi-walled carbon nanotubes (SMWCNs) to PNIPAM$_{101}$-*b*-PAAEB$_{37}$. Next,

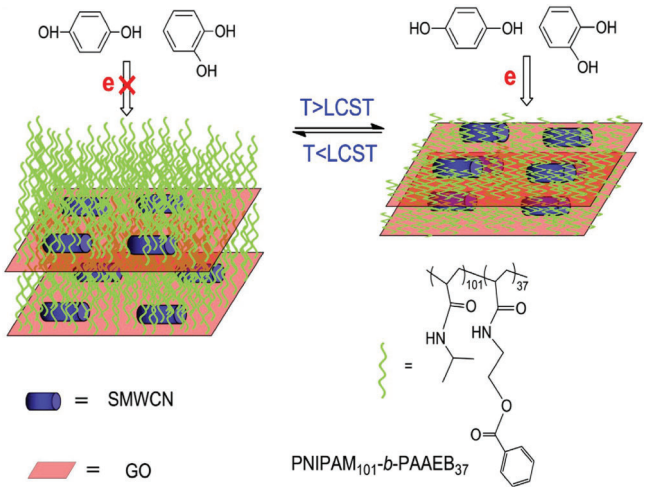

Figure 49. The sensing mechanism of the polymer where the electronic transition occurred when temperature less than LCST. Reproduced with permission.[232] Copyright 2016, Elsevier Ltd.

a $PNIPAM_{101}$-*b*-$PAAEB_{37}$/GO/SMWCNs (PGS) solution was formed by mixing the PG and PS solutions and the resulting solution was placed on glass carbon electrode (GCE) by dropping. At a temperature lower than the LCST, the PNIPAM chain is in the swollen state, which increases the distance between GO sheets and interfacial electron transfer resistance is high. Whereas, above the LCST, the polymer chain collapses and the distance between GO sheets decreases, resulting in well-defined redox peaks (**Figure 49**). This approach enabled electrochemical "on/off" detection of dihydroxybenzenes as low as 2.7×10^{-5} mol L^{-1}.

Another "On-Off" electrochemical detection system for HQ was developed by Zhao et al. based one triblock copolymer PS-PNIPAM-PS prepared via RAFT polymerization.[233] The copolymer solution was dispersed uniformly on the GCE. The copolymer forms a core–shell structure with PS in core and PNIPAM in shell. At low temperature, HQ can exchange electrons with electrode surface via the gap between polymer micelles. However, above LCST, PNIPAM-loop collapses and micelles agglomerate, which prevents HQ from undergoing redox reactions on the electrode surface causing no response (**Figure 50**). HQ has been detected with a good detection range for hydroquinone (6×10^{-7} to 2.35×10^{-3} M) and a low LOD (490×10^{-9} M) and observed via differential pulse voltammetry (DPV).

Nitroaromatic explosives draw wide attraction due to their powerful explosivity and serious environmental hazards. So rapid, sensitive, and selective detection of it is gaining increasing concern. Ahmad et al. reported an electrochemical sensor for detecting 4-nitrophenol (4-NP).[234] Here they prepared a single-chain stimuli-responsive templated polymer with a target analyte. A random template copolymer consisting of NIPAM, methacrylic acid (MAA), and 4-vinylpyridine (VP) and 4-NP was prepared via the RAFT process using DDMAT (2-dodecylthiocarbonothioylthio-2-methylpropionic acid) as RAFT agent for functionalization onto the electrode surface. In parallel, a homopolymer of PNIPAM was also prepared by the RAFT process. After template (4-NP) removal, the copolymer was grafted on an Au electrode with the help of tris(2-carboxyethyl)phosphine (TCEP) which reduces the trithiocarbonyl group to sulfur (**Figure 51**). The resulting polymer was incorporated with 4-NP and grafted on the electrode and underwent distinct conformational changes upon target binding as above LCST the volume of hydrogel increased with the increase of template concentration. This conformational change induces a distinguishable change in the electrochemical signals via altering the interface charge transfer kinetics. This signal corresponds to the presence of 4-NP.

Babu et al. designed a fluorescence-based nitroaromatics detection via π-electron-rich anthrapyrazolone-derived fluorophore moiety with PNIPAM.[235] By using free radical polymerization NIPAM unit was incorporated with the dye with enhanced solubility. In the presence of nitrophenol compounds (dinitrophenol, trinitrophenol and para-nitrophenol), quenching of the emission intensity was observed due to PET occurring from the pyrazoloanthrone units on the crosslinked polymer to the electron-deficient nitrophenol molecules. At elevated temperatures above the LCST phase transition, PNIPAM gets dehydrated and subsequently, the fluorophore unit also becomes aggregated. Hence PL intensity get quenches. The LOD was exhibited as 0.12×10^{-9} M (**Figure 52**).

Dopamine (DA) is an organic chemical in the catecholamine family that plays a critical role in the function of the central nervous system (CNS), endocrine system, and cardiovascular system. Its concentration indicates various types of diseases, such as Parkinson's disease, schizophrenia, and dementia.[236–238] Thus, its detection is particularly useful in biomedicine. Two different sensor platforms, namely

SPR and microcantilevers (MCL) were used to detect DA as demonstrated by Jiang et al.[239] Their system made use of a statistical copolymer poly(*N*-isopropylacrylamide-*st*-5-methacrylamido-1,2-benzoxaborole) (P(NIPAM-*st*-MAAmBO)), which was prepared via RAFT polymerization. The polymer was subsequently immobilized on an Au substrate for SPR detection via the dithioester group at the polymer terminal introduced from the RAFT agent. In the next step, the immobilized copolymer was coupled to a maltosylated polyacrylamide, poly(2-lactobionamidoethyl methacrylamide) (PLAEMA) through dynamic covalent boronate ester bonds. When this system was exposed to DA, the PLAEMA is released, as the formation of boronate esters with the cis diol group of DA is preferred (**Figure 53**). This displacement of PLAEMA induced a change in the local refractive index and the reflection angle change on the SPR sensor surface. Moreover, in the presence of DA, swelling of the polymer occurs which increases the local refractive index. The authors demonstrated that the same approach could also be applied to an Au microcantilever system, whereby DA-induced release of PLAEMA resulted in surface stress variation of the cantilever. The SPR biosensor can detect DA in the concentration range of 1×10^{-9} to 1×10^{-4} mol L^{-1} while the MCL sensor exhibited a LOD of 5×10^{-11} mol L^{-1}.

Wang et al. prepared a microgel-based dopamine sensor using an optical device named etalon.[240] Etalons, photonic materials were synthesized by depositing a single layer of microgels on an Au-coated glass substrate, and then another layer of Au was deposited on the microgels to form a sandwiching structure and the reflection wavelength was dependent on the Au-Au

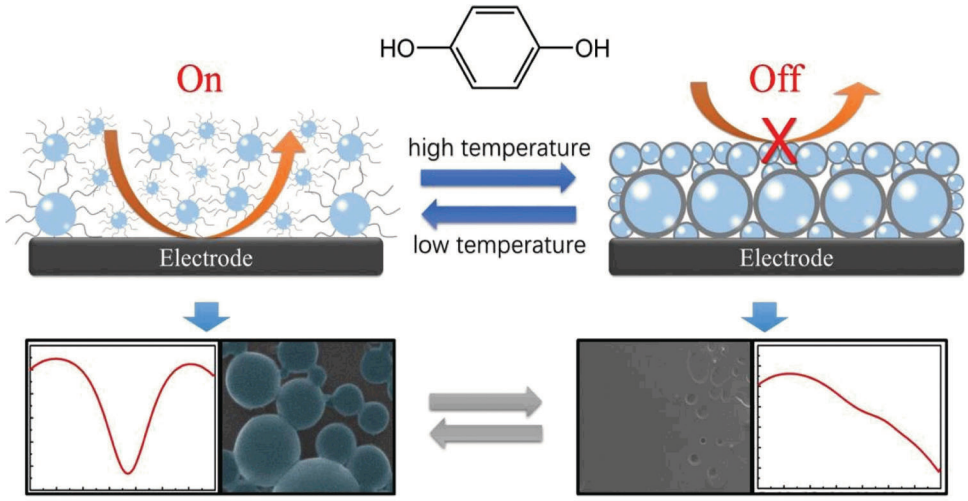

Figure 50. Electrochemical "On-Off" detection of the system. Reproduced with permission.[233] Copyright 2020, Wiley-VCH.

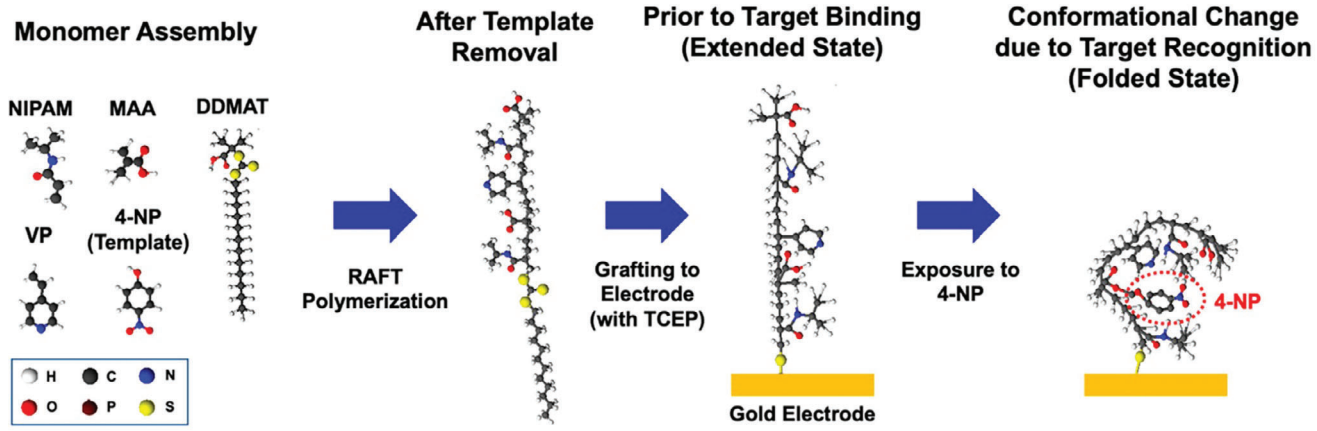

Figure 51. Synthesis of polymer with detection mechanism. Reproduced with permission.[234] Copyright 2021, American Chemical Society.

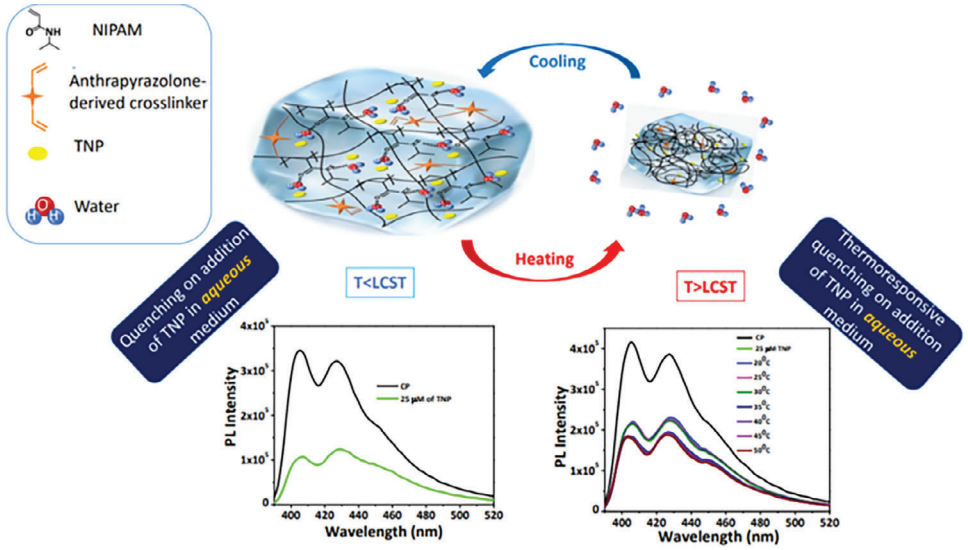

Figure 52. Sensing property dependence on thermoresponsive behavior of PNIPAM. Reproduced with permission.[235] Copyright 2023, Elsevier Ltd.

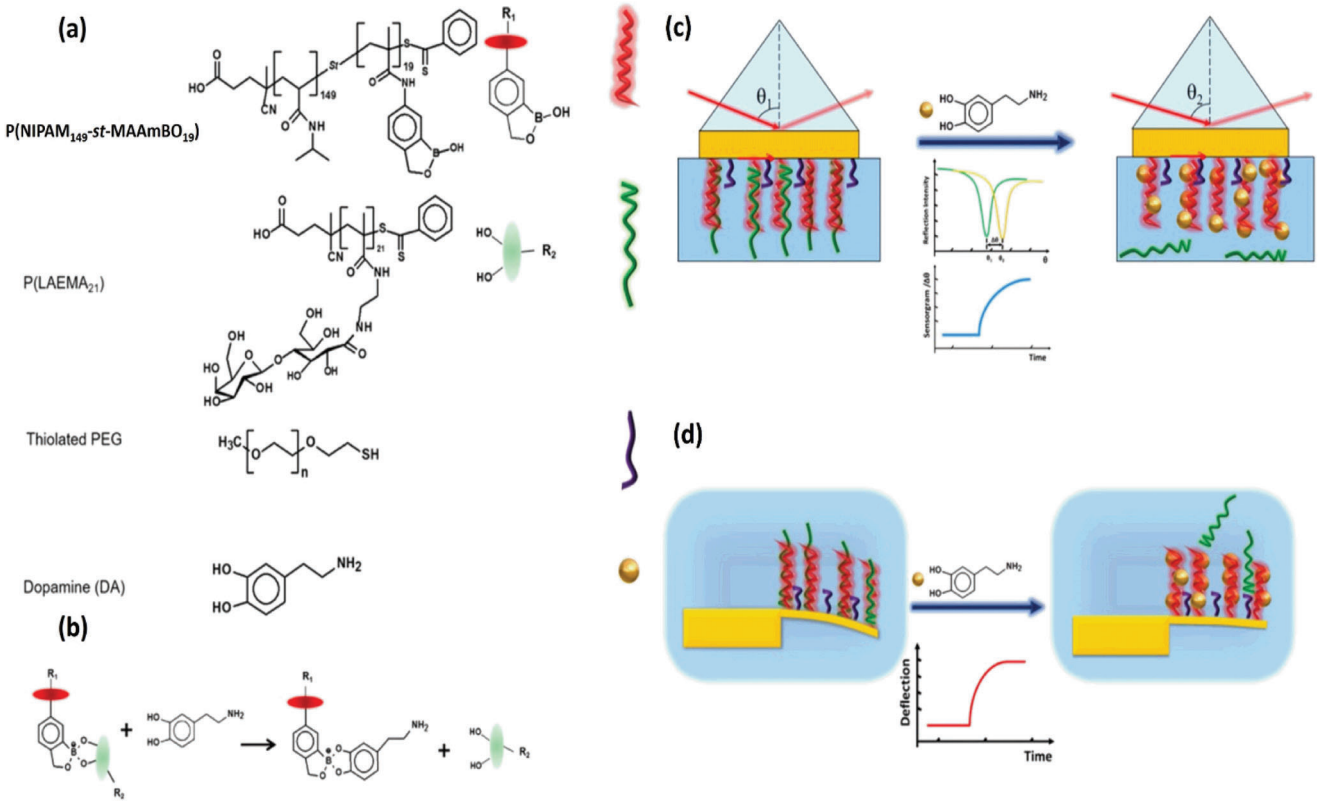

Figure 53. a) Chemical structures of the P(NIPAM-st-MAAmBO), P(LAEMA21) and DA, b) Pictorial representation of adsorption-displacement reaction on the sensor surface, c) Schematic representation of light reflection angle change due to the SPR change, d) Change of microcantilever deflection due to DA displacement. Reproduced with permission.[239] Copyright 2017, American Chemical Society.

distance. The microgel was fabricated by the precipitation polymerization of NIPAM, AAc, MBAM (crosslinker). The etalon was prepared by sandwiching the microgel between two Au layers, followed by the fixation of tyrosinase on etalon surfaces. In the presence of dopamine, tyrosinase oxidizes the dopamine to form a film (**Figure 54**). Then $ZnCl_2$ was added to the etalon, whereby the formed dopamine films inhibited the $ZnCl_2$ diffusion into the etalon which previously changed the volume of microgel, resulting in a DA concentration-dependent response concerning the optical properties of the device. The sensor showed a LOD for dopamine of 11.5 ppm in DI water, 18.7 ppm in urine, and 21.4 ppm in serum.

Volatile organic compounds (VOCs) readily go into the vapor phase due to their low vapor pressure. Biogenic VOCs are very important in the survival of plants and animals, as they can serve in inter/-intra-species communication (i.e., attract pollinators, seed dispersers, finding suitable mates, marking territory) as well as a defense mechanism. Some VOCs are soluble in the aqueous medium, and therefore easily detected. The Serpe group designed a novel optical device named etalon in which a PNIPAM microgel-based monolayer was inserted between two Au layers.[241] Here, 1.27×10^{-3} M THF could be detected within 4 min. The microgel was made with NIPAM monomer and MBAM crosslinker, and an etalon device was created with it. The etalon device was placed in water and hexane, cyclohexane, petroleum ether, chloroform, and tetrahydrofuran (THF) vapors were inserted through bubbling. Upon exposure to the aqueous VOCs, the size of the microgels changed, which depended on PNIPAM's solubility in the specific aqueous VOC solution. The variation in microgel size changed the distance between the two Au layers, and consequently the wavelength (λ) of other reflected light. Compared to others THF has better solubility in water and both are good solvents for PNIPAM. Hence PNIPAM became swollen and the distance between two Au changed.

In this fashion, specific absorbances were generated for different VOCs, which facilitated their straightforward identification. Within 4 minutes, 1.27×10^{-3} M THF may be detected (**Figure 55**).

Organic dyes are extensively used in textile, leather, cosmetics, garments, printing, and paper industries. However, the dyes are harmful to the human body and cause serious water pollution. Therefore, the detection of these dyes draws growing attention. Plasmonic-active metal nanostructures can be used as optically triggerable catalytic systems, extremely sensitive sensor platforms, and photonic modulators with unprecedented speed. Their surface modification allows for the design and development of a new generation of sensor devices, related to the area of so-called smart plasmonic systems. Guselnikova et al. reported a PNIPAM grafted Au grating for surface-enhanced Raman scattering (SERS) detection of azo-dyes.[242] SERS is a method to determine the composition, structure, conformation, and interaction of molecules, exhibiting great potential in various fields including analytical chemistry, food science, and biology due to its prominent sensitivity, anti-interference performance, fast and

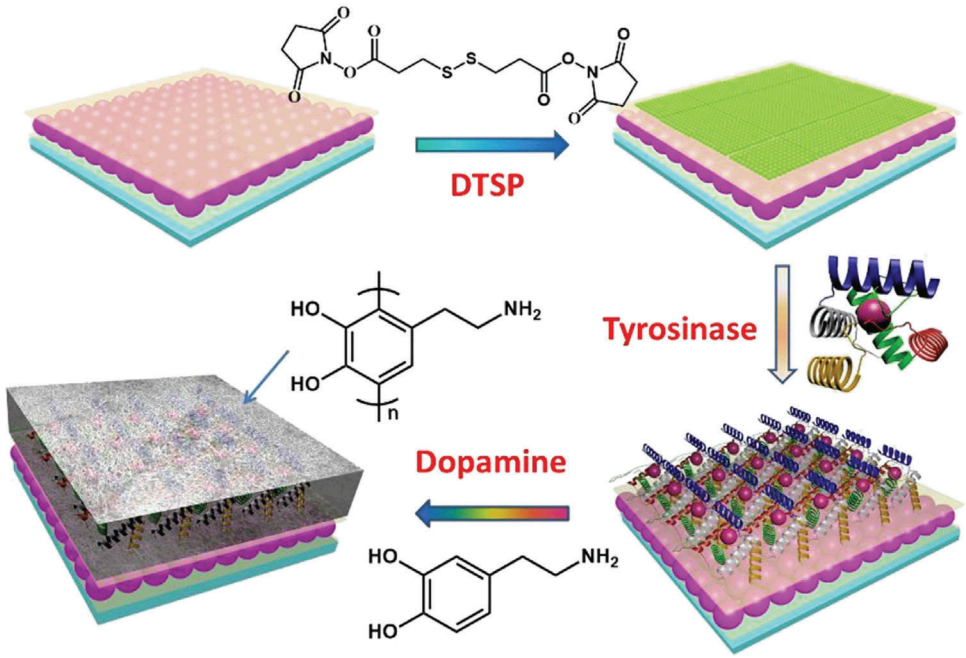

Figure 54. Fabrication of etalon device.[240]

facile detection through plasmon-enhanced excitation, and scattering.

4-Carboxybenzenediazonium tosylate (ADT-COOH) was used to modify the gold grating. Then the grafting-to approach was performed with PNIPAM-NH_2 via NHS-carbodiimide coupling to prepare a 7 nM thick layer (**Figure 56**). Various azo-dyes, such as crystal violet (CV), disperse red 1 (DR1), and metanil yellow (ME) could be detected. The sensor utilized PNIPAM's thermal response to trap and enrich the dye concentration near the surface of the detector, thus increasing the Raman response by several orders of magnitude. In this fashion, the prepared plasmonic sensor could detect azo dyes down to femtomolar concentrations. Finally, the authors demonstrated the sensor could be regenerated by exploiting the reversibility of the thermal response of PNIPAM.

It has been noted that PNIPAM introduces a fascinating feature to the detection of organic molecules. Using a PNIPAM-based design, a range of organic compounds can be sensed, including alcohol (0–30 vol%) by virtue of its influence on the PNIPAM phase transfer process. While, nitroaromatic compounds can be detected selectively, as demonstrated by the analysis of a sample of river water. DA can be detected from complex systems like serum and urine. Within a 4-minute response time, VOCs can be detected using PNIPAM microgel-based system. These examples demonstrate the broad applicability in terms of dealing with complex media, allowing the detection of various analyte classes and the medium response times necessary for the detection process.

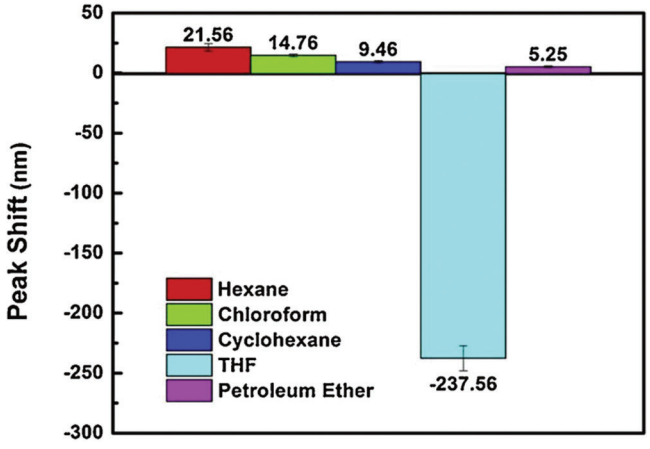

Figure 55. Color exhibited by etalon device in presence of different VOCs. Reproduced with permission.[241] Copyright 2019, Elsevier Ltd.

2.5. Pressure Sensors

Pressure is characterized as force per unit area. Measurement of pressure has a wide range of applications such as in aircraft, satellites, weather, and barometric applications. In medicine, pressure measurements give an idea about pulse rate, blood pressure, and various other physiological measures. Therefore, pressure sensing is gaining increasing interest. PNIPAM hydrogels draw increasing attention to form pressure sensors due to their excellent mechanical properties. Nanocomposite hydrogels are extensively used due to their remarkable physical properties, such as a high degree of mechanical toughness, elastic response over large deformations, high swelling ratios, rapid swelling-deswelling responses, and optical transparency. Cellini et al. synthesized a laponite crosslinked P(NIPAM-*co*-Py-PEGMA) nanocomposite hydrogel, whereby PEGMA units were fluorescently labeled with

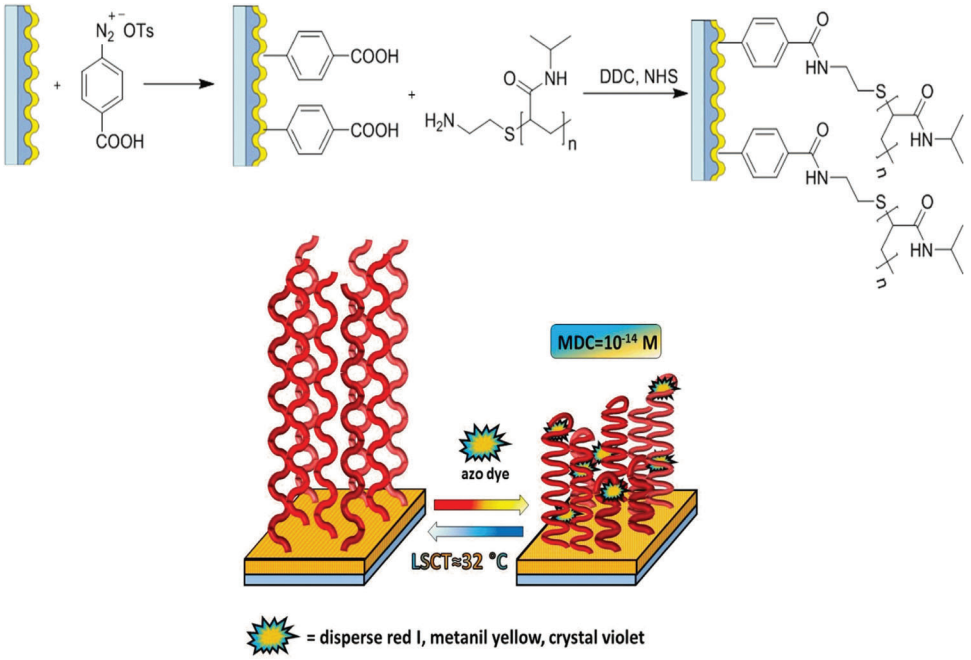

Figure 56. Synthesis of plasmonic nanostructure with sensing mechanism. Reproduced with permission.[242] Copyright 2017, Wiley-VCH.

pyrene butyric acid.[243] When the nanocomposite hydrogel is exposed to pressure, the pyrene groups undergo progressive reorganization during the stretching of the network which leads to a detectable change in fluorescence emission (**Figure 57**). The model can detect pressures on the order of 10^2 Pa.

A hydrodynamic pressure sensor inspired by the canal lateral line system of fish, was designed by Jiang et al.[244] The sensor consisted of a microfluidic PDMS canal and four microcantilevers based on biomimetic neuromasts (BN) containing poly(vinylidene fluoride-trifluoro ethylene) (P(VDF-TrFE))/polyimide (PI) cantilever, a microheater, and a PNIPAM hydrogel cupula (dome-shaped cap) (**Figure 58**). The hydrogel was formed in the presence of MBAM crosslinker. When the heating is turned off (below LCST) PNIPAM forms a clathrate

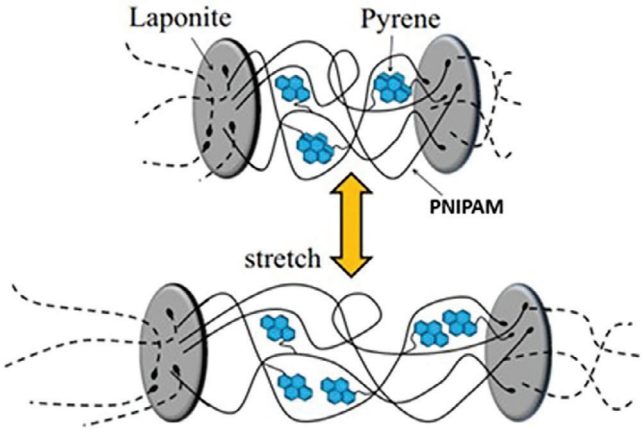

Figure 57. Mechanical response of hydrogel. Reproduced with permission.[243] Copyright 2016, Elsevier Ltd.

which was hydrophobically hydrated in water. Above LCST (heater on) the structure of the clathrate was deformed due to the temperature and volume of the hydrogel cupula decreased. Upon application of pressure, the height of the hydrogel cupula was reduced which induced a cantilever deflection, which corresponded to the applied pressure. Using an electrochemical method, the model exhibited a sensitivity of approximately 0.31 Mv/Pa/m at heater on state.

Another pressure sensor was fabricated using DN hydrogels. It showed fracture toughness, fracture tensile stress, and fracture tensile strain which improved the mechanical properties of hydrogels. As described earlier,[151] the volume of the fabricated DN hydrogel decreased upon exposure to pressure, which caused a decrease in resistance due to the improvement of electronic transmission between continuous layer structures of GO and the tight DN structure of hydrogels (**Figure 59**). The hydrogel could bear pressure up to 0.754 MPa. PNIPAM hydrogels are utilized as pressure sensors because of their exceptional mechanical properties.

Wang et al. synthesized a dually synergetic network hydrogel that has properties like integrated mechanical stretchability, thermal responsiveness, and electrical conductivity. Its structure is described in the "Temperature Sensor" section.[152] In the presence of pressure shape of the hydrogel changed which induced electric signals, like current or resistance when the hydrogel was connected to a circuit. The brightness of the LED was diminished with tensile deformation and increased with the releasing process. This hydrogel was used to prepare a wearable sensor to detect the bending motion of fingers and wrist, swallowing motion and pulse rate. A wearable sensor for detecting strain was designed by Feng et al.[150] They designed triple-network hydrogel with excellent conductivity (≈170 Ω mm^{-1}), mechanical tolerance (1.1 MPa), and rapid recoverability (within

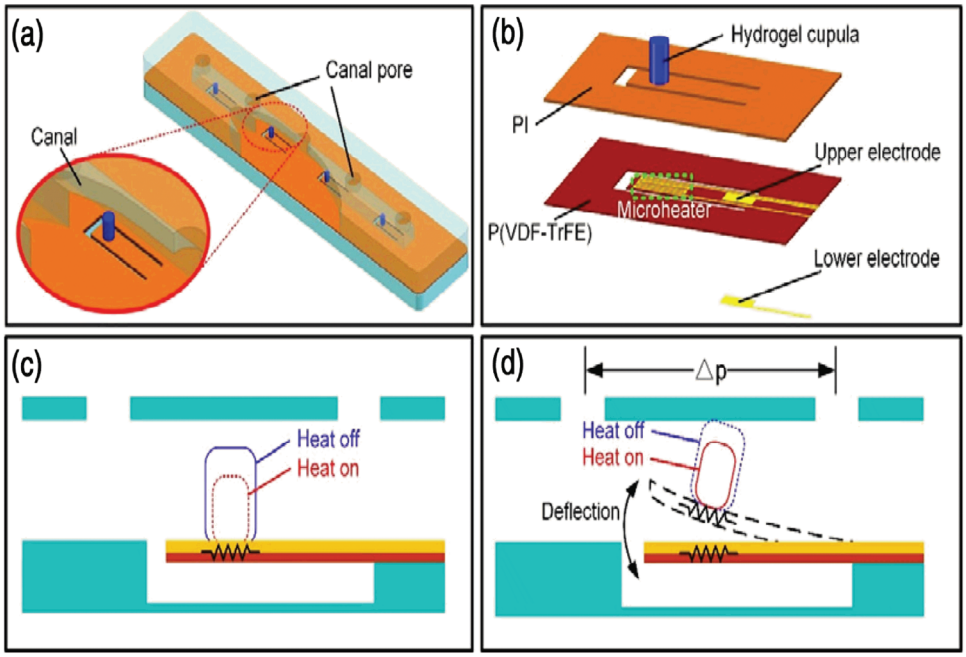

Figure 58. a) 3D image of the pressure sensor, b) Image of the sensing cantilever, c,d) Mechanism of tunable sensitivity depends on the volume change of hydrogel cupula. Reproduced with permission.[244] Copyright 2020, Wiley-VCH.

0.5 s). Here also deformation occurs in the application of pressure which gives an electrical signal that corresponds to the applied pressure. The incorporation of PNIPAM in the hydrogel introduced recoverability. Another hydrogel PNIPAM/CMCS/-MWCNT/PANI was utilized as a pressure sensor.[153] With the increase of strain, the relative resistance of hydrogel increased.

In the pressure sensor field, PNIPAM has received comparatively little attention. In some cases, electric conduction was incorporated to enable pressure sensing. Investigations are underway in this field, and we may see some pressure sensors in the future. The PNIPAM/PANI hydrogel-based strain sensor has been shown to have a response time of as low as 0.4 s, in addition to the hydrogel's exceptional mechanical properties. This sensor

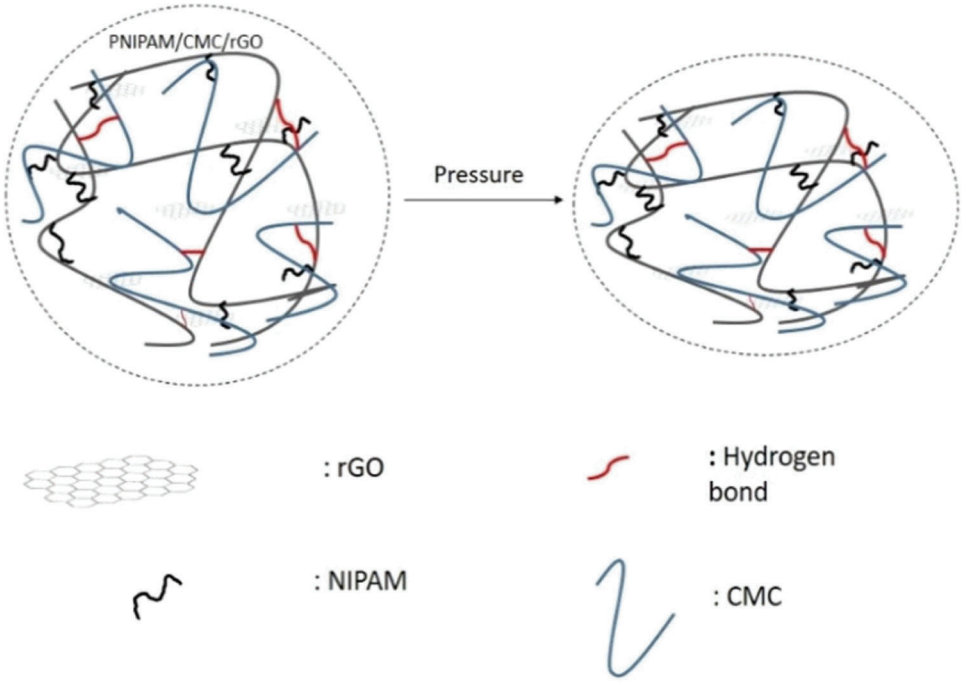

Figure 59. Effect of pressure on DN hydrogel.[151]

has been used in the development of wearable sensors to track movements of the human body and, with careful engineering, to monitor disease.

2.6. Gas Sensors

Hydrogen chloride (HCl) gas is emitted from burning fuels containing chlorine and incinerating plastic-containing waste. However, HCl gas may cause toxic effects on the human body and has been identified as a cause of acid rain. As a result, reliable detection of HCl gas has been required from the standpoint of emission control and air-quality monitoring. Matsuguchi and Tada designed quartz crystal microbalance (QCM)-based HCl gas sensors because of their simplicity and high sensitivity.[245] PNIPAM was synthesized via atom transfer radical polymerization (ATRP), and NPs were generated by spray coating its aqueous solution onto a heated quartz resonator surface at 50 °C (above PNIPAM's LCST). Due to HCl adsorption, the frequency shift of the resonator was observed. Additionally, the sensor showed a 90% recovery.

Their group also developed an HCl gas sensor utilizing the same process, with the exception that they used a water-methanol binary solvent and used the cononsolvency effect on the phase transition of PNIPAM aqueous solutions.[246] Cononsolvency is a phenomenon where the LCST of PNIPAM is affected by the addition of good organic solvents. Although, the fabricated system exhibited reusability of less than 90% at the first cycle, which is improved to almost 100% at the third cycle.

3. PNIPAM-Based Biochemical Sensors

3.1. Biomolecules Sensing

Molecules with a biological function or found in living organisms, i.e., biomolecules, come in a wide range of sizes, shapes, and structures, each with its specific function. There are four major types of biomolecules, namely carbohydrates, lipids, nucleic acids, and peptides/proteins. The ability to characterize detect and quantify biomolecules plays a significant role in our understanding of life, its function in physiological processes in health and diseased states. Here, PNIPAM-based systems have demonstrated the ability to aid in the detection of a variety of biomolecules, which will be outlined below.

3.1.1. Glucose Sensing

Glucose is one of the most important energy sources in the human body and a crucial agent in the food industry.[247] In medicine, monitoring of blood glucose levels is routinely measured for people suffering from diabetes, during pregnancy and to diagnose liver diseases.[248,249] The normal range of glucose concentration is between 3.9×10^{-9} M to 7.8×10^{-3} M in blood, and 0×10^{-3} to 0.8×10^{-3} M in urine. In diabetes patients, glucose concentrations vary from about 10×10^{-3} to 21.1×10^{-3} M in blood and 1.0×10^{-3} to 2.8×10^{-3} M in urine. This hyperglycemia, if left unchecked, is the cause of many secondary symptoms and

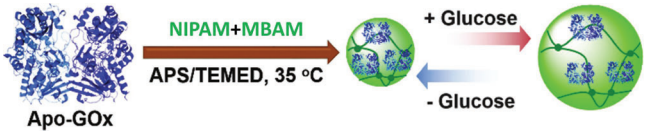

Figure 60. Synthesis of microgel with glucose induce phase transition. Reproduced with permission.[253] Copyright 2016, Royal Society of Chemistry.

worsening of the health condition of diabetes patients, and monitoring glucose levels enables timely insulin treatments to manage blood glucose levels. Besides diabetes, glucose also plays an important role in cancer, as cancer cells consume glucose more rapidly than normal cells, and their growth is therefore highly dependent on glucose metabolism.[250] Hence, glucose is an important indicator of health, diet, and age.

Huang et al. synthesized a glucose sensor by calculating O_2 production by glucose oxidation.[251] For this purpose, they first introduced the PNIPAM-immobilized glucose oxidase (GOD) complex (PIGC) for fiber optic glucose sensing. PIGC was synthesized by polymerizing NIPAM, MBAM and GOD immobilized SiO_2 NPs. At a temperature lower than the LCST, the hydrogel is in the swollen state allowing the enzyme to contact the substrate, resulting in an enzymatic catalysis reaction forming O_2. This O_2 quenches the fluorescence. The prepared sensor shows glucose-sensing in the range of 50–700 mg dL^{-1} in the real sample.

The prepared sensor might sense cholesterol in addition to glucose, according to their forthcoming study on glucose sensors.[252] Here GOx and cholesterol oxidase (COD) were immobilized on the SiO_2 NPs to prepare a multiparameter fiber-optic biosensor based on the same PIGC and immobilized COD. Above the LCST the incorporated GOx was isolated from the substrate, so no oxidation of glucose occurred but COD can oxidize cholesterol, while below the LCST the swollen hydrogel enabled GOx contact with glucose and oxidation occurred. In both reactions, O_2 is emitted which quenches the fluorescence. The hydrogel detects cholesterol concentration in the range of 20–250 mg dL^{-1} and glucose concentration in the range of 50–700 mg dL^{-1}.

In vivo, glucose sensors can be prepared from an apo-enzyme, such as apo-GOx which is an inactive (non-metabolizing) form of an enzyme with the cofactor/coenzyme being removed. In this fashion, the high specificity of enzymes towards their substrates and associated conformational changes of the enzyme can be exploited without the transformation of the substrate, which is ideal for sensing applications. A recent example of such an apo-Gox sensor can be found in the work of Ye et al., who introduced apo-GOx in a microgel for glucose recognition and monitoring in physiological concentrations.[253] The Apo-enzyme apo-glucose oxidase (apo-GOx) was prepared by removing the coenzyme flavin adenine dinucleotide (FAD), and subsequently, apo-GOx@PNIPAM microgels were synthesized via free radical precipitation copolymerization using NIPAM and MBAM crosslinker in the presence of apo-Gox (**Figure 60**). The microgels displayed characteristic swelling in the presence of glucose, due to the charge-dipole and hydrogen-bond interactions formed between the apo-enzyme and its substrate, which was confirmed via DLS measurement. Furthermore, the authors demonstrated the high selectivity for β-D-glucose, as the observed swelling was

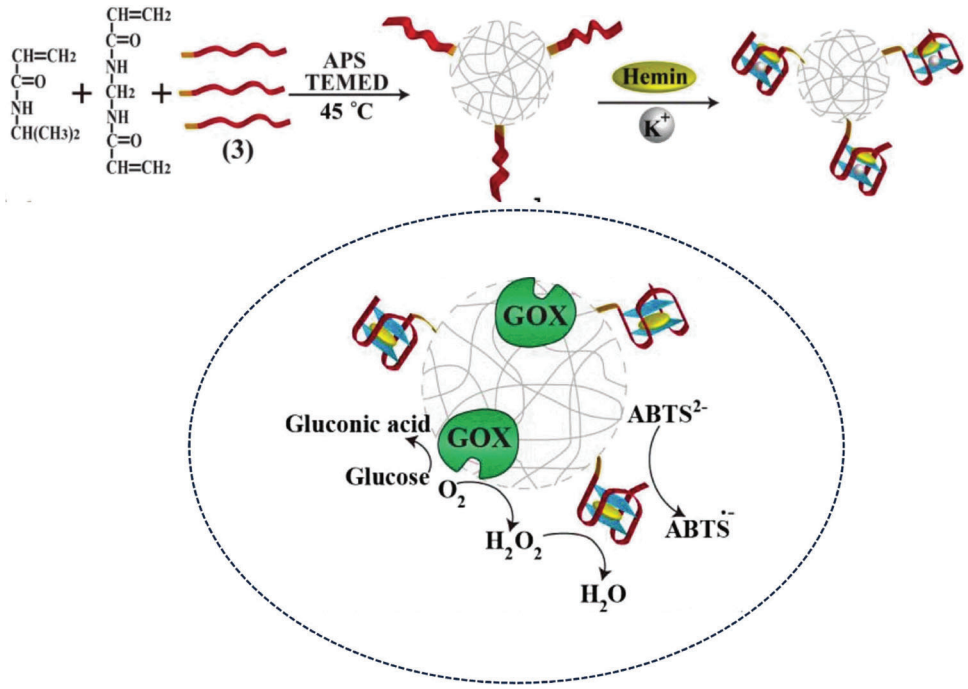

Figure 61. Synthesis of the system with glucose detection mechanism. Reproduced with permission.[254] Copyright 2018, Wiley-VCH.

absent in the presence of other glycogens (fructose, galactose, mannose), polysaccharides, and glycoproteins. The fabricated microgel can selectively detect β-D-glucose with a sensitivity range of 0–20 × 10^{-3} M. This study demonstrates a useful use in diabetic mice.

DNAzymes are oligonucleotides with the ability to catalyze chemical reactions, therefore exhibiting similarities to enzymes. Hence, they can be applied as a useful tool in sensing applications. The utility of DNAzymes in glucose sensing has been explored in combination with PNIPAM microgels by Li et al.[254] In their system, the authors combined the hemin-G-quadruplex horseradish peroxidase (HRP) mimicking DNAzyme on PNIPAM microgel surface by a one-step precipitation polymerization (**Figure 61**). The porous structure of the PNIPAM microgel was encapsulated with an enzyme and GOx. The GOx catalyzed the reaction to form H_2O_2 from the reaction with O_2 and glucose. The H_2O_2 further oxidized 2,2′-Azino-bis(3-ethylbenzothiazoline-6-sulfonic acid) diammonium salt ($ABTS^{2-}$) salt to generate colored $ABTS^{\bullet-}$ in the presence of HRP mimicking DNAzyme, to produce readout signals. At a temperature higher than LCST of PNIPAM, PNIPAM/DNAzyme transforms to a shrunken state and gets separated from water solvent. Subsequently, after centrifugation, this polymer can be reused.

Another type of glucose sensor was prepared by Chen et al. using sonochemistry.[255] Due to its unique qualities, such as cheap cost, customizable nanostructure, high sensitivity, quick reaction, and long-term stability, they developed a CuO-based nanocomposite. Using N_2 aeration the ultrasonic synthesis of CuO@PNIPAM hybrid nanomaterial was performed, followed by modification with GCE. Initially, due to the Cu(II)/Cu(III) redox couple, a peak at about +0.65 V was observed. However, in the presence of glucose, Cu(III) was reduced to Cu(II), which showed a peak at 0.55 V on the CV curve, and glucose converted to gluconic acid as a result of the presence of powerful oxidant Cu(III). At lower temperatures, the hydrophilic PNIPAM allowed glucose to diffuse to electroactive CuO. When the temperature was higher than the LCST, PNIPAM turned into a hydrophobic state that prevented glucose contact with CuO and displayed an "off" state.

Phenylboronic acid (PBA) derivatives are prominently used probes for glucose sensing. In alkaline media, PBAs form a tetrahedral boronic acid anion. This anion is reactive towards diols, such as the 1,2- or 1,3 diols found on glucose, thus yielding the corresponding boronic esters.[256] Therefore, with the introduction of PBA moieties into the PNIPAM chain, various types of glucose sensors are prepared. Several PNIPAM sensors have been developed for glucose sensing, utilizing VPTT and size-changing of the polymer,[74–78] polymerized crystalline colloidal array (PCCA) glucose sensor was reported.[104] Other examples of optical glucose sensors are inverse opal[105] and photonic crystal.[257] A FRET process was also introduced in polymer chain by incorporating a FRET pair.[104] Tang et al. prepared a contraction type glucose-sensitive microgels for glucose sensing and a new type of mechanism was proposed in which glucose changes its swelling degree via changing the ionization degree or crosslink degree.[258] Here they first prepared P(NIPAM-AAc) microgel and by reacting with 2-acrylamidophenylboronic acid (2-AAPBA) in the presence of 1-ethyl-3-(3-dimethylaminopropyl)carbodiimide hydrochloride (EDC) target microgel P(NIPAM-2-AAPBA) was formed. In addition to glucose, the VPTT of the polymer decreased with a decrease in the size of the polymer. Therefore, by measuring the particle size by DLS the amount of glucose can be calculated (**Figure 62**).

In the next example, for the first time, the same group synthesized a glucose sensor by introducing, a colloid crystal capable

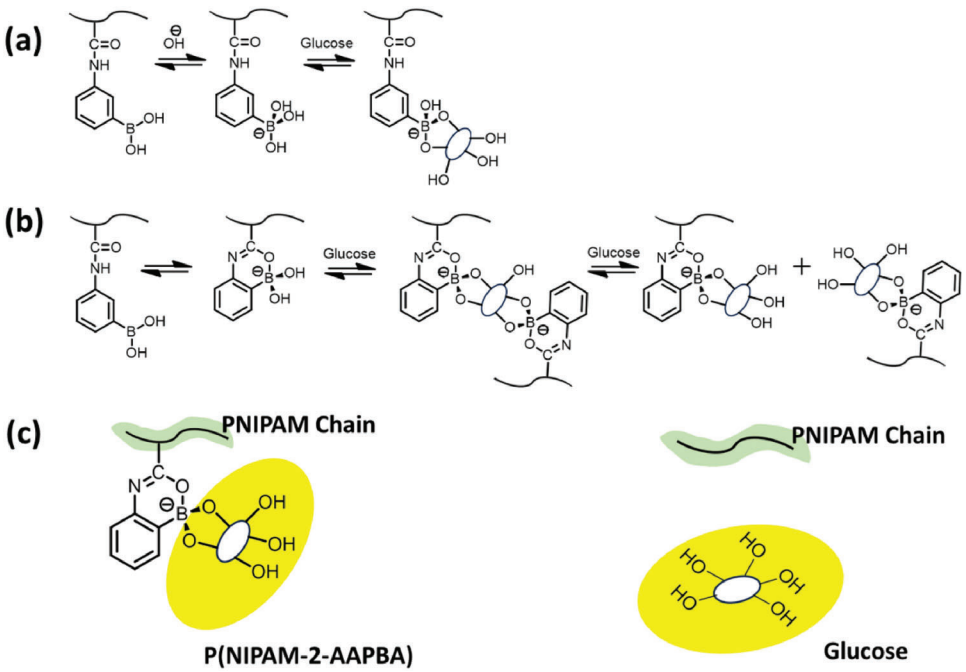

Figure 62. a) Formation of 1:1 glucose–boronate complex, b) Formation of 1:2 glucose–boronate complex, c) Correlation between the glucose and PNIPAM chains in the P(NIPAM-2- AAPBA) microgel (left) and PNIPAM microgel (right). Reproduced with permission.[258] Copyright 2018, Royal Society of Chemistry.

of undergoing transition among three states in response to external stimuli, e.g., glucose.[259] PNIPAM microgel was prepared and doped with P(NIPAM-2-AAPBA) microgel. The doped microgel was larger than the host microgel. In the presence of glucose at pH 7.4 the doped microgel began to shrink and with an increase of glucose concentration, the size of the doped microgel decreased than the host microgel (**Figure 63**). This observation was confirmed by examining the transmission spectra. The glucose concentration in the range 0–60 × 10^{-3} M can be measured.

Further, a glucose sensor based on a similar concept was described by their group.[257] P(NIPAM-3-AAPBA) and 3-AAPBA create the doped microgel. Since the doped microgel was smaller

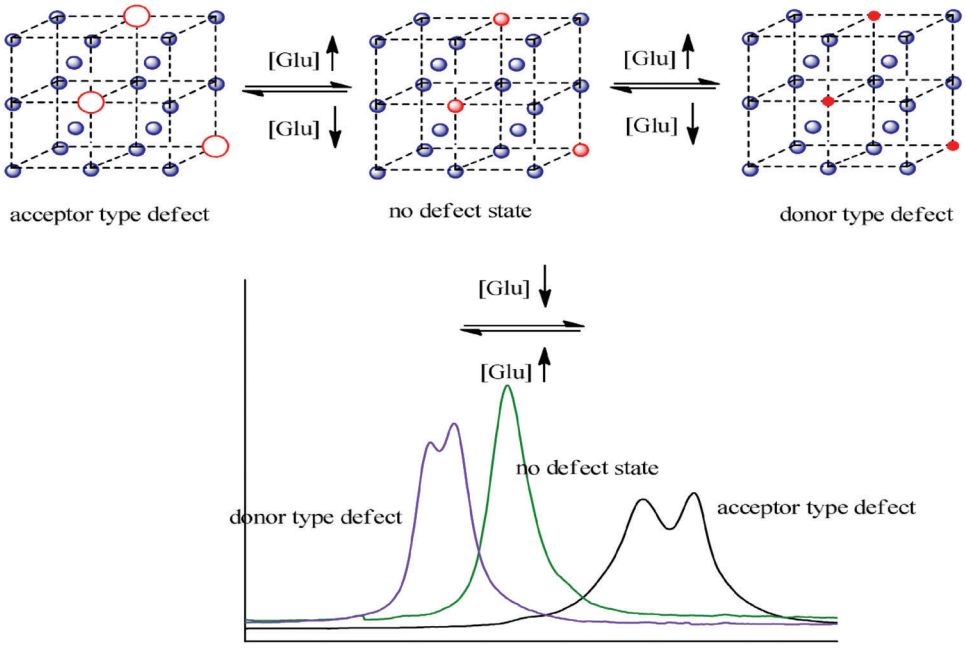

Figure 63. In the presence of glucose, the microgel shrinks. Reproduced with permission.[259] Copyright 2018, American Chemical Society.

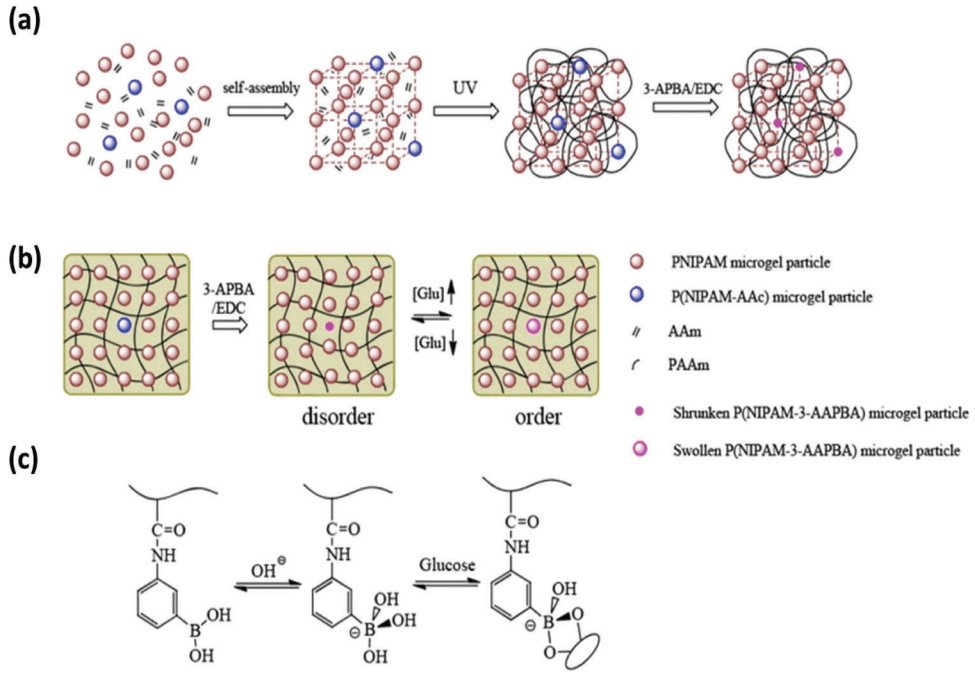

Figure 64. a) Formation of P(NIPAM-3-AAPBA) microgel-doped PNIPAM microgel, b) Introduction of defects to get order–disorder transition induced by glucose, c) Interaction between PBA and glucose inside the gel. Reproduced with permission.[257] Copyright 2018, American Chemical Society.

than the host microgel, in this case, a defect in the transmission window was found. Swelling of doped microgels occurred in the presence of glucose at pH 8.5 (phosphate buffer), and the size difference between the two microgels was reduced.

The size of two microgels becomes comparable at a particular glucose concentration, therefore eliminating the defects. Further, the addition of glucose increased the size of the doped microgel relative to the host microgel, causing a defect to appear once more, as detected by transmission emission (**Figure 64**).

Peng and co-workers prepared a nanogel in order to develop a glucose sensor with low LODs and a visual output.[260] The nanogel was synthesized with a glucose-responsive VPBA and thermo-sensitive monomer NIPAM via emulsion precipitation polymerization. In ammonium chloride-ammonia buffer solution (pH 9.50), the nanogel colloid formed a complex with glucose causing nanogel swelling which allowed the red-shift and the distinct change in the structure color from blue to green. The nanogel detected a very low concentration of 1×10^{-3} M of glucose.

Another naked-eye glucose-detecting sensor was prepared by their group by introducing colloidal photonic crystals (CPCs) made from interpenetrating nanogels (IPN).[261] Poly(*N*-isopropylacrylamide)/poly(acrylic acid) nanogels were first prepared followed by the formation of P(NIPAM-VPBA)@IPN-BAC nanogels with VPBA, NIPAM, and *N,N′*-bis(acryloyl)cystamine (BAC) crosslinker, and the nanogels were allowed to self-assemble into colloidal photonic crystals (CPCs). The VPBA in the nanogel could complex with glucose, which allowed the swelling of the lattice space in the crystal structure and a rapid increase in the lattice distance. As the concentration of glucose increased from 0 to 2 mM, the color of CPCs changed from bright blue to green.

Nanoparticle-based glucose sensors can also be prepared which contain PBA moiety. Fluorescent CdS QDs were immobilized with a PBA-containing polymer to prepare an optical glucose sensor.[124] Other fluorescent CdS QDs incorporated which convert the biochemical signal into an optical signal corresponding to the amount of glucose.[125] Noble metal NPs, such as AuNPs were introduced in polymer chains for optical sensing and ability to improve storage ability and reusability.[262] Nanosized CDs are also used for their excellent optoelectronic property.[126] There was another example of using ZnO QDs for glucose sensing.[263] Inspired by the "fishing" or "selective capture and controllable detection" concept Qiao et al. fabricated poly(maleic anhydride-styrene-N-isopropylacrylamide-4-aminophenylboronic acid) P(MAn-St-NIPAM-PBA) to fabricate the nanoreactor for the detection of D-glucose (Glu) in the rat microdialysates of brain ischemia.[264] Block copolymer P(MAn-St-NIPAM-PBA) was synthesized by the RAFT polymerization process followed by the enzyme (GOx) filled and Myo-filled nanoreactors were fabricated in the self-assembling method.

The PBA unit in block copolymer selectively binds Glu and GOx in a nanoreactor converted Glu to D-glucono-δ-lactone and H_2O_2. The prepared H_2O_2 was used as a cosubstrate for a Myo-based catalyst to oxidize guaiacol into quinone, which was observed using UV–vis spectroscopy (**Figure 65**). At a temperature higher than LCST enzyme was blocked by shrinking of PNIPAM and so it exhibited "off" state. Additionally, the model selectively detects Glu over other saccharides in the range of $0.30–10.0 \times 10^{-3}$ M with a LOD of 0.20×10^{-3} M.

The glucose in saliva was measured using AuNPs modified with polymer. In this context, Yang et al. fabricated an Au-decorated glass nanopore where the inner wall was modified with copolymer poly(3-(acryloylthioureido)phenylboronic

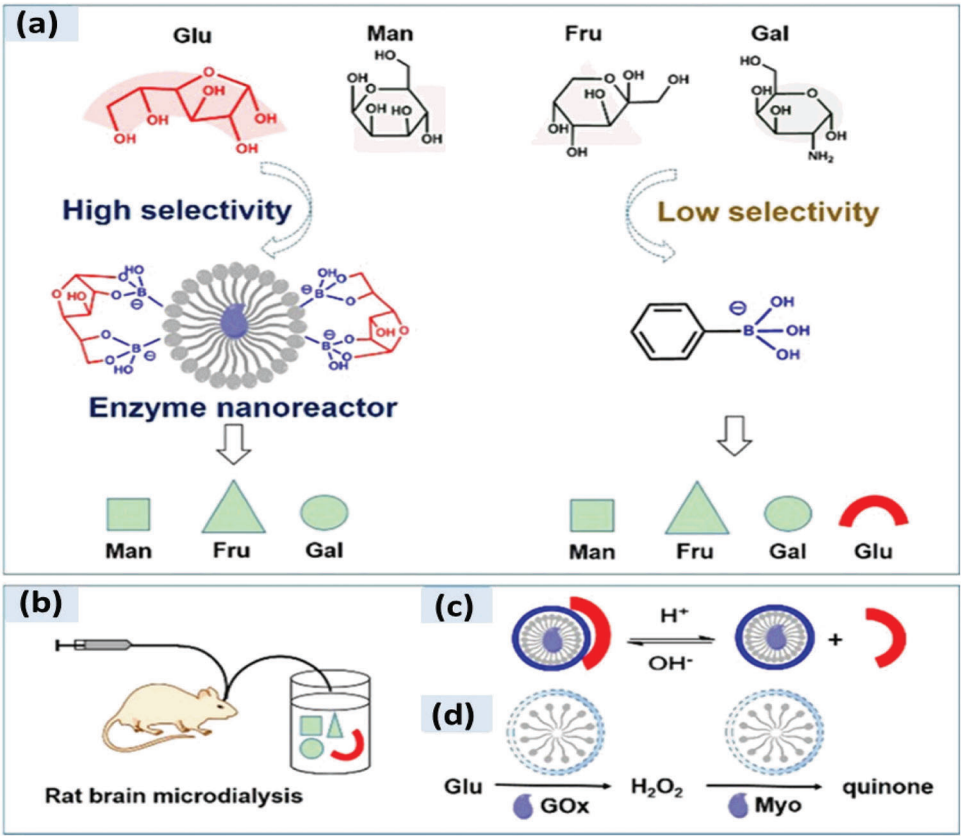

Figure 65. a) Selective capture of Glu by PBA unit over other saccharides, b) schematic illustration of the rat brain microdialysis process, c) reversibility nature of the hollow nanoreactor towards Glu, d) immobilizing the hollow nanoreactors with GOx enzyme and myoglobin (Myo)-based catalyst for the controlled monitoring of Glu in the rat brain. Reproduced with permission.[264] Copyright 2020, American Chemical Society.

acid-*co*-*N*-isopropylacrylamide) P(ATPBA-*co*-NIPAM) via Au–S interaction.[265] In the presence of glucose by H-bonding interaction, the conformation was changed from a coiled to a stretched state leading to an increase in ionic flux. Again, the pKa value of the corresponding polymer was 6.8 and upon the addition of glucose at pH 9 boronate copolymer became a polyanion with the ionic current change (**Figure 66**). The system selectively detected glucose over other biological molecules (xylose, fructose, galactose, mannose, sucrose, lactose, and maltose) with a LOD of 1×10^{-9} M.

PBA-based micro/nanogels usually take a long time to reach the de-swelling equilibrium under decreasing glucose concentration conditions. To overcome this problem a nanogel was prepared with Concanavalin A (ConA), as the glucose recognition moiety.[102] ConA is a plant lectin protein tetramer that consists of two dimers and has four binding sites for non-reducing D-glucose, D-mannose, and polysaccharide. Wei et al. introduced a microgel-based surface plasmon resonance transducer for glucose detection using ConA.[266] The microgel poly(*N*-isopropylacrylamide-*co*-glycosyloxyethyl methacrylate (P(NIPAM-*co*-GEMA)) was synthesized using MBAM crosslinker via free radical precipitation polymerization followed by adding ConA through pendent glycosyl groups of microgel (**Figure 67**). ConA has a greater glucose affinity than GEMA. Therefore, the deswelling microgel, in the presence of ConA again began to swell in the presence of glucose as ConA leached from the microgel to bind with glucose. This process was examined by monitoring the contraction/expansion process of the microgels bound to an Au surface via SPR. This process was observed up to 5×10^{-3} M glucose concentration.

A glucose-responsive phenyl boronic moiety was typically included int the polymer backbone for designing glucose sensor systems. The polymer matrix can also be modified by including glucose oxidase. Many strategies were employed to produce glucose sensors using a glucose-responsive mechanism. For instance, AuNPs and CDs were utilized to track glucose. Glucose was detected with a LOD as low as 0.2×10^{-3} M using a PNIPAM-based sensor, and also sensed from complex mediums such as human saliva and rat brain with high selectivity. Therefore, the PNIPAM-based designed sensors have the potential of practical application.

3.1.2. Hydrogen Peroxide Sensing

Hydrogen peroxide (H_2O_2) has a vital role in the regulation of many physiological processes and it is also a by-product of many metabolic processes in living systems. The variation of its concentration can affect cell proliferation, death, and signal transduction.[267] Hydrogen peroxide is also an important

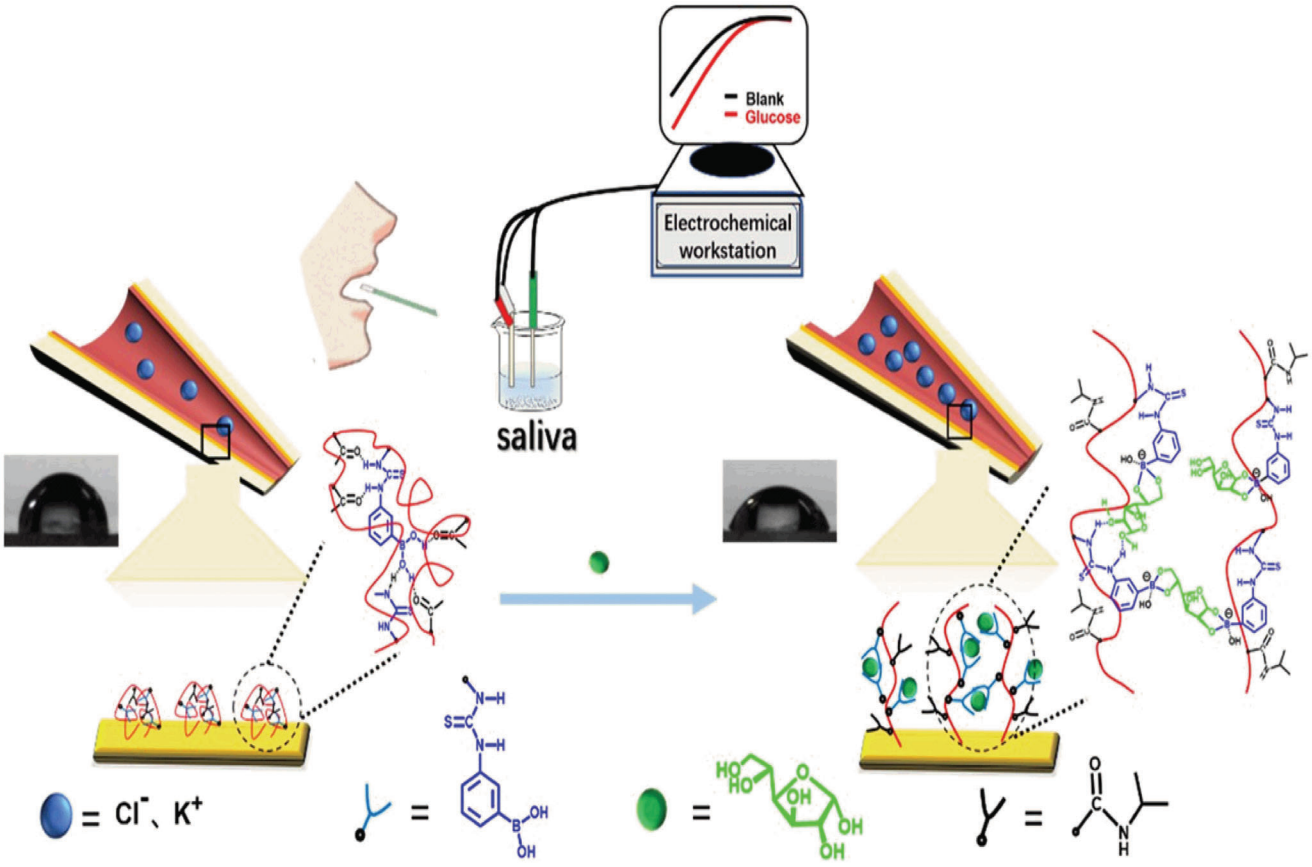

Figure 66. Demonstration of glucose detection from saliva. Reproduced with permission.[265] Copyright 2019, American Chemical Society.

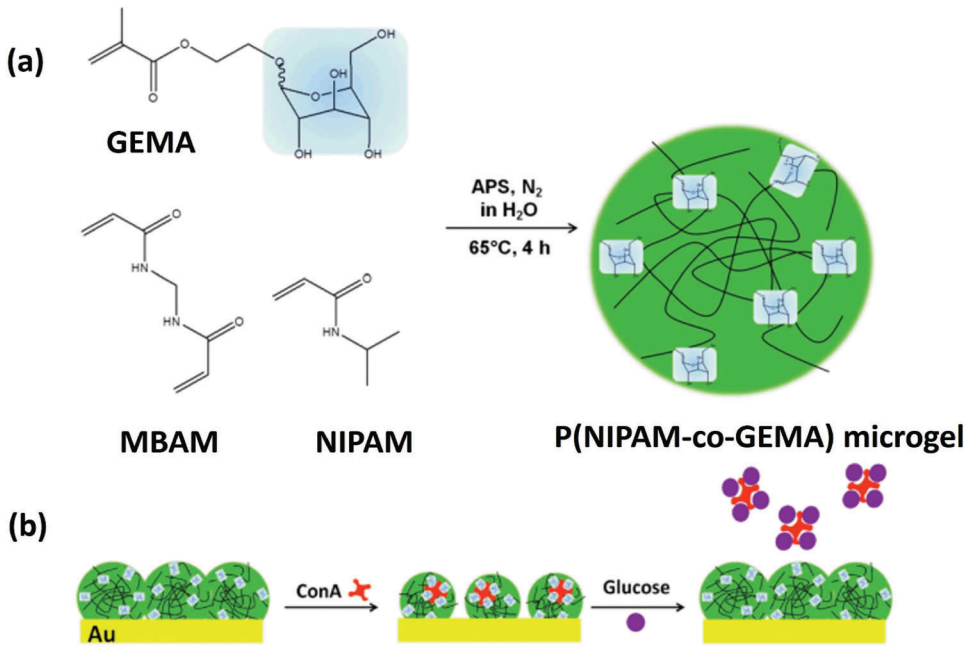

Figure 67. a) Synthesis of microgel; b) design for SPR platform. Reproduced with permission.[266] Copyright 2019, American Chemical Society.

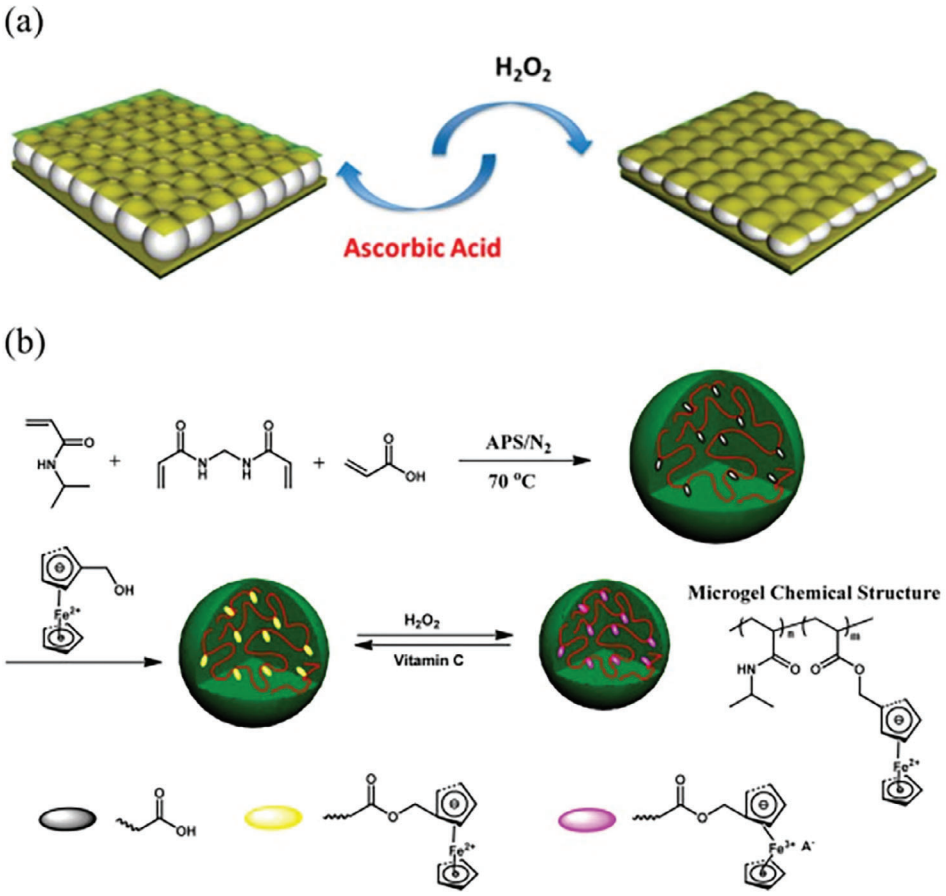

Figure 68. a) Peroxide responsive change in etalon device structure; b) formation of microgel with sensing property. Reproduced with permission.[268] Copyright 2016, American Chemical Society.

intermediate in food, pharmaceutical, clinical, and industrial processes; environmental analysis; and many other fields. PNIPAM has taken an important role in peroxide sensing due to its temperature response character which increased the sensitivity of the sensor. Peroxide-sensitive fluorescent Calcon dye assemblies were reported to prepare a sensor.[174] Sensing based on photonic materials takes significant attention due to their low cost and easy signal readout property. The Serpe group demonstrated a novel optical device named etalon where microgel was sandwiched between two Au layers. Optical properties vary depending on the distance between two Au layers. To prepare a peroxide sensing etalon, first a microgel was prepared via free radical precipitation polymerization with monomer NIPAM, AAc, and crosslinker MBAM.[268] Then ferrocenylmethanol monomer was added to the microgel followed by etalon fabrication. When the microgel was exposed to H_2O_2, Fe^{2+} of ferrocene oxidized to Fe^{3+}, causing it to transition to a +1-charge state of ferrocene. The compound with +1 charge was reported to interact with the polar amide group of the microgel resulting in a decrease in microgel diameter and the formation of a characteristic multipeak reflectance spectrum (**Figure 68**). Peroxide emitted from the enzymatic reaction between glucose oxidase and glucose can be detected using this etalon device, and the device can be reused by the reduction of ferrocene done by exposure to the reducing agent.

Another etalon device was fabricated by the same group introducing silver nanoparticles (AgNPs) in a P(NIPAM-*co*-AAc) microgel instead of the ferrocene moiety for H_2O_2 sensing.[269]

This was made possible by introducing Ag^+ to the etalons composed of deprotonated microgels, followed by its subsequent reduction with $NaBH_4$. AgNPs were decomposed in the presence of H_2O_2, which enabled the microgel layer to swell resulting in a red-shift in the reflectance peaks from the etalon and an increase in the intensity of the reflectance peaks (**Figure 69**). Additionally, the NPs could be regenerated and reused at least seven times without losing performance efficiency.

Peroxide sensors can be prepared by incorporating redox enzymes into polymer-based films such as hydrogel polymers, biopolymers, and polyelectrolytes. It can enhance the direct electron exchange between the enzymes and underlying electrodes. Hemoglobin (Hb) shows a couple of well-defined redox peaks with a formal potential of −0.371 V (vs SCE) and exhibits intrinsic electro-catalytic activity toward H_2O_2. This property was used to prepare a composite film containing MWCNTs.[118] Another Hb-based peroxide sensor was fabricated by Zhou et al. using GO having good hydrophilicity, moderate conductivity, and excellent electrochemical properties.[270] Block co-polymer

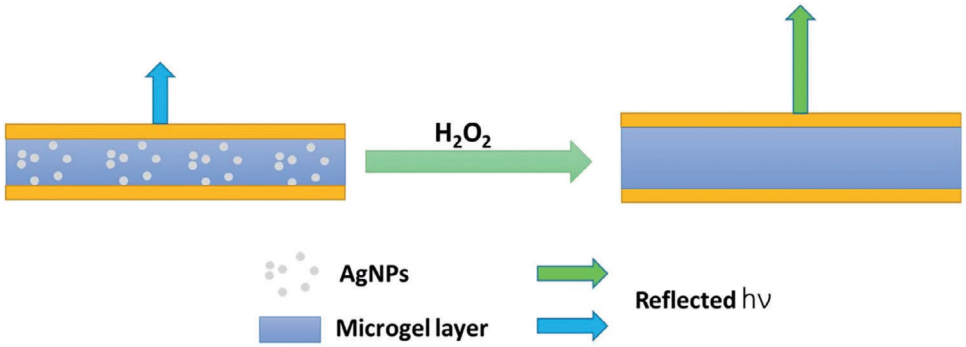

Figure 69. Peroxide induced change in etalon.[269]

poly(*N*-isopropylacrylamide)-*b*-poly(2-acrylamidoethyl benzoate) (PNIPAM-*b*-PAAE) was fabricated using the RAFT process and mixed with GO to form PNIPAM-*b*-PAAE/GO. Then Hb was added to get PNIPAM-b-PAAE/GO/Hb (PGH) solution which was used to prepare a film on GCE, marked as PGH/GCE. In the presence of H_2O_2, a significant reduction peak was observed which suggested the reduction of peroxide in the presence of Hb. At temperature above LCST PNIPAM-*b*-PAAE underwent a dehydrated state inducing "expansion-to-contraction" (**Figure 70**) of the PGH film which resulted in wider linear detection ranges and lower LOD existing above 32 °C. The system detected H_2O_2 with a detection range of 0.1 to 3.72 µmol L^{-1} at that temperature.

In parallel, Manivannan et al. designed an electrochemical sensor where the enzyme Hb was used with inorganic particles, modified with PNIPAM, to prepare a composite for detecting H_2O_2.[271] To prepare the composite, first a SiO_2 dispersion was treated with (3-aminopropyl)triethoxysilane (APTES) to form NH_2-functionalized SiO_2 microspheres (NH_2-SiO_2). Then 2-bromoisobutyrate-functionalized SiO_2 microspheres (Br-SiO_2) were prepared using 2-bromoisobutyryl bromide (BiBB) followed by adding NIPAM, methanol, water, and CuBr/$CuBr_2$/PMDETA to prepare composite PNIPAM@SiO_2 core–shell microspheres through surface-initiated ATRP. Finally, Hb was immobilized onto the surfaces of PNIPAM@SiO_2 microspheres via hydrophobic and π-π stacking interactions and modified on GCE to prepare the electrode (**Figure 71**). Electron transfer occurs between Hb and PNIPAM@SiO_2 causing a redox peak at −0.38 V corresponding to Fe(III)/Fe(II) redox couple. H_2O_2 was reduced by Hb and reduction currents at −0.29 V increased linearly upon increasing the H_2O_2 concentrations at pH 7.2. The system detected H_2O_2 over a wide linear concentration range (0.1×10^{-3} M to 333×10^{-3} M) with a LOD of 0.07×10^{-6} M.

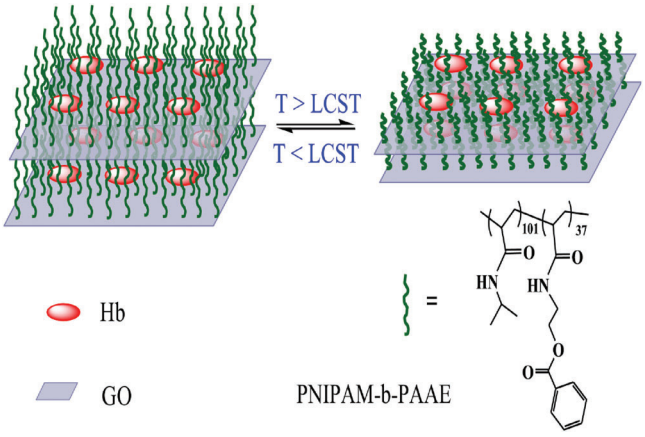

Figure 70. Temperature-responsive volume change of polymer. Reproduced with permission.[270] Copyright 2016, Springer Nature.

Fe_3O_4 NPs can be used as an alternative to enzymes in the fabrication of peroxide sensors, due to their enzyme-like activity. In this context, Wang et al. reported a nonenzymatic switchable bioelectrocatalytic sensor for H_2O_2.[272] The first PNIPAM microgel was synthesized via emulsifier-free polymerization followed by mixing with Fe_3O_4 NPs to generate Fe_3O_4-PNIPAM microgels and a GCE was modified with it. At temperatures below the LCST of PNIPAM, due to swelling the Fe_3O_4 NPs were open to the electrode surface and the Fe_3O_4 NPs can catalyze oxidation reaction of H_2O_2, yielding the "on" state.

Above the LCST the NPs were not exposed to H_2O_2 due to the collapsed polymer resulting in the "off" state (**Figure 72**). The fabricated system detected 0.005×10^{-6} M H_2O_2 at 26 °C by seeking an electrochemical response.

Electrochemical changes resulting from peroxide reduction are a common technique for detecting H_2O_2. PNIPAM is often applied to the electrode surface. These interfaces have been demonstrated to have temperature-controlled electro-catalysis or switchable/tunable interfacial electron transport. With a high degree of selectivity, the peroxide sensor can identify concentrations as low as 0.005×10^{-6} M. The sensor has been used to detect peroxide in actual samples, including milk and fruits. According to some reports, scientists have developed a low-cost peroxide sensor and assessed its application in biological enzymatic reactions.

3.1.3. Protein Sensing

Proteins are another main class of biomolecules, having the largest size among all biomolecules and macromolecules. Its structure has one or more long chains of amino acid residues. Proteins are very important as they are responsible for many functions within organisms, including catalyzing metabolic reactions, DNA replication, responding to stimuli, providing structure to cells and organisms, and transporting molecules from one location to another. Due to their vast applications, there is a tremendous interest in protein detection. The PNIPAM-based

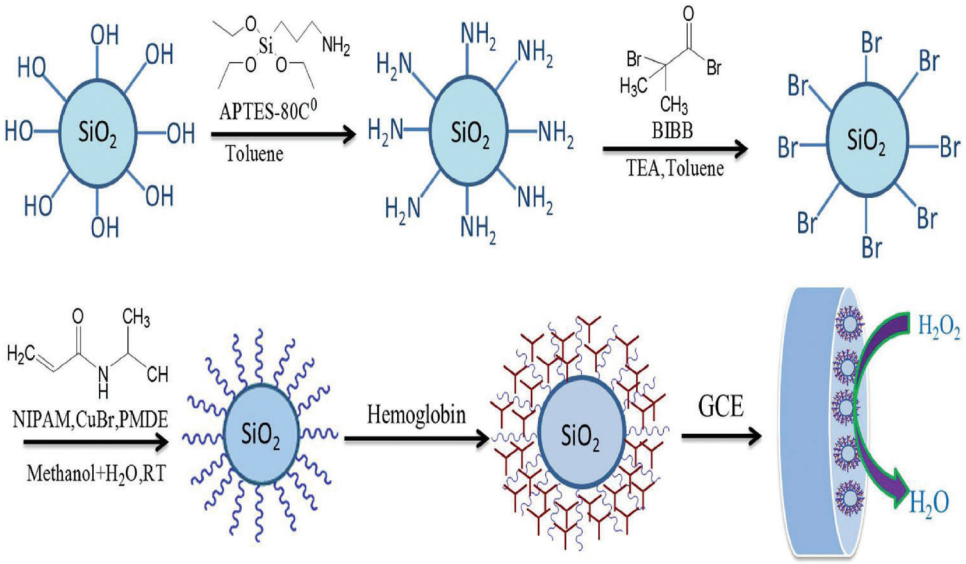

Figure 71. Synthesis of PNIPAM coated SiO_2 microsphere and immobilization of Hb. Reproduced with permission.[271] Copyright 2017, Wiley-VCH.

system offers a variety of protein detection methods. Molecular imprinting is a popular method among them. Here affinity to template molecules is done by copolymerization of the functional monomers and cross-linkers around them. Then removal of templates is done to form a cavity complementary to the template molecules. Lysozyme (*N*-acetylmuramide glycanohydrolase), a single-chain protein consisting of 129 amino acids is detected using this method. Lysozyme in body tissues and secretions takes part an important physiological role in the innate immune system and the abnormal concentration of lysozyme in body fluids and tissues causes diseases such as renal diseases, leukemia, and meningitis. Chen et al. reported a PNIPAM hydrogel-based molecularly imprinted polymer (MIP) for lysozyme detection.[273] Another PNIPAM hydrogel-based MIP was designed for lysozyme sensing.[99] Fang et al. incorporated silanized CDs into MIP to prepare a fluorescent probe using their fluorescence signal reporting ability.[274] Silica-coated CDs (CDs/ SiO_2) were prepared. Then, the MIP-coated CDs/ SiO_2 composites (CDs/SiO_2/MIP) were synthesized via surface imprinting method with CDs/SiO_2, NIPAM, AAm as the

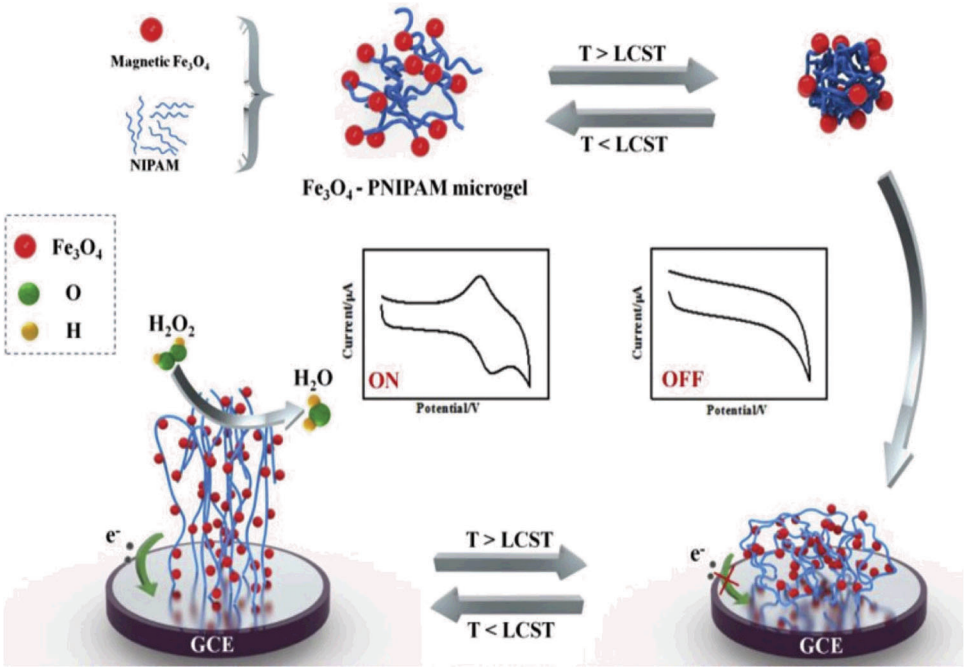

Figure 72. Fabrication of microgel with H_2O_2 response. Reproduced with permission.[272] Copyright 2019, Elsevier Ltd.

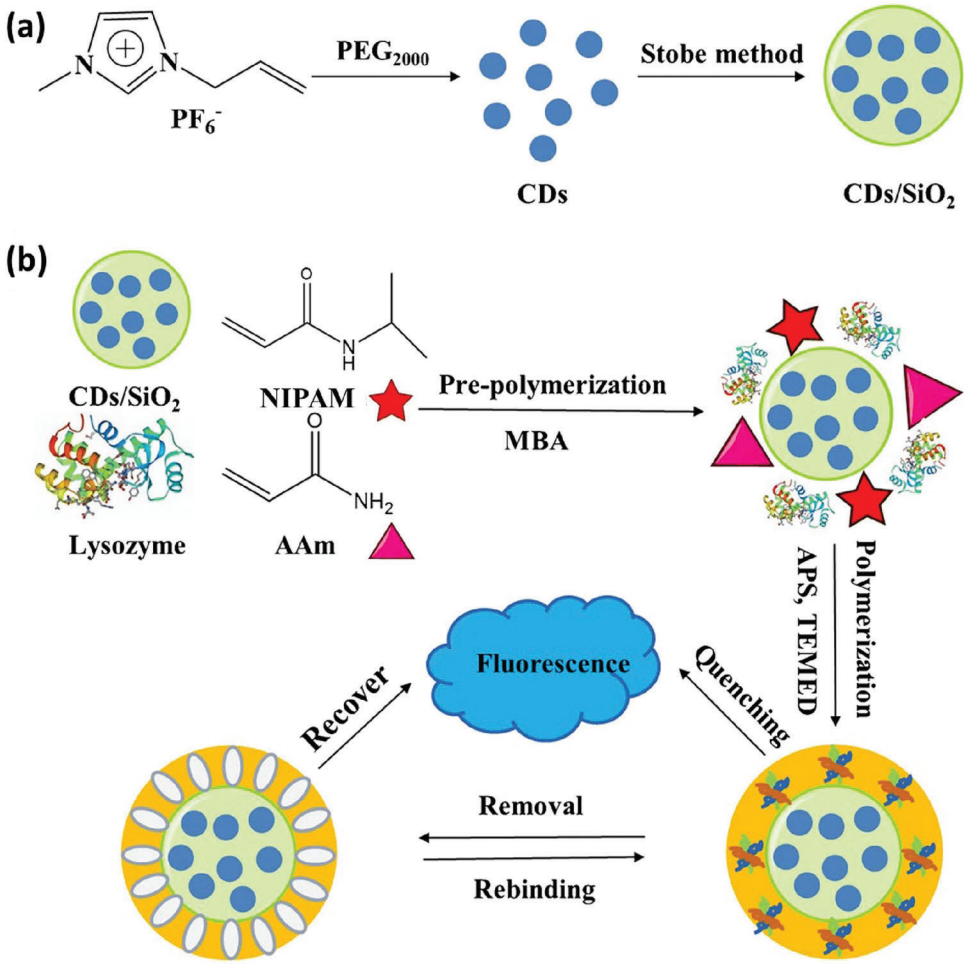

Figure 73. a) Synthesis of CDs/SiO_2, b) Fabrication of MIP with lysozyme sensing property. Reproduced with permission.[274] Copyright 2019, Springer Nature.

functional monomer, and lysozyme as the template (**Figure 73**). After removal of the template molecule, the MIP selectively bound lysozyme due to the similarity of cavity shape and size with lysozyme, inducing fluorescence quenching of the CDs due to the transfer of electrons of the hydroxyl group of lysozymes into the amino group of CDs/SiO_2/ MIP causing the energy of the CDs into the complex. The MIP detected lysozyme in body fluids and tissues with a wider detection range (0.001–0.01 mg mL^{-1}), a low LOD 0.55 µg mL^{-1}, and a high selectivity. The system acted as a temperature-dependent "on-off" as at high temperatures due to the shrinking of PNIPAM, lysozyme could not bind to the imprinted site and the fluorescence intensity decreased.

By introducing magnetic NPs (Fe_3O_4) into MIP, a lysozyme detector was synthesized which could separate lysozyme from egg whites depending on temperature and light, dual-dependent rebinding, and release characteristics for lysozyme. In this context, Jia et al. synthesized magnetic imprinted NPs by grafting nanogel on NPs.[275] At first, the 3-(trimethoxysilyl)propyl methacrylate group was added onto Fe_3O_4 NPs and with it MIPs were formed with thermoresponsive NIPAM, lysozyme (Lys) as the protein template, an azobenzene monomer (MAZoA) as the functional photo-sensitive monomer, AAm containing amino group, and *N*-[3-(dimethylamino) propyl]methylacrylamide (DMAPMA) containing positively charged tertiary amines and crosslinker MBAM via surface graft polymerization (**Figure 74**).

Non-imprinted Fe_3O_4 NPs were also made using similar materials as used in the previous example but without a template. The polymer contracted above the LCST at 37 °C, changing the shape of the imprinted sites and making it easier to capture the protein. However, below LCST, owing to polymer swelling, there was a weaker connection between the nanogel and the protein leading to its release.

Without MIP, lysozyme can be sensed using a turbidimetric sensor array by introducing PNIPAM nanogel as protein receptors.[276] Here a nanogel P(NIPAM-*co*-MAA) was prepared via precipitation polymerization. Then using a carbodiimide-coupling strategy amine-containing molecules were linked to the carboxyl groups of MAA to introduce sulfate, guanidinium, secondary amine, or primary amine groups (unmodified nanogels are referred to as R1 and modified nanogels are marked as R2–R5 corresponding to the ligands with which they were modified). The protein made a bond with nanogel by electrostatic interactions. The anionic nanogels (R1 and R2) preferentially interacted with high p^I proteins, while the cationic nanogels (R4 and R5)

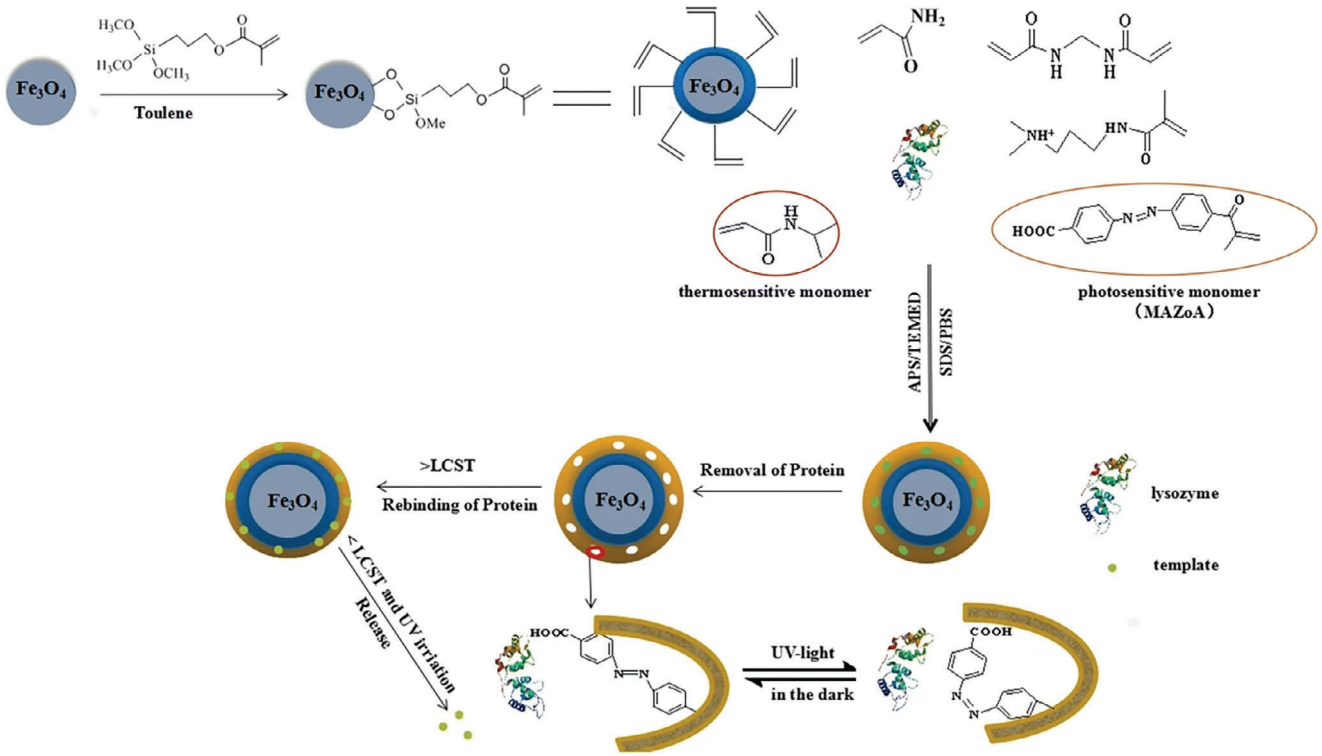

Figure 74. Synthesis of MIP and detection of lysozyme. Reproduced with permission.[275] Copyright 2020, Springer Nature.

preferred low p^I proteins (**Figure 75**). Interaction with nanogel caused particle agglutination or aggregation. Due to the larger size of these aggregates compared to individual particles, light scattering was increased and, consequently, increasing the turbidity of the solution. Turbidity changes were measured by measuring the absorbance of the solution. Here without lysozyme, ten more proteins can be sensed, e.g., cytochrome c, trypsin, lactoferrin, myoglobin, hemoglobin, gamma globulins, bovine serum albumin, ovalbumin, ovomucoid, and fetuin. Additionally, the nanogel was able to detect lysozyme in tear fluid.

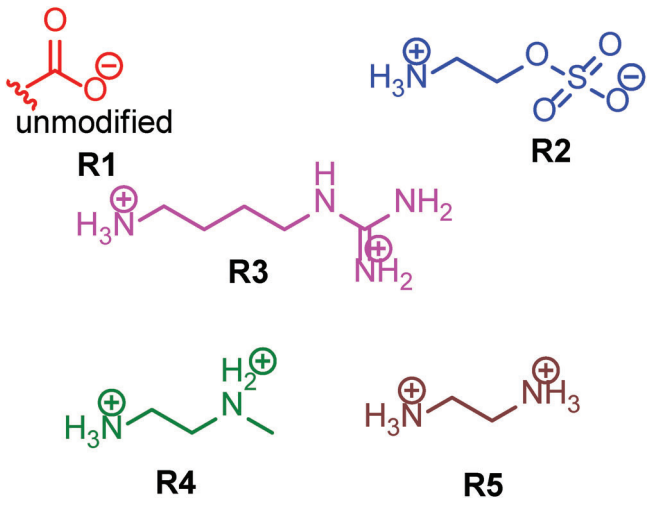

Figure 75. Structures of ligands used to modify P(NIPAM-co-MAA). Unmodified nanogels (R1) contain a carboxylic acid group. 2-aminoethyl hydrogen sulfate (AEHS, R2), agmatine sulfate (AGS, R3), *N*-methylethylenediamine (NMEDA, R4), and ethylene diamine dihydrochloride (ED, R5) were used to introduce sulfate, guanidinium, secondary amine, and primary amine functional groups, respectively.[276]

However, at low protein concentrations, the number of proteins per nanogel decreased and this is due to the misbalance between protein concentration and refractive index. Therefore, achieving a low LOD became hard. To overcome this limitation, they designed the nanogel P(NIPAM-*co*-MAA) (PNM) in a localized surface plasmon resonance (LSPR) based biosensor.[277] For this PNM coated silica gold nanoshells (AuNS@PNM) was prepared.

A significant red shift was seen as a result of proteins' enhanced electrostatic interactions with the PNM nanogel at higher protein concentrations. By using this technique, two protein biomarkers for chronic dry eye were identified: lactoferrin and lysozyme. Due to differing pI values (lactoferrin 8.8, lysozyme 11.3), lactoferrin was sensed at a lower pH (5.5), whereas lysozyme was detected at a higher pH (7.4). Another example of protein is bovine serum albumin (BSA) derived from cows and is a basic component in blood. It is very commonly used in biochemical tests and can be detected using MIPs. The hydrogel of PNIPAM is used to detect BSA using MIP.[99] Dong et al. prepared an MIP using SiO_2 NPs for the recognition of BSA.[278] First silica NPs were formed and the —COOH group was formed on them obtaining SiO_2@COOH and coated with chitosan (CS). After that NIPAM and diammonium cerium (IV) nitrate (CAN) was grafted to it forming SiO_2@CS-*g*-NIPAM and the MIP was formed by adding AAm, template BSA, and crosslinker

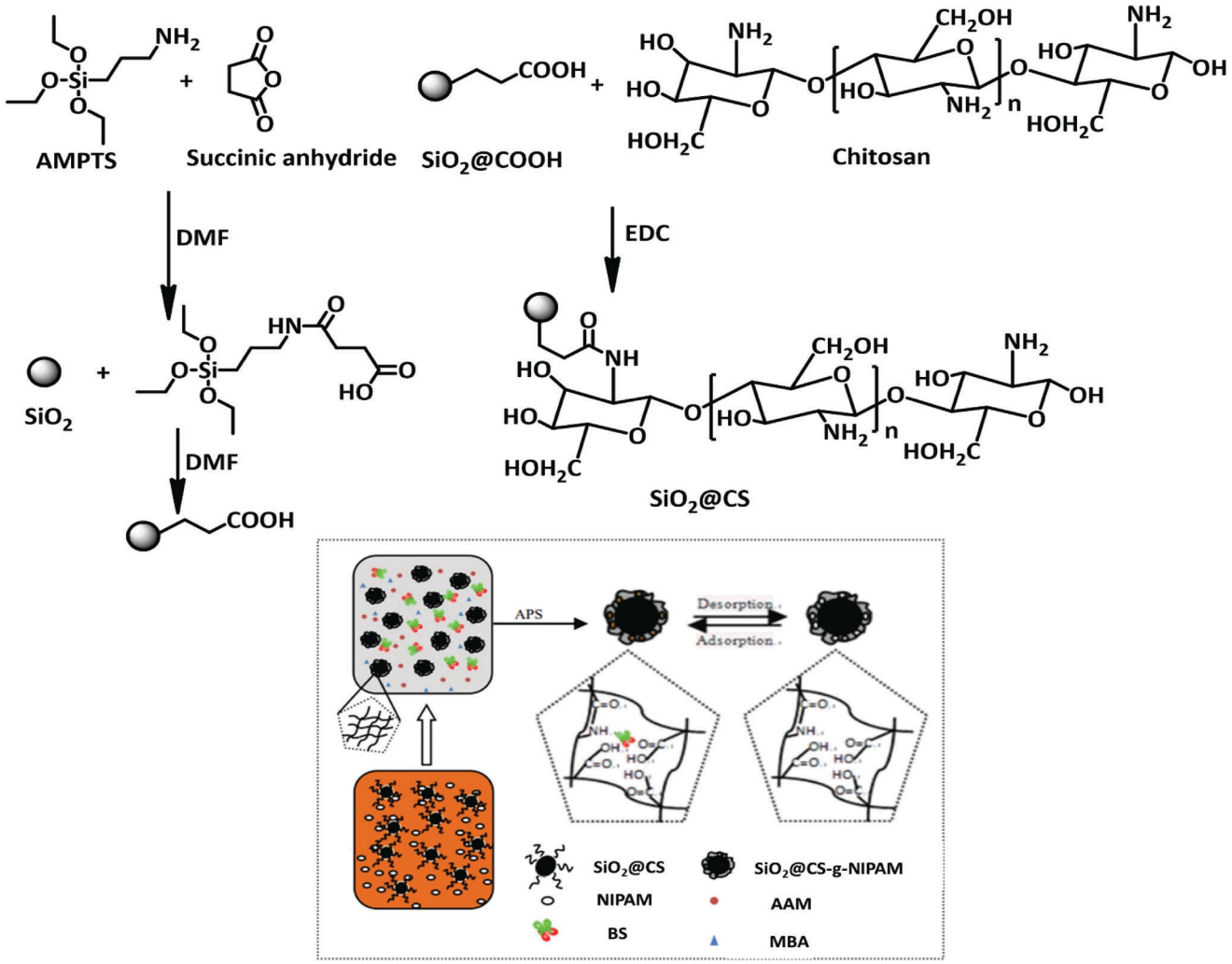

Figure 76. Schematic representation of MIP prepared by Dong et al. Reproduced with permission.[278] Copyright 2019, Wiley-VCH.

MBAM (**Figure 76**). A non-imprinted polymer (NIP) is also prepared without a template molecule. Here, BSA was incorporated in the MIP based on strong electrostatic attraction and the hydrophobic interaction between SiO_2@BSA-MIP and BSA and confirmed by adsorption measurement. At a temperature higher than LCST, PNIPAM shrink and imprinted cavity were deformed which blocked BSA from attaching. The MIP can be used in the real sample with excellent specificity properties. Yang and coworkers introduced a nanogel for detecting multivalent protein binding (MPB) using SPR.[214] First P(NIPAM-*co*-AAc) nanogel was fabricated via radical polymerization in water followed by immobilizing biotin through EDC coupling. Initially, they check the system in the presence of streptavidin where it binds with four biotin molecules. This binding enhances the cross-linking degree of the nanogel network through MPB resulting in deswelling of the nanogels followed by an increase in the RI of the nanogel layer.

These RI changes affected the SPR signal which was not that much affected by monovalent binding (**Figure 77**). Instead of biotin, antigen Fc-tagged PD-1 and protein A were used to detect PD-1 antibodies with a LOD down to 10×10^{-9} M.

Hemoglobin (Hb) is one of the main components of red blood cells. It transports oxygen and carbon dioxide. Again, glycated hemoglobin (HbA1c) plays an important role in diabetes diagnostics. Its deficiency causes anemia, palpitations, and lack of blood color. Therefore, Hb is very important in biological analysis. PNIPAM-based MIP draws wide attention for detection of it. Zhao et al. fabricated a fluorescent sensor by incorporating silanized CDs (CD@SiO_2) into MIP to detect bovine hemoglobin (BHb).[279] The silica-coated CD (CD@SiO_2) was prepared first then taking thermoresponsive NIPAM, functional monomer MAA, and template BHb molecular imprinted polymer was synthesized using the surface imprinting method and coated with CD@SiO_2 to fabricate CD@SiO_2@MIP (**Figure 78**). BHb caused fluorescence quenching due to the special interactions of the template molecules with the imprinting cavities. Here temperature played as a switch of the MIP as at high temperature it acted as a hydrophobic part with weak fluorescence signal. The sensor showed a detection range of $0.31–1.55 \times 10^{-6}$ M and a LOD of 1.55×10^{-6} M.

Alternatively, CDs-based MIP was reported by Sun et al. to detect alpha-fetoprotein (AFP).[280] AFP, an oncofetal glycoprotein

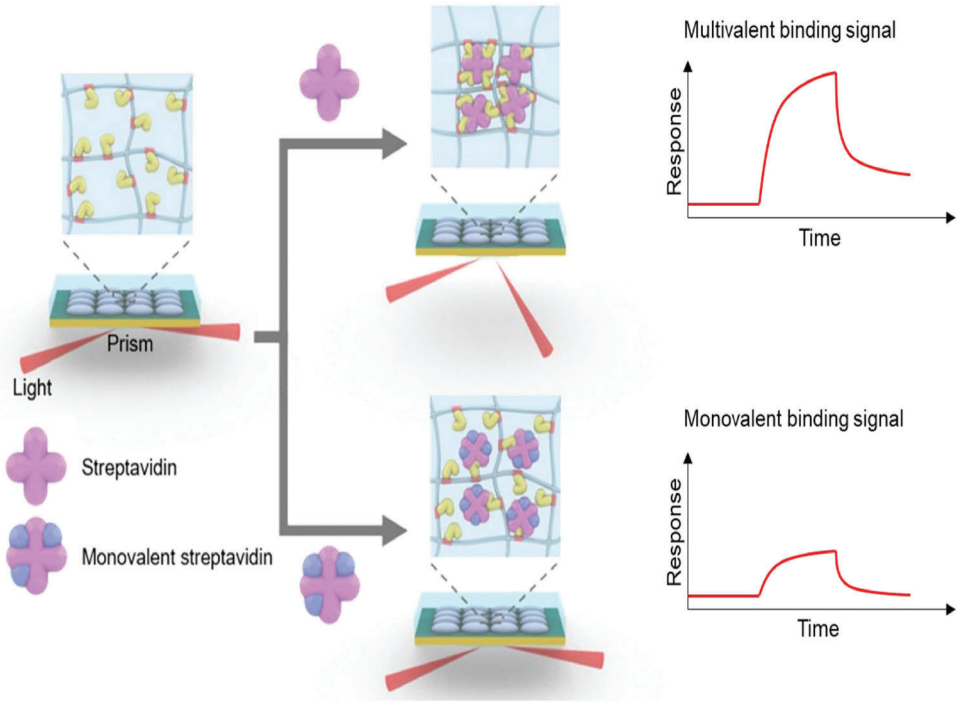

Figure 77. SPR analysis of monovalent/multivalent analytes. Reproduced with permission.[214] Copyright 2020, American Chemical Society.

used as a tumor marker of hepatocellular carcinoma, plays an important role in clinical diagnostics. The MIPs with different compositions were prepared with vinyl-functionalized CDs (V-CDs) as transducer elements and support materials, AFP as the template protein, NIPAM and VPBA as thermo-responsive, and pH-responsive monomer, APS and MBAM as initiator and cross-linker, respectively (**Figure 79**). Under basic conditions and above LCST, VPBA units interact with the *cis*-diol groups of AFP and exhibit enhancement of fluorescence spectra. The MIPs showed a good linear response to AFP in a concentration range of 10 to 100 ng mL^{-1}, with an LOD of 0.474 ng mL^{-1}. Using PNIPAM-based MIP other proteins like myoglobin,[281] and fibrinogen[282] can be detected. Peptides, units of protein,[283] could also be detected using the same method.

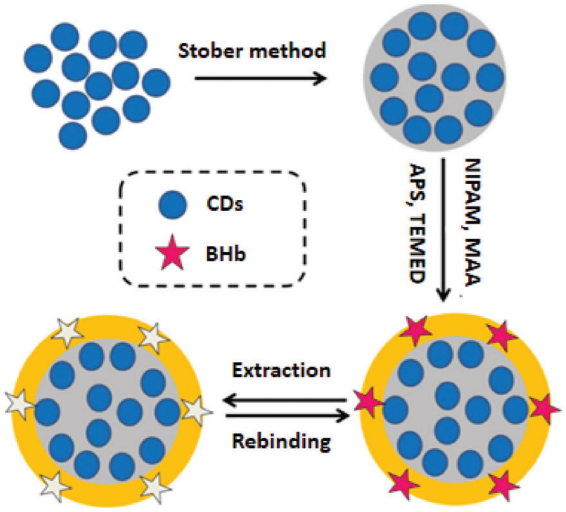

Figure 78. Preparation of MIP CD@SiO_2@MIP. Reproduced with permission.[279] Copyright 2020, Springer Nature.

Protein detection using the etalon device is another interesting work of the Serpe group.[113,114] They have demonstrated the use of PNIPAM microgels for the detection of Estradiol-17β (E2) using the etalon device.[284] E2, considered one of the most active estrogens, is necessary for the development and maintenance of female reproductive tissues. Varying the concentration of it causes health problems like sexual precocity in young females, and feminization in males. As a result, detecting it is extremely vital. In this report poly(*N*-isopropylacrylamide-*co*-acrylic acid) [P(NIPAM-*co*-AAc)] microgels were formed via surfactant-free, free radical precipitation polymerization using cross-linker MBAM, and etalon device was fabricated using Au layer. Then the Au layer of etalon was modified with thiol-modified 75-mer anti-E2 DNA aptamer (E2-Ap75: 5′- HS-(CH2)6-ATACGAGCTTGTTCAATACGAAGGGA TGCCGTTTGGG CC-CAAGTTCGGC ATAGTGTGGTGAT AGTAAGAGCAATC-3′) and 35-mer anti-E2 DNA aptamers (E2-Ap35: 5′-HS-(CH2)6-AAGGGATGCCGTTTGGGCCC AAGTTCG GCATAGTG-3′) via S–Au binding. In the presence of E2 aptamer, etalon binds to it and forms a rigid structure that prevents salt or ions from passing through the microgel; however, when E2 aptamer is absent, it forms a loose structure that allows salt to pass through and causes a change in optical property (**Figure 80**). So, observing optical property E2 can be detected. The etalon exhibited a dynamic range of 0.9–200 pg mL^{-1} with a calculated LOD of 0.9 pg mL^{-1} (3.2×10^{-12} M) E2, and the lowest measured concentration of E2 is 5.0 pg mL^{-1}.

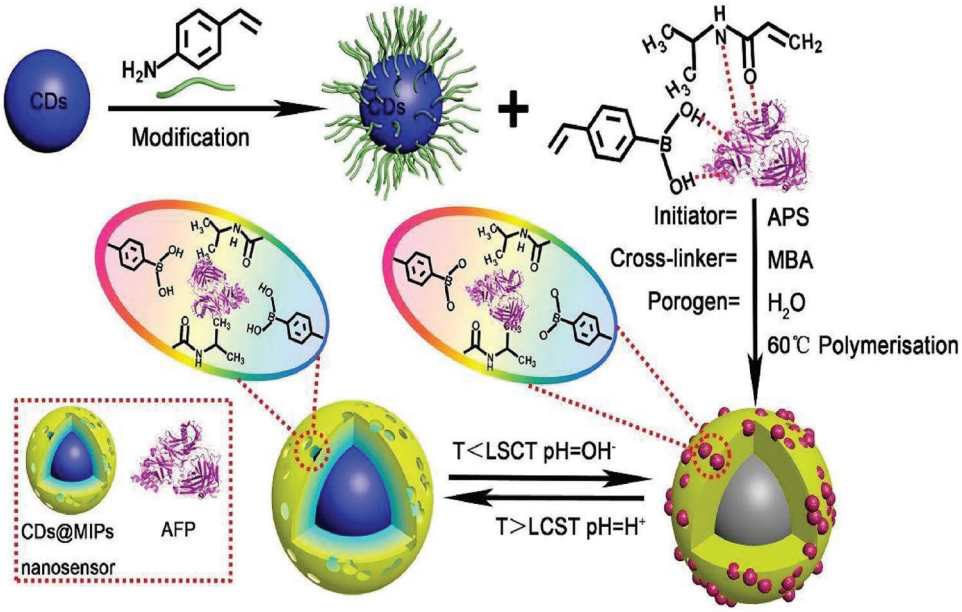

Figure 79. Synthesis of MIP with sensing assay. Reproduced with permission.[280] Copyright 2019, Royal Society of Chemistry.

The same group in another example reported an etalon device having progesterone (P4) sensing ability.[285] P4 is an important steroid hormone due to participation in the reproduction cycle and is necessary for the maintenance of pregnancy in humans and animals. Here also P(NIPAM-*co*-AAc) microgel was prepared using temperature-ramp, surfactant-free, free-radical precipitation polymerization, and etalon was made by this microgel. Then anti-P4 antibody E2 was attached to a microgel with EDC and *N*-hydroxysuccinimide (NHS). In the presence of P4 microgels collapsed, forming a blue shift in the optical properties of the device. By observing the shift of the reflectance peaks the amount of P4 can be detected. The fabricated sensor showed a linear detection range of 0.28 to 30 ng mL^{-1} P4 with a LOD of 0.28 and 0.25 ng mL^{-1} at room temperature and 30 °C, respectively.

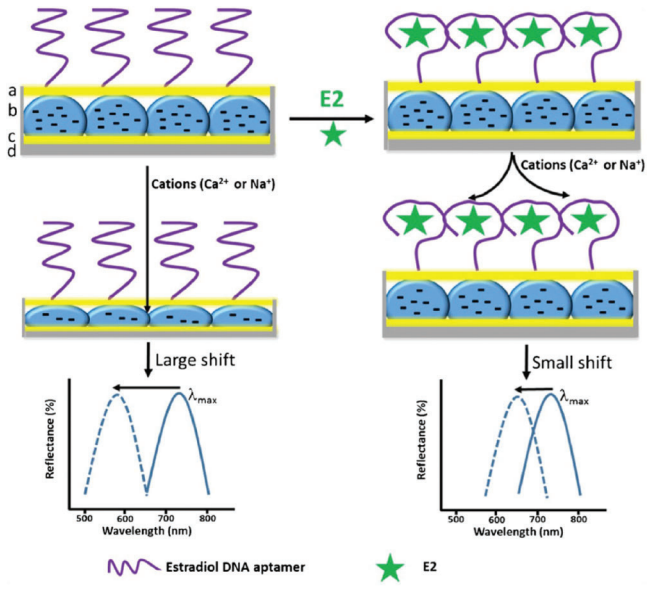

Figure 80. Response of etalon towards E2. Reproduced with permission.[284] Copyright 2018, Springer Nature.

A biosensor for mouse immunoglobulin G (IgG), a glycoprotein was prepared using an etalon device.[286] Here PNIPAM-*co*-*N*-(3-aminopropyl) methacrylamide hydrochloride (APMAH) microgel-based etalons coated with enzyme-responsive/reactive species were used to detect biomolecules. First, alkaline phosphatase-modified goat anti-mouse IgG (AP-GAM) ($F(ab')_2$ fragment specific to mouse IgG) and mouse IgG were mixed in solution, and after sometime unbound AP-GAM isolated in the presence of the magnetic field. The unbound AP-GAM was added to the microgel in the etalon device to neutralize the positive charge APMAH on the microgel due to the degradation of a phosphate-containing polymer layer on top of the etalon produces negative phosphate group which caused a change in reflection peak corresponding to mouse IgG (**Figure 81**).

It has been demonstrated that the use of MIPs can lead to the development of highly sensitive and selective methods for identifying proteins and peptides, with a sensitivity increase of at least two times compared to non-imprinted polymers. Most of the time, the thermoresponsiveness of PNIPAM has been found to increase the sensor's sensitivity. Since the majority of the examples were assessed using real samples—such as serum, bodily fluid, or tissue—and their low cytotoxicity was verified, these sensors have been demonstrated to be suitable for imaging living cells. The developed sensor showed strong selectivity and a LOD as low as 10×10^{-9} M.

3.1.4. DNA Sensing

Deoxyribonucleic acid or DNA is the hereditary material in humans and almost all other organisms. It consists of two polynucleotide chains that coil around each other to form a double

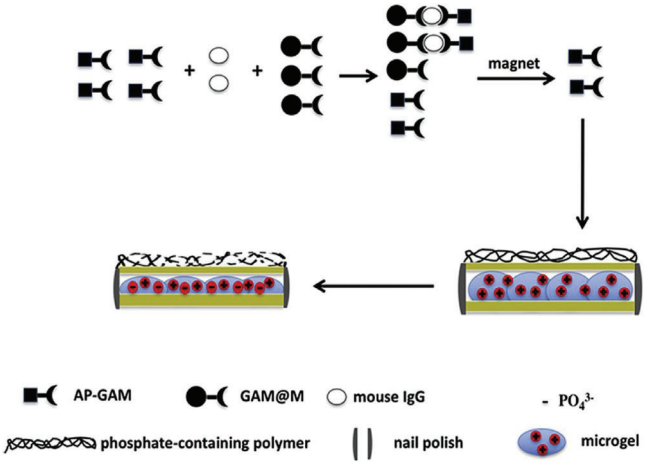

Figure 81. The sensing mechanism of etalon. Reproduced with permission.[286] Copyright 2017, Elsevier Ltd.

helix carrying genetic instructions for the development, functioning, growth, and reproduction. Detection of DNA in body fluids can provide the possibility of early disease diagnosis and hence the chance to improve quality of life. Scientists have reported many techniques and along with them, the thermoresponsive PNIPAM-based system draws considerable attention. The Serpe group in their reports explored a device named etalon. Using this etalon DNA can be detected.[108,109] In another example, nucleobase containing PNIPAM was prepared for the DNA sensor.[287] A fluorescent sensor was also prepared for the sensing of DNA.[288] Chen et al. prepared a DNA sensor by using a microfluidic device where PNIPAM was tethered on a silicon surface.[92,289,290] Their group designed a block copolymer that can identify DNA single-base mismatches.[291] Azido-terminated PNIPAM brushes were grafted onto thin Au films on silicon as a bottom electrode and single-stranded DNA (ssDNA) presenting a 4-pentynoic acid succinimidyl ester unit were grafted onto the azido-terminated PNIPAM brushes through a click reaction, forming PNIPAM-*b*-ssDNA copolymer brushes (**Figure 82**). The complex was stabilized via bio-multiple hydrogen bonds (BMHBs) by which the resistivity of the structures decreased by enhancing the proton transfer. Whereas, in the presence of DNA, a competition between BMHBs and complementary HBs occurred which caused phase transformation and inhibition of proton transfer followed by increasing resistance. Again, in the absence of a DNA base pair "proton leakage" occurred to decrease the resistivity at temperatures below the LCST for adenine and guanine units. Above LCST thymine and cytosine mismatches were identified due to disruption of the BMHBs at increased temperatures.

3.1.5. Other Biomolecules Sensing

There are some other examples of biomolecules that can be detected by PNIPAM. Urea is the chief nitrogenous end-product of the metabolic breakdown of proteins in all mammals and some fishes. Chronic kidney disease (CKD) is on the rise these days, making urea sensing a critical tool. Goh et al. introduced urease-loaded PNIPAM hydrogel to develop an osmotic urea sensor.[292]

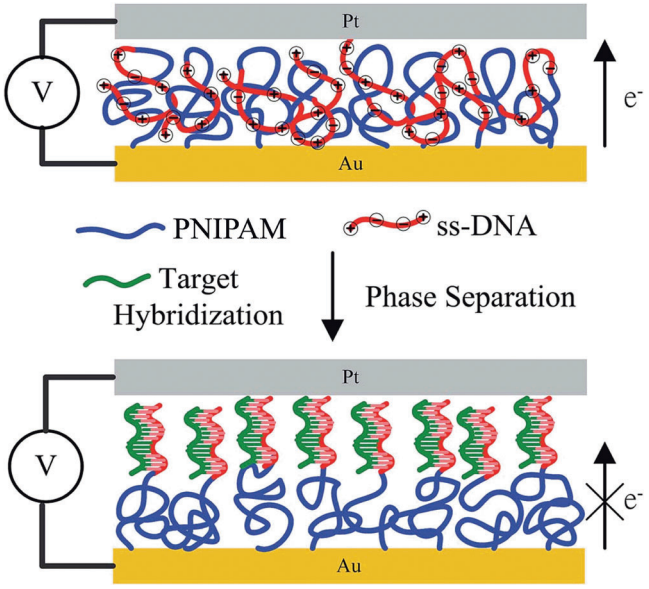

Figure 82. Fabrication of system with DNA sensitive mechanism. Reproduced with permission.[291] Copyright 2017, Royal Society of Chemistry.

The introduction of urea in a salt solution caused binding with urease and the osmotic pressure was increased corresponding to urea concentration using a multiphysics model.

Cyclodextrins (CDs) are cyclic polysaccharides composed of several glucopyranose units. In comparison to α-CD and β-CD, γ-CD has a larger internal cavity, higher bioavailability, and higher solubility. Therefore, it is widely used in the food and pharmaceutical industries. Wei et al. reported a microgel for γ-CD detection using adsorption property.[293] Here poly(*N*-isopropylacrylamide-*co*-acryloylamidobenzo-12-crown-4) (PNB) microgel was prepared by the formation of poly(*N*-isopropylacrylamide-*co*-acrylic acid) (PNA) microgels followed by modification benzo-12-crown-4 ($B_{12}C_4$) units via condensation reaction (**Figure 83**). Since the pore size of crown ether and γ-CD are similar, the crown ether complex preferentially adsorbed γ-CD, increasing the volume of the microgel.

3.2. Drug Sensing

A drug is a chemical substance or construct that has a biological impact when consumed by a living organism. It has wide application in the biological system. Its wide range of applications makes the detecting process vital. PNIPAM-made systems can have the potential to detect drugs and the most popular method is a MIP based system. Glycopeptide antibiotics are utilized in the treatment of serious gram-positive bacterial infections. Chen et al. prepared fluorescent MIP incorporating Mn-doped ZnS QDs as a fluorescent probe for detecting telavancin, a semisynthetic glycopeptide antibiotic.[294] The MIP was synthesized with amino-capped Mn-doped ZnS QDs, VPBA, NIPAM, AAm, and mannose-tryptophan (MT) as a template. The boronic moiety presented here can bind with the template over glucose due to the shape exclusion of the imprinted cavity and fluorescence intensity was increased. The temperature should be more than LCST as at low-temperature swelling of PNIPAM deformed the

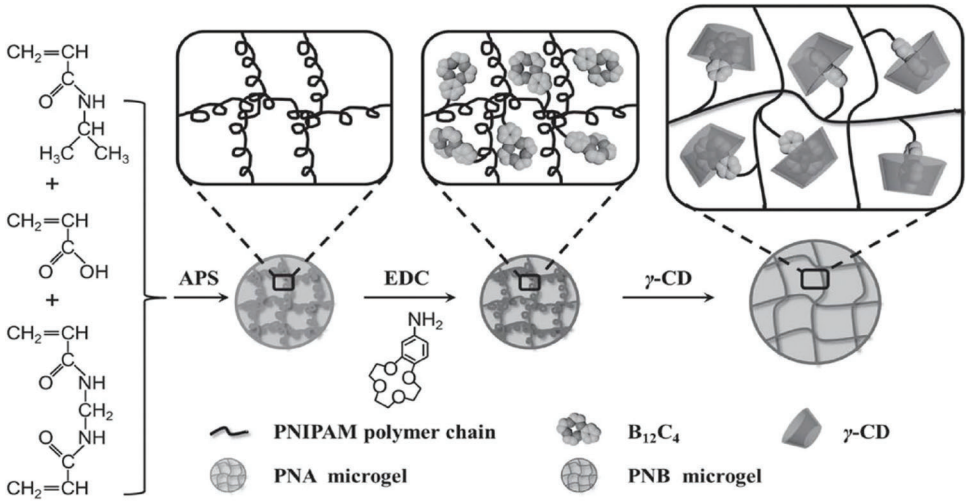

Figure 83. Synthesis of microgel with adsorption property. Reproduced with permission.[293] Copyright 2017, Wiley-VCH.

imprinted cavity. The MIP showed good linear correlations over the concentration range of 3.0 to 300.0 μg L^{-1} and with a low LOD of 1.0 μg L^{-1}.

The electrochemical approach is an alternative to the MIP method for detecting drug molecules. Antipsychotic drug sensor consisting of PNIPAM microgel for antipsychotic drug

Chlorpromazine (CPZ).[295] Here, in a first step, a PNIPAM microgel was prepared via a temperature-ramp, surfactant-free, free-radical precipitation polymerization method with MBAM cross-linker, and a GCEwas modified with the microgel (**Figure 84**). An oxidation peak was observed at 0.67 V in the presence of CPZ due to the direct electro-oxidation of nitrogen atoms in the CPZ structure. Due to the higher surface area of the PNIPAM microgel, it adsorbed CPZ molecules and oxidized them. The fabricated system exhibited sensitivity and LOD, 0.084 μA/μM/cm^2 and 0.016 × 10^{-6} м, respectively.

Their group also published another electrochemical sensor for detecting the drug 5-fluorouracil (5-fluoro-1 hpyrimidine-2,4-dione, 5-FU).[296] 5-FU is one of the major antineoplastic agents used in chemotherapeutic regimens for metastatic colorectal, breast, stomach, pancreatic, and cervical cancer worldwide. Here conducting polymers, poly(3,4-ethylenedioxythiophene) (PEDOT) was immobilized on the PNIPAM chain to get the direct electron transfer from the microgel to the electrode. First PDEOT was synthesized from DEOT monomer by oxidative polymerization and PNIPAM microgel was formed by seeded precipitation polymerization of NIPAM monomers in the presence of MBAM crosslinker. Following that, PNIPAM microgel-encapsulated PEDOT was synthesized by seeded precipitation polymerization of NIPAM monomer in the presence of PEDOT and finally, it was dispersed on GCE to get PNIPAM-PEDOT/GCE (**Figure 85**). An oxidative current was found at temperatures over LCST due to the electron exchange mechanism,

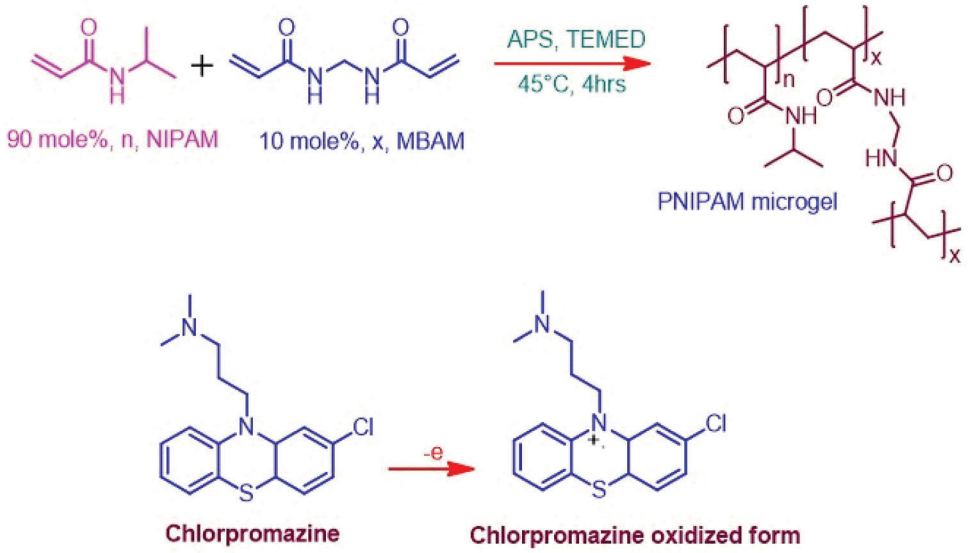

Figure 84. Synthesis of microgel and oxidation of CPZ.[295]

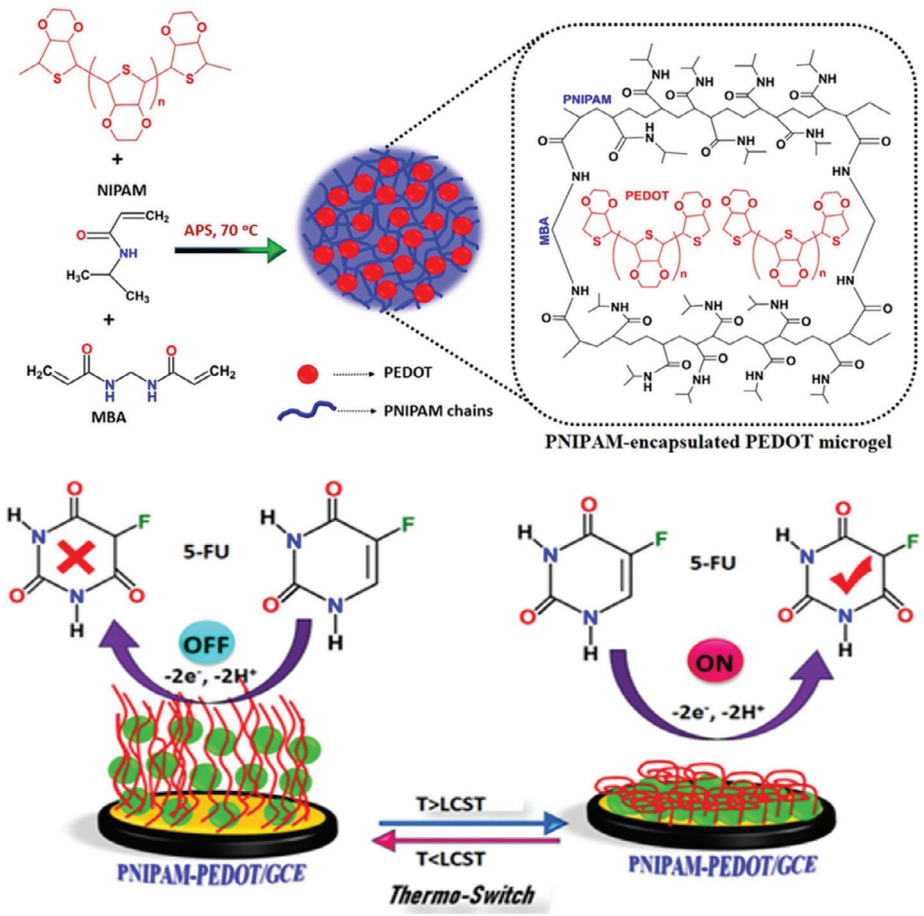

Figure 85. Synthesis of microgel with temperature-responsive "off-on" character. Reproduced with permission.[296] Copyright 2019, Elsevier Ltd.

which decreased the distance between materials and the surface of GCE, resulting in an "on" state. The sensor exhibited an LOD of 15×10^{-9} M at 40 °C.

Their group this time detected metoprolol (MTP) [2-propanol, 1-[4-(2-methoxyethyl)phenoxy]−3-[(-methylethyl)amino]-,(±)-,[R-(R*,R*)]−2,3-dihydroxy butanediol ate] with a polymer nanocomposite using a nanocomposite.[297] MTP is a very popular antihypertensive drug belonging to the class of β-blockers (β(1)-adrenergic receptor antagonists), used for the treatment of hyperthyroidism, angina, arrhythmia, hypertension, and myocardial infarction diseases. It is so sensitive that alittle extra intake may cause harmful effects like the provocation of cardiac failure, bradycardia, fatigue, bronchospasm, hypotension, and hypoglycemia. Here, the nanocomposite based on poly(styrene-*co*-*N*-isopropylacrylamide) hybrid tungsten dioxide (WO_2@PS-*co*-PNIPAM) was synthesized by facile ultrasonic irradiation.

The same technique was used here also, that is below LCST polymer chain extension buried electroactive sites of WO_2 to occur electronic transfer and indicate the "off" state. However, above LCST, WO_2 was underwent an electro-oxidation reaction, and the response current indicated "on" state (**Figure 86**). The composite exhibited a sensitivity of 2.21 μA/μM/cm^2, a wide dynamic range of 0.05–306 × 10^{-6} M, and a low LOD of 0.03 × 10^{-6} M for MTP.

Using the same temperature-responsive "on-off" switch sulfamethazine [(4-amino-N-(4,6-dimethyl-2-pyrimidinyl)benzenesulfonamide, (SFZ)] was detected.[298] It is mainly used to provide relief from respiratory tract diseases and gastrointestinal in veterinary clinical treatment. However,

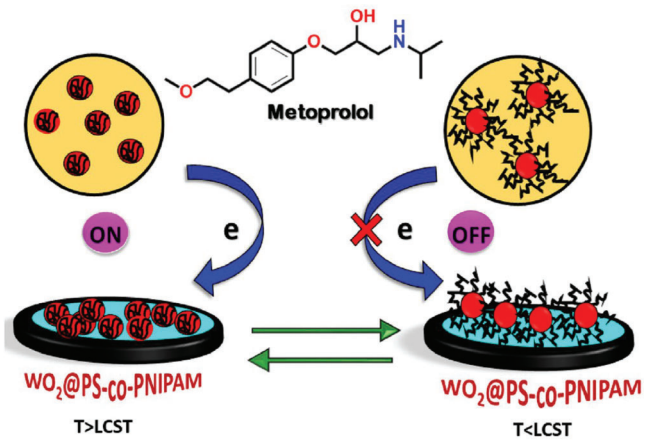

Figure 86. The sensing mechanism of composite proposed by Mutharani et al. Reproduced with permission.[297] Copyright 2020, Elsevier Ltd.

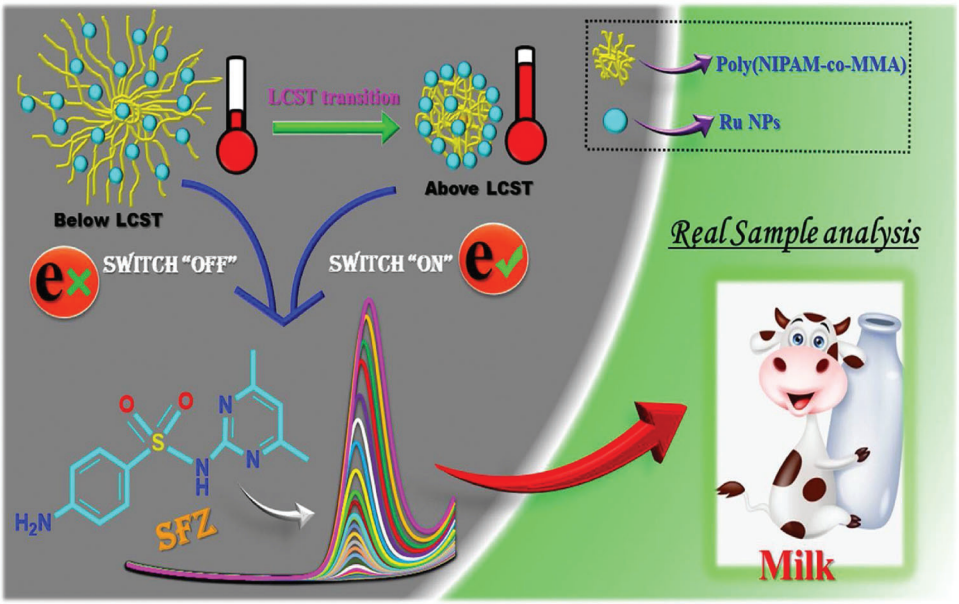

Figure 87. The detection process of SFZ. Reproduced with permission.[298] Copyright 2020, Elsevier Ltd.

excessive intake can cause harmful effects on the human body. First, P(NIPAM-*co*-MAA) was prepared by precipitation polymerization and nanocomposite was designed with ruthenium nanoparticles (RuNPs) by coordination of carboxylic —COOH groups with the surface of metal oxides. Then the GCE was modified with composite. Below the LCST the electroactive sites of Ru were closed to oxidation of SFZ leading to a "switch-off" state and above LCST due to the shrinking of polymer electroactive sites were exposed to oxidation of MGC leading to as "switch-on" state (**Figure 87**). The corresponding peak current refers to the concentration of MGC. The sensor exhibited a linear concentration of $0.01–491 \times 10^{-6}$ M and a very low LOD of 5×10^{-6} M SFZ at 40 °C in the real sample.

Another electrochemical sensor was reported by Zhao et al. for sensing the drug paracetamol.[299] Paracetamol (*N*-acetyl-para-aminophenol or APAP), is a very popular antipyretic analgesic, commonly used for treating colds, headaches, fever, neuralgia, arthritis, and post-operative pain symptoms. However, excessive intake of APAP can result in liver damage and even coma or death in severe cases. Here electrochemical "on/off" detection of APAP (paracetamol) was achieved using the thermosensitive PS-PNIPAM -PS, carboxylated multi-walled carbon nanotubes (MWCNTs-COOH), and amino-functionalized graphene quantum dots (N-GQDs). Among them, MWCNTs provide excellent electrochemical performance and electrocatalytic performance for sensors. Graphene quantum dots (GQDs) can enhance the stability and dispersibility of carbon nanotubes, and promote close bonding of the polymer and MWCNTs. The triblock polymer was prepared with RAFT polymerization. Then the obtained PS-PNIPAM-PS/MWCNTs-GQDs were dropped onto GCE to form PS-PNIPAM-PS/MWCNTs-GQDs/GCE electrodes. At the temperature below LCST due to stretching the electroactive sites of the carbon nanocomposite were buried and consequently APAP could not penetrate through the polymer to achieve electronic exchange, representing the "closed" state (**Figure 88**). Whereas above the LCST, the polymer shrank to expose the electroactive sites and enlarge background currents, the paracetamol underwent the redox reaction normally and generated the response current, representing the "on" state. The sensor exhibited a wide detection range ($0.1–7.0 \times 10^{-6}$ M and $7.0–103.0 \times 10^{-6}$ M) and a low LOD of 66×10^{-9} M for paracetamol.

To design drug sensors, scientists took advantage of the reduction of functional groups present in drug molecules. GCEs featuring PNIPAM layers and their electrochemical response were notable means for detection. Below its LCST the polymer layer covers the GCE surface and inhibits the electron transfer to the GCE surface. Whereas, the opposite phenomena were observed above the LCST which introduced off-on characteristics. The sensor applicability was tested with real samples such as milk, human urine, and human blood serum, and the results were satisfactory. The developed sensor demonstrated a low LOD of 5×10^{-9} M, good selectivity, and a wide detection range.

3.3. Biomarker Sensing

Biomarkers are molecules that measure a biological state. They are indicative of normal biological processes, pathogenic processes, or pharmacologic responses to therapeutic intervention, and easily monitored by using blood, urine, or soft tissue samples. PNIPAM-based systems were prepared which exhibits responsive character in the presence of biochemical stimuli and can sense the biomarkers. Adenosine is utilized as a possible biomarker for monitoring the progress of lung cancer. Wang et al. synthesized AgNPs-embedded PNIPAM electrospun nanofiber mats to detect the biomarker adenosine in urea solutions using SERS, which is a powerful technique for the ultrasensitive detection of biological and chemical species.[300] At first, PNIPAM/2- aminoethyl methacrylate hydrochloride (AEMA) copolymer (PNIPAM-NH_2) was prepared via radical

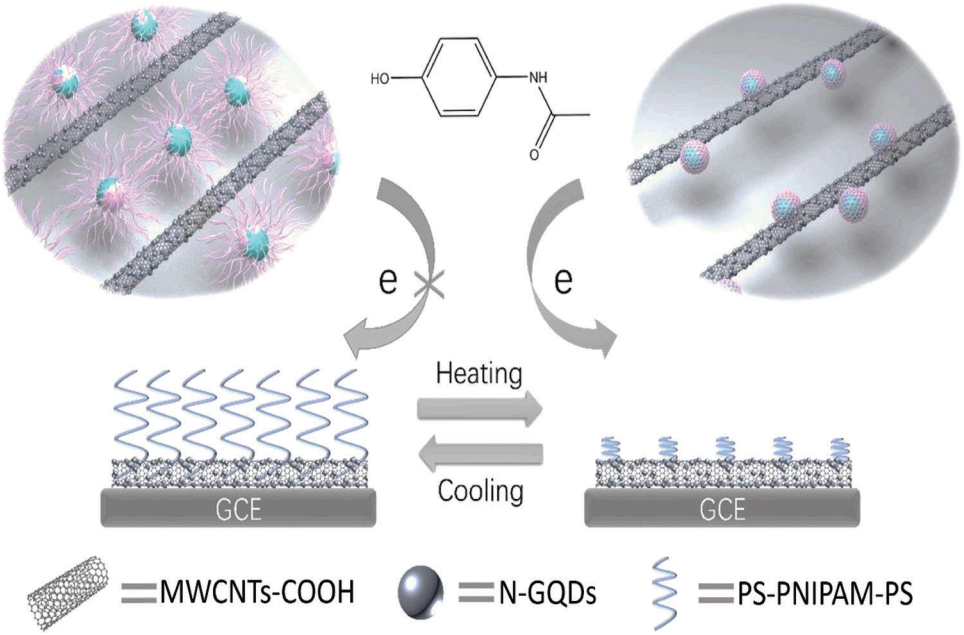

Figure 88. Temperature dependence electrochemical response of polymer. Reproduced with permission.[299] Copyright 2019, Royal Society of Chemistry.

polymerization and by electrospinning PNIPAM-NH_2 nanofiber was formed. Again, after adding AgNPs to the PNIPAM-NH_2 solution, AgNP/PNIPAM nanofibers were synthesized by electrospinning. Finally, AgNP/PNIPAM nanofibers mats were formed by adding glutaric dialdehyde (GA) which acted as a crosslinker (**Figure 89**). Above LCST, the hydrophobic PNIPAM entraps more hydrophobic adenosine and excludes more hydrophilic urea molecules with the greatest enhancement in SERS spectra. The fabricated system exhibited a LOD as low as 10^{-7} M.

Lactate is a biomarker for cellular anaerobic metabolism or glycolysis. It acts as an energy storage molecule produced during physical exertion and low muscle oxygen. Mugo and Dhanjai detected lactate in sweat by preparing an imprinted polymer.[222] In the salt sensing section, we have discussed its structure. Lactate responsiveness was achieved by modifying the surface of PNIPAM@CNC/CNT with lactate imprinted PANI polymerized in the presence of PBA. The PBA unit made a bond with lactate and due to the matching of imprinted cavities lactate bounded with MIP and capacitance was increased. Due to insulation, PNIPAM increased electron transfer resistance. The system exhibited an LOD as $0.10 \pm 0.04 \times 10^{-3}$ M, and a limit of linearity of approximately25×10^{-3} M.

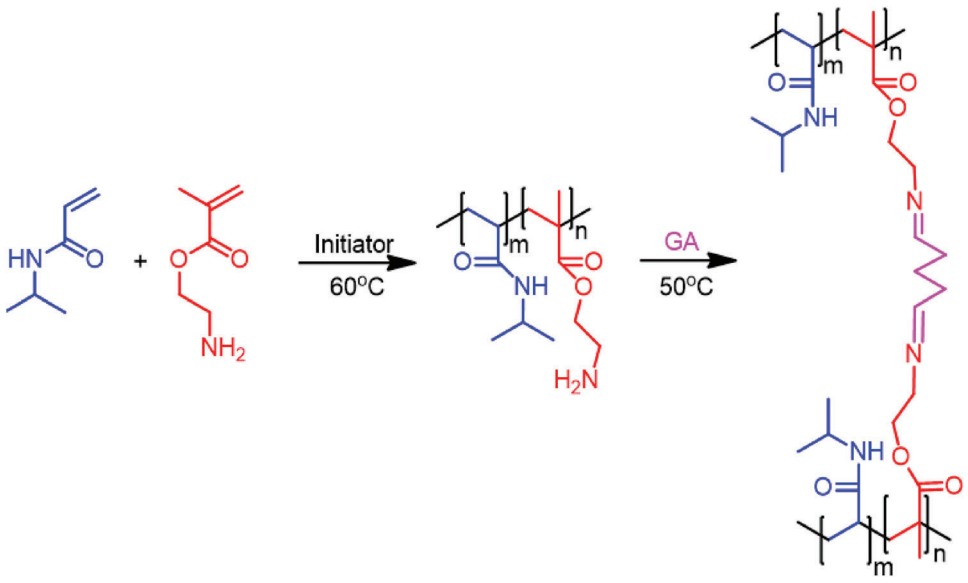

Figure 89. Schematic diagram of polymer synthesis by Wang et al.[300]

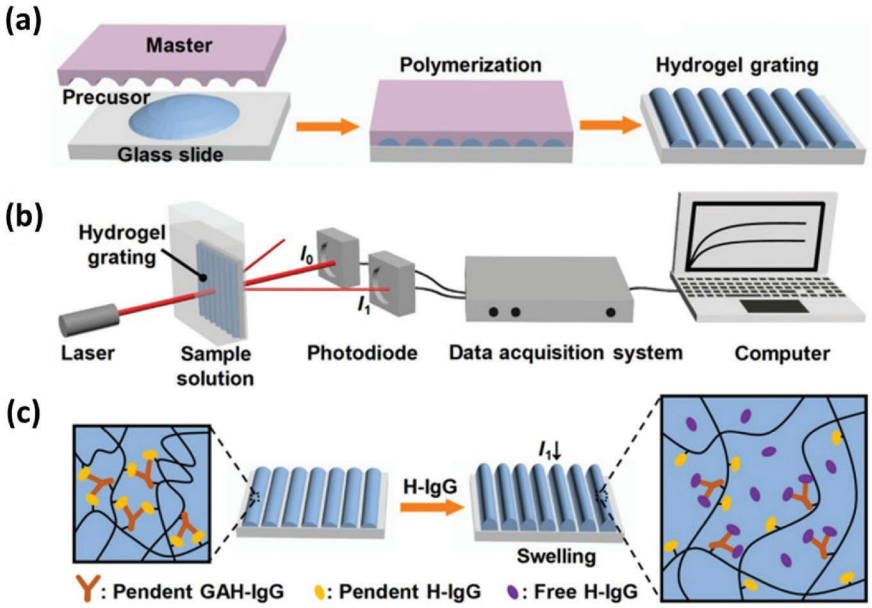

Figure 90. a) Schematic representation of the preparation of hydrogel grating by polymerization, b) Formation of the optical detection platform, c) Pictorial representation of the mechanism for H-IgG sensing. Reproduced with permission.[301] Copyright 2020, American Chemical Society.

Biomarker human immunoglobulin G (H-IgG) can indicate diseases such as primary or secondary immunodeficiency and infection diseases. Zhao et al. fabricated a hydrogel grating immunosensor for detecting the biomarker human immunoglobulin G (H-IgG).[301] First, vinyl-modified H-IgG and goat anti-human immunoglobulin G (GAH-IgG) were synthesized with previously prepared silanized glass slides and *N*-acryloxysuccinimide. Then adding NIPAM monomer and biocompatible crosslinker tetra-arm star-polyethylene glycol-acrylamide (PEG-AAm) hydrogel grating was formed (**Figure 90**). Primarily GAH-IgG made a bond with pendant H-IgG. However, upon the introduction of free H-IgG, the pendent GAH-IgG in the hydrogel interacts with it and the binding constant is higher than the previous one. Therefore, the previously formed complex started decomplexation, and swelling of hydrogel occurred. Therefore, the refractive index and diffraction efficiency changed. Observing this optical change H-IgG can be detected with an LOD as low as 1.3×10^{-8} M.

The use of the thermoresponsive polymer PNIPAM has not been investigated extensively in the field of biomarkers. However, novel MIP approaches and an antigen–antibody association technique were used to detect several biomarkers. The applicability of the fabricated sensor was utilized with a real sweat sample, showing satisfactory results. The LOD was noted as 0.1×10^{-9} M for lactate (biomarker) with high selectivity. The sensor's applicability was verified in lake water, tap water, and milk samples

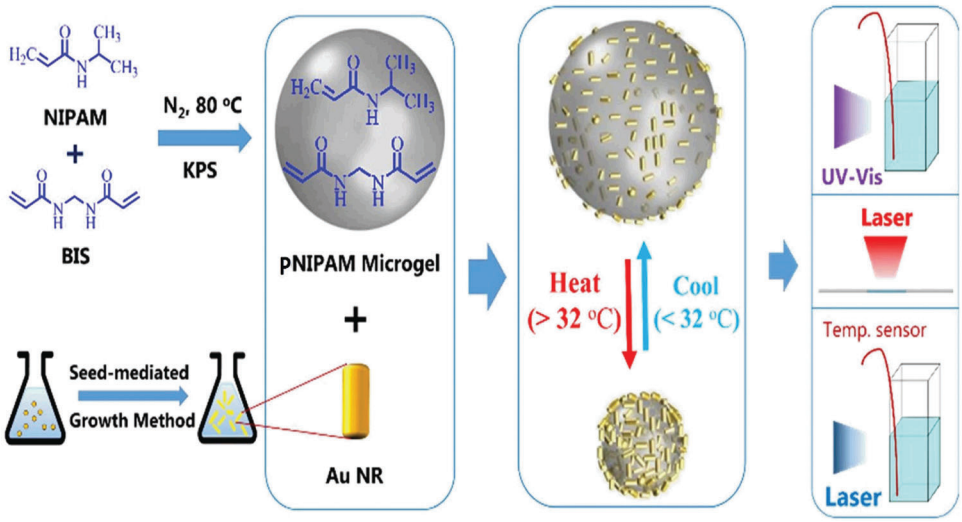

Figure 91. Preparation of PNIPAM@AuNRs composites. Reproduced with permission.[304] Copyright 2020, Elsevier Ltd.

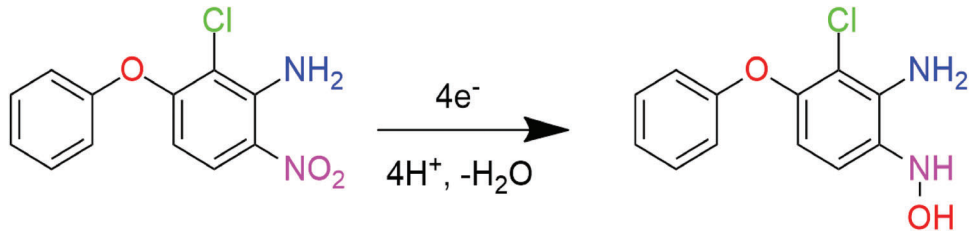

Figure 92. Electrochemical reaction of AFN.[305]

for living cell detection. The calculated LOD was as low as 0.01×10^{-9} M with relatively fast response time (6–10 min).

3.4. Living Cell Detection

Bacterial living cells have been detected by using PNIPAM. The hydrophilic to hydrophobic transfer in physiological temperature allows bacteria growth. Currently, the majority of diseases are caused by infection. As a result, the need for pathogen detection grows every day. The use of PNIPAM over other systems gets an advantage due to its sensitivity at physiological temperature. Khan et al. reported an electrically-receptive membrane by combining graphene-nanoplatelet (GR) with thermo-responsive polymer (PNIPAM) for detecting bacterial strains (*E. coli*, *S. Mutans*, and *B. Subtilis*).[302] Electrically receptive membrane graphene-nanoplatelet (GR) combined with thermo-responsive polymer (PNIPAM) to get a composite using the optimized spin-coating technique. Interdigitated microelectrodes (IDμE) were prepared on a thin layer of PNIPAM-GR composite by depositing Au electrodes. In the presence of bacteria, the polymer shrinks which makes a change in the electrical properties of GR. Resistance increased in Gram-negative bacteria (*E. coli*), whereas resistance in Gram-positive bacteria (*B. subtilis* and *S. mutans*) decreased by about 10.31 ± 2.43% and 37.88 ± 5.25% percent, respectively, compared to *E. coli*. The system exhibited a wide range of concentration 10^1–10^5 cells mL^{-1} and a lower LOD of 5 cells mL^{-1}.

Highly branched PNIPAMs were used to identify Gram-positive bacteria (Staphylococcus aureus). In this context, Swift et al. synthesized the polymer using self-condensing reversible addition–fragmentation transfer polymerization (SCVP-RAFT).[303] Where, Nile red was added to the main chain, and Vancomycin was added at the end of the chain. The fluorescence intensity was increased in bacteria due to the use of highly branched PNIPAM.

3.5. Pesticide Sensing

Pesticides are introduced to control pests, mostly killing caterpillars and other critters that feed on crops. However, pesticides cause severe effects on several other species besides their intended targets, including humans. Pesticides contain a wide range of compounds including insecticides, fungicides,

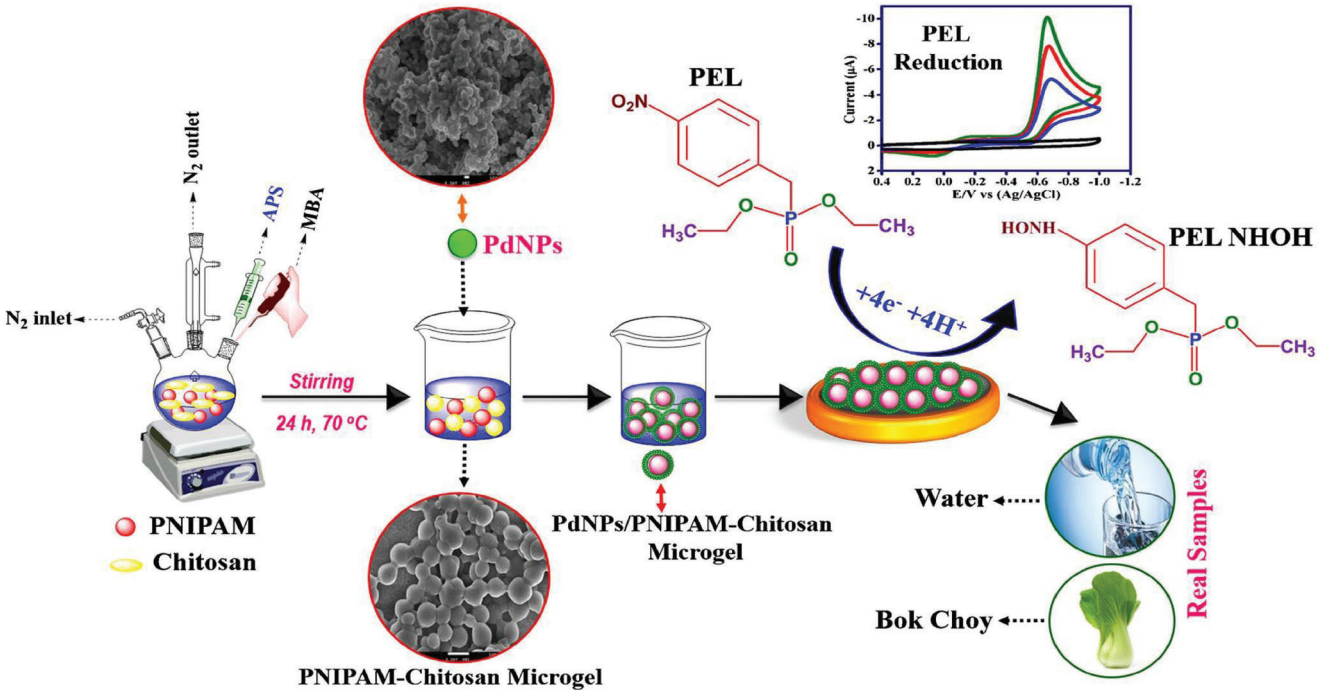

Figure 93. Fabrication of electrode with the detection process. Reproduced with permission.[306] Copyright 2019, Springer Nature.

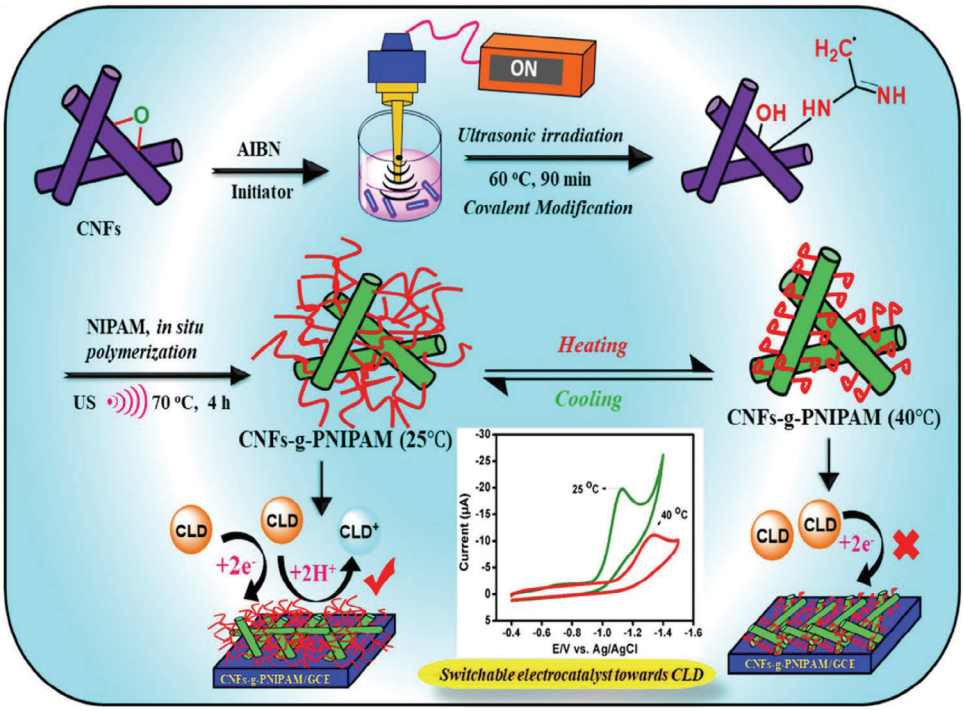

Figure 94. Synthesis of the sensor with the fabrication of a detection mechanism with "on/off" switchability. Reproduced with permission.[307] Copyright 2019, Elsevier Ltd.

herbicides, rodenticides, molluscicides, nematicides, plant growth regulators, and others. Due to their harmful effects, most of the developed countries have banned the use or import of produce treated with specific pesticides. Considering their harmful effects, careful detection and quantification techniques are needed, preferably with a straightforward readout. Also here, PNIPAM has been explored as a material in the development of SERS, electrochemical, and pesticide sensors, which will be outlined in detail below. By loading PNIPAM on AuNPs, SERS microsensors were produced for detecting effective dynamic SERS substrates malachite green.[304] Using the electrochemical method pesticides can be detected. For this purpose, the excellent conductive property of polyaniline (PANI) was utilized and Cu NPs were taken for using their stability, and sensitivity to make composite materials with PNIPAM.[305] In another example, PdNPs are immobilized on PNIPAM due to their excellent electrocatalytic activities and are used for pesticide detection.[306] Carbon nanofibers (CNFs) also can be used due to their conductive property and PNIPAM was grafted on it to make it more useful for sensory use for pesticides.[307] Immobilizing electrochemiluminescence (ECL) molecules into the PNIPAM matrix can lead to the formation of thermosensitive ECL hydrogels which can detect pesticides using a variation of electrochemiluminescence property.[308]

The fungicide malachite green (MG) is harmful and causes serious risk due to its teratogenicity, mutagenicity, and carcinogenesis. Hu et al. introduced surface-enhanced Raman scattering (SERS) using AuNRs for the detection of MG in fish fillets.[304] They first created AuNRs utilizing a seed-mediated growth technique in the presence of CTAB, as well as a PNIPAM microgel. The interaction of positively charged CTAB on AuNRs with negatively charged PNIPAM microgel produced PNIPAM@AuNRs nanocomposites (**Figure 91**). For SERS, prominent enhancement from localized surface plasmon resonance (LSPR) on the surface of nanostructures, while surface-enhanced resonance Raman scattering (SERRS) provided additional enhancement effect through molecular resonance for analytes that contain chromophore with the electronic transition at the wavelength near the excitation wavelength. Above the LCST due to the collapsed state of the nanocomposite, the density of "hot-spots" was increased, so SERS intensity was increased significantly. Besides MG, the additives, sodium cyclamate (SC) and sodium saccharin (SS) can be detected. The LOD was 1.3×10^{-9} M for MG, 5.8×10^{-9} M for SC, and 3.5×10^{-8} M for SS, respectively.

Herbicides are another example of pesticides, which can also cause prominent and substantial health issues when irresponsibly released into the environment. Mutharani et al. prepared a composite sensing film (PNIPAM/PANI-Cu) by mixing PNIPAM, the conducting polymer poly(aniline), $Cu(NO_3)_2.3H_2O$ via chemical polymerization method and drop cast onto bare GCE to prepare an electrochemical device to detect herbicides, aclonifen (AFN) or 2-chloro-6-nitro-3-phenoxyaniline.[305] The cathodic peak was shown due to the reduction of the $-NO_2$ group to $-NHOH$ group with the four electrons (e^-) and four protons (H^+) (**Figure 92**). The cathodic peak current was recorded by cyclic voltammetry (CV). The sensor exhibited a two-detection range ($0.01–10 \times 10^{-6}$ M and $18–76 \times 10^{-6}$ M) with the low LOD was found to be 0.009×10^{-6} M. The authors demonstrated that at a temperature lower than LCST no significant signal was formed owing to the obstacle of the polymer and difficulty in changing electrons during the AFN reduction process. Whereas, at a temperature above the LCST, significant

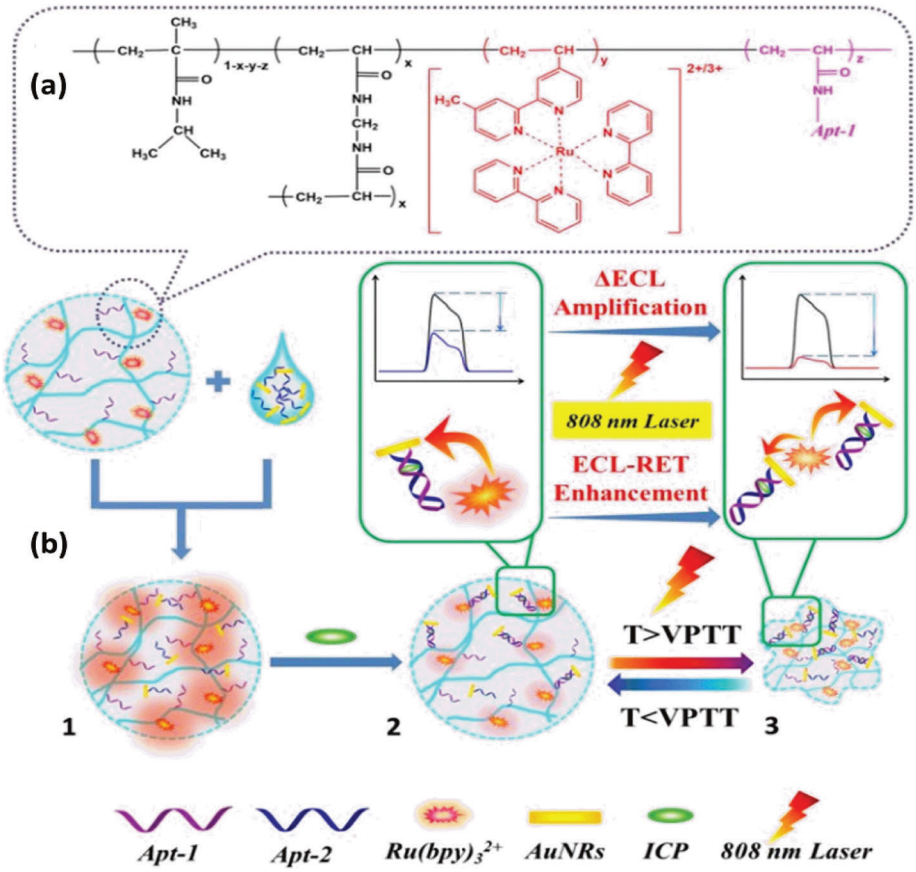

Figure 95. a) Structure of T-ECL hydrogel, b) Schematic illustration of PT-ECL hydrogel for ICP detection where 1 is T-ECL hydrogel, 2 is PT-ECL hydrogel and 3 is ICPPT-ECL hydrogel at swollen state. Reproduced with permission.[308] Copyright 2020, American Chemical Society.

signal was observed which proves temperature reversibility and stability.

Alternatively, the same group introduced an electrochemical sensor for the detection of organophosphorus pesticide paraoxon-ethyl (PEL) based on a GCE modified with a composite material containing palladium nanoparticles (PdNPs).[306] The cross-linked PNIPAM-Chitosan microgel was synthesized by a surfactant-free emulsion polymerization method by MBAM crosslinker. Then PdNPs were synthesized and microgel was decorated with it to make a composite. Finally, the composite was

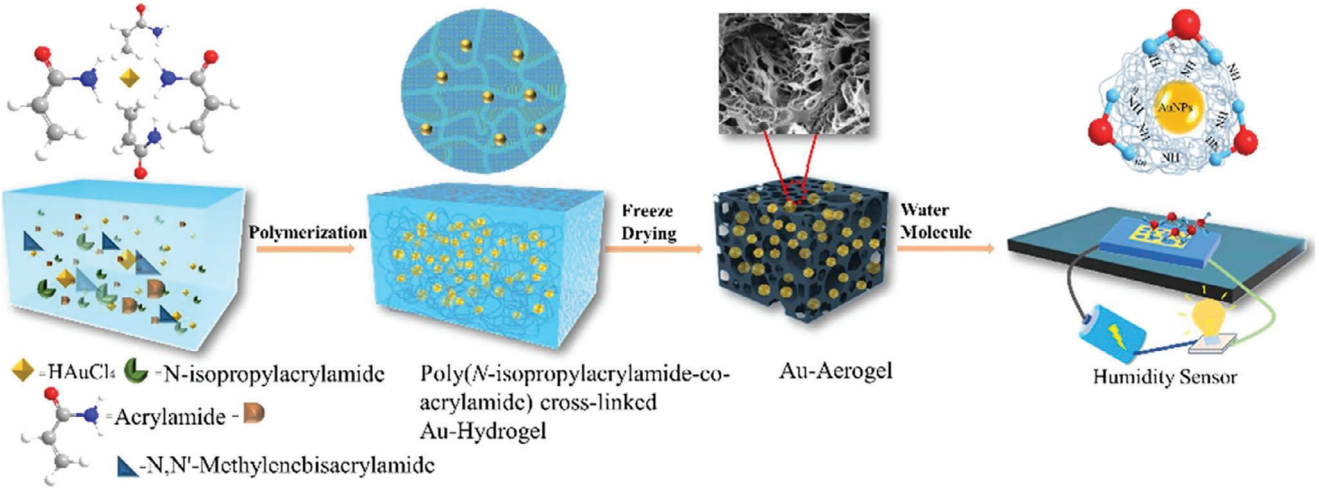

Figure 96. Fabrication of aerogel and application in humidity sensing. Reproduced with permission.[309] Copyright 2018, American Chemical Society.

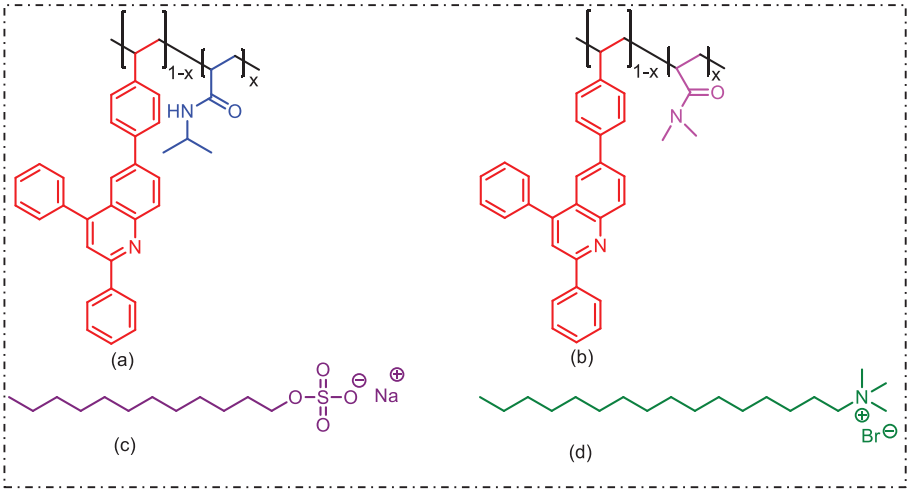

Figure 97. Chemical structure of a) P(NIPAM-*co*-SDPQ), b) P(DMAM-*co*-SDPQ), c) sodium dodecyl sulfate (SDS), d) gexadecyltrimethylammonium bromide (CTAB).[311]

formed on GCE by the drop-casting method. The PNIPAM microgel stabilized the composite by electronic interaction between positively charged chitosan and negatively charged PNIPAM, resulting in the decrease of size of PNIPAM. In the presence of PEL prominent cathodic peak and redox couple observed which is attributed to the reduction of PEL involves a transfer of four electrons ($4e^-$) and four protons ($4H^+$) leading to the formation of phenylhydroxylamine.

By using differential pulse voltammetry, the model detected PEL in bok choy and water in the 0.01×10^{-6} M to 1.3×10^{-3} M PEL concentration range with a LOD of 0.7×10^{-6} M (**Figure 93**). Their team also developed a carbon nanofiber (CNF)-based sensor to detect another neonicotinoid pesticide, clothianidin (CLD), electrochemically.[307] They used AIBN to generate a radical on the surface of the CNFs, which then initiated the polymerization with an ultrasonic horn to prepare covalently grafted CNFs-*g*-PNIPAM using the "grafting-from" strategy and adding it on GCE. In the presence of CLD two peak currents were observed, peak I current due to the reduction of $-NO_2$ group in CLD to $-NHOH$ group, and peak II ascribed to the further reduction of $-NHOH$ group to an $-NH_2$ group. At higher temperatures, PNIPAM shrinks and blocks electron transfer from CLD to CNF showing the "off" state. The system detected CLD with a sensitivity of 2.32 μA/μM/cm^2 with an LOD of 0.03×10^{-6} M (**Figure 94**).

Sun et al. reported a novel photocontrolled thermosensitive electrochemiluminescence hydrogel (PT-ECL hydrogel) for detecting the pesticide isocarbophos (ICP).[308] First T-ECL was prepared with NIPAM, one split aptamer (Apt1: acrydite-modified aptamer), and $Ru(bpy)_3^{2+}$ via free radical polymerization. Another split aptamer (Apt2: thiol-modified aptamer) was conjugated with AuNRs to form AuNRs-Apt2. Finally, PT-ECL was formed by mixing T-ECL and AuNRs-Apt2. In the presence of ICP, the conjugation of two split aptamers induced the ECL–resonance energy transfer (ECL-RET) between the Au nanorods and the $Ru(bpy)_3^{2+}$ centers. However, upon exposure to NIR light, the photothermal effect of AuNRs initiated the shrinkage of the hydrogel, resulting in the enhancement of the ECL-RET (**Figure 95**). The system exhibited ICP detection with a low LOD of 20×10^{-12} M and a wide linear range from 50×10^{-12} M to 4×10^{-6} M, with great stability and repeatability.

Similar to "drug sensing," the electrochemical method is used to detect pesticides. Here also the electron transfer phenomena are utilized to design the sensor. Electric conductive AuNR, CNF, and GCE were mixed to PNIPAM. The thermoresponsive nature controls the interaction between the pesticide and electric conductive moiety. Bok Choy extract water samples were tested to check the presence of pesticides. The designed sensor demonstrated the LOD value as 0.07×10^{-9} M and with proper design that can be used in the food industry.

3.6. Miscellaneous

A PNIPAM-based humidity sensor was designed by Ali et al.[309] They took advantage of the conductivity of AuNPs and the high surface area of a highly porous structure hybrid PNIPAM/AuNPs aerogel. This aerogel-based humidity sensor was used to detect human breath in different states such as normal breath, fast breath, and deep breath, or by different individuals such as the person in illness, smoking, and normal. AuNPs were prepared and from it, PNIPAM/AuNPs hydrogels were synthesized with NIPAM monomer. PNIPAM/AuNPs hydrogel formed PNIPAM/AuNPs aerogel which did the sensing (**Figure 96**). The aerogel having a hydrophilic group made a hydrogen bond with water. During the breathing process, the variance of water vapor was observed whereby increasing water vapor content increased the conductivity of the aerogel. Using this property a wearable sensor was prepared.

Visualization of microwaves is another fascinating use of the PNIPAM-based technology.[310] Nakamitsu et al. introduced polydiacetylene (PDA) in PNIPAM hydrogel.[310] Upon irradiation of microwaves, the color change of PDA occurred through heating of water in the hydrogel and subsequent volume shrinkage and exhibited the color change.

Surfactants are a wide range of chemicals that are characterized by their amphiphilic nature as they contain hydrophilic

and hydrophobic parts together. They are widely used in washing, wetting, emulsifying, and dispersing agents. Nevertheless, their extensive use causes damage depending on their concentration and so their detection draws attention in modern times. Ionic surfactants can also be detected using a copolymer of PNIPAM. In this context, Thivaios and co-workers designed poly(*N*-isopropylacrylamide-*co*-2,4-diphenyl6-(4-vinylphenyl) quinoline) (P(NIPAM-*co*-SDPQ)) (**Figure 97**).[311] The authors exploited the emissive properties of the SDPQ dye to detect surfactants selectively. At 22 °C and acidic conditions, the protonated form of SDPQ showed intense emission, and at a higher temperature, a weak band corresponding to the unprotonated form was predominated. Upon addition of SDS, the band corresponding to the unprotonated form disappeared and the red shift of the band observed corresponds to the protonated structure. However, in the presence of an anionic surfactant at a low temperature, the emission band corresponding to protonated form was observed and persisted until the concentration reached the critical aggregation concentration (cac) value. Further, increased concentration leads to a band corresponding to an unprotonated form. The authors used *N,N*-dimethylacrylamide (DMAM) to show the thermoresponsive character.

Studies have shown that sensors can be developed with sensitivities and detection limits appropriate for monitoring the analytes discussed in this section. A number of intriguing applications for the sensor were explored, including noise identification, voice recognition, and song note recognition. These applications show promise for use in flexible wearable devices for human health monitoring and other advanced applications that will be readily portable in the near future. In the case of surfactant detection, the proposed design can be utilized to quantify cationic surfactants in daily items, such as hair conditioners and shampoos, as well as in highly polluted water samples.

4. Conclusion

One of the major topics in polymer science are stimuli-responsive polymers. Among them, PNIPAM is the most researched, and their LCST around body temperature, as well as their appealing and tunable properties, make them an excellent choice for a variety of in vivo and in vitro applications. The applications of sensing and bio-sensing are discussed in depth in this review. The described polymers were made utilizing a number of processes, e.g., ATRP, RAFT, and free radical polymerization. In certain situations, the sensor tag was added to the polymers by post-polymerization modification. The sensors performed admirably in terms of selectivity and sensitivity. Despite their accomplishments, PNIPAM-based sensors experienced certain difficulties in practical implementations. In this context, the fabrication of sensors on an industrial scale is a primary major challenge that should be cheap in cost and should be without any cracks and defects. However, a prevalent issue is the slow response time and mechanical strength, both of which are major roadblocks to their continued growth. For PNIPAM-based hydrogels, a basic requirement is effectively dissipating mechanical energies under large deformations while maintaining original configurations. By changing different factors such as degree of crosslinking, initial monomer concentration, polymerization temperature, test temperature, and swelling degree scientists are trying to improve the mechanical strength. Reusability is another main condition for practical application, if the thermoresponsive cycle or heating/cooling cycle provides durability is less than 100 times then it is quite hard to use in real conditions. Therefore, in practice, there is still a long way to go before we can use these polymers in our daily lives. If we want to use them for health monitoring or as wearable devices then it has to be sufficiently biodegradable with selectivity and sensitivity. PNIPAM homopolymers are intrinsically not biodegradable, unlike other natural polymers like chitosan, cellulose, and gelatine. This can lead to long-term bioaccumulation at the implantation site. However, it is noncytotoxic in many biological applications, and when utilized as sensors typically very small quantities of materials are necessary. As a result, the main application area appears to be in healthcare systems for biosensing purposes and reusable sensors for a broad range of applications, rather than commodity single-use applications for textiles or food. Nonetheless, there is a long road ahead to go from initial proof-of-concept to real-world applications. Stimuli-responsive polymers feature a low responsivity rate, which may be in the order of an hour. To overcome this challenge, we shall need to consider the alteration of the mechanical properties (stress, elasticity modulus) and the micro/ nano structure (size, shape, porosity, and thickness) of the materials. As a result, PNIPAM has not been employed on a regular basis, and additional research into PNIPAM-based polymer sensors is required. To increase the use of PNIPAM-based smart sensors, in the future, more attempts shall be required to construct novel structures and enhance their properties with the integration of multi-functionality (e.g., multi-response, self-healing, and self-power) into the PNIPAM-based system. Therefore, cooperation across disciplines is required. Accelerating research in this field is necessary to ensure that innovations meet public demand.

We may anticipate that merging the efforts of multidisciplinary specialists from various backgrounds will shed new light on the potential uses of PNIPAM-based sensor systems. We do foresee that PNIPAM-based sensors will most likely excel at (medical) applications where portability is a key feature, providing an accessible technology in environments with limited infrastructure.

Acknowledgements

A.D. and A.B. thanks SRM IST for providing a fellowship to support the Ph.D. program. S.M. acknowledges SRMIST for providing SRMIST seed grant and Science and Engineering Research Board (SERB), India for a core research grant (CRG/2021/004203). R.H. thanks FWO and Ghent University for financial support.

Conflict of Interest

The authors declare no conflict of interest.

Keywords

biosensor, poly(*N*-isopropyl acrylamide), sensor, smart material, thermoresponsive polymer

Received: February 7, 2024
Revised: April 16, 2024
Published online: May 11, 2024

[1] S. Amador-Vargas, M. Dominguez, G. León, B. Maldonado, J. Murillo, G. L. Vides, *Plant Ecol.* **2014**, *215*, 1445.
[2] Y. Forterre, J. M. Skotheim, J. Dumais, L. Mahadevan, *Nature* **2005**, *433*, 421.
[3] M. Schneemann, R. Cathomas, S. T. Laidlaw, A. M. El Nahas, R. D. G. Theakston, D. A. Warrell, *QJM* **2004**, *97*, 717.
[4] J. C. Bradley, B. S. Galil, *Proc. Entomol. Soc. Wash.* **1977**, *79*, 176.
[5] K. Kuba, E. Kato, E. Kumamoto, K. Koketsu, K. Hirai, *Nature* **1981**, *291*, 654.
[6] S. Ebashi, M. Endo, *Prog. Biophys. Mol. Biol.* **1968**, *18*, 123.
[7] D. Roy, W. L. A. Brooks, B. S. Sumerlin, *Chem. Soc. Rev.* **2013**, *42*, 7214.
[8] K. Nagase, J. Kobayashi, T. Okano, *J. R. Soc. Interface* **2009**, *6*, S293.
[9] D. Crespy, R. M. Rossi, *Polym. Int.* **2007**, *56*, 1461.
[10] M. E. S. Miranda, C. Marcolla, C. A. Rodrígues, H. M. Wilhelm, M. R. Sierakowski, T. M. B. Bresolin, R. A. de Freitas, *Polym. Int.* **2006**, *55*, 961.
[11] S. Maji, Z. Zhang, L. Voorhaar, S. Pieters, B. Stubbe, S. Van Vlierberghe, P. Dubruel, B. G. De Geest, R. Hoogenboom, *RSC Adv.* **2015**, *5*, 42388.
[12] S. Dai, P. Ravi, K. C. Tam, *Soft Matter* **2008**, *4*, 435.
[13] D. Schmaljohann, *Adv. Drug Delivery Rev.* **2006**, *58*, 1655.
[14] J. Rodríguez-Hernández, S. Lecommandoux, *J. Am. Chem. Soc.* **2005**, *127*, 2026.
[15] F. D. Jochum, L. zur Borg, P. J. Roth, P. Theato, *Macromolecules* **2009**, *42*, 7854.
[16] J. Jiang, X. Tong, Y. Zhao, *J. Am. Chem. Soc.* **2005**, *127*, 8290.
[17] S. Ramanathan, L. H. Block, *J. Controlled Release* **2001**, *70*, 109.
[18] G. Filipcsei, J. Fehér, M. Zrínyi, *J. Mol. Struct.* **2000**, *554*, 109.
[19] D. Roy, J. N. Cambre, B. S. Sumerlin, *Chem. Commun.* **2009**, 2106.
[20] P. D. Thornton, R. J. Mart, R. V. Ulijn, *Adv. Mater.* **2007**, *19*, 1252.
[21] M. Czaun, L. Hevesi, M. Takafuji, H. Ihara, *Chem. Commun.* **2008**, 2124.
[22] H. Liu, S. Lin, Y. Feng, P. Theato, *Polym. Chem.* **2017**, *8*, 12.
[23] J. S. Scarpa, D. D. Mueller, I. M. Klotz, *J. Am. Chem. Soc.* **1967**, *89*, 6024.
[24] J. Nicolas, Y. Guillaneuf, C. Lefay, D. Bertin, D. Gigmes, B. Charleux, *Prog. Polym. Sci.* **2013**, *38*, 63.
[25] K. Matyjaszewski, J. Xia, *Chem. Rev.* **2001**, *101*, 2921.
[26] J. M. O'Donnell, *Chem. Soc. Rev.* **2012**, *41*, 3061.
[27] C. W. Bielawski, R. H. Grubbs, *Prog. Polym. Sci.* **2007**, *32*, 1.
[28] O. Nuyken, S. Pask, *Polymers* **2013**, *5*, 361.
[29] C. R. Becer, R. Hoogenboom, U. S. Schubert, *Angew. Chem., Int. Ed.* **2009**, *48*, 4900.
[30] A. Bratek-Skicki, *Appl. Surf. Sci. Adv.* **2021**, *4*, 100068.
[31] T. Chen, R. Ferris, J. Zhang, R. Ducker, S. Zauscher, *Prog. Polym. Sci.* **2010**, *35*, 94.
[32] H. Lee, J. Pietrasik, S. S. Sheiko, K. Matyjaszewski, *Prog. Polym. Sci.* **2010**, *35*, 24.
[33] M. Motornov, Y. Roiter, I. Tokarev, S. Minko, *Prog. Polym. Sci.* **2010**, *35*, 174.
[34] I. Dimitrov, B. Trzebicka, A. H. E. Müller, A. Dworak, C. B. Tsvetanov, *Prog. Polym. Sci.* **2007**, *32*, 1275.
[35] R. Liu, M. Fraylich, B. R. Saunders, *Colloid Polym. Sci.* **2009**, *287*, 627.
[36] J.-S. Park, K. Kataoka, *Macromolecules* **2006**, *39*, 6622.
[37] J. Tang, M. F. X. Lee, W. Zhang, B. Zhao, R. M. Berry, K. C. Tam, *Biomacromolecules* **2014**, *15*, 3052.
[38] S. F. Medeiros, A. M. Santos, H. Fessi, A. Elaissari, *Int. J. Pharm.* **2011**, *403*, 139.
[39] J. Karppi, S. Åkerman, K. Åkerman, A. Sundell, K. Nyyssönen, I. Penttilä, *Int. J. Pharm.* **2007**, *338*, 7.
[40] E. Gil, S. Hudson, *Prog. Polym. Sci.* **2004**, *29*, 1173.
[41] A. Hakeem, F. Zahid, G. Zhan, P. Yi, H. Yang, L. Gan, X. Yang, *Int. J. Nanomed.* **2018**, *13*, 1029.
[42] S. E. Burke, C. J. Barrett, *Biomacromolecules* **2003**, *4*, 1773.
[43] Q. Tang, D. Zhao, H. Yang, L. Wang, X. Zhang, *J. Mater. Chem. B.* **2019**, *7*, 30.
[44] B. P. Bastakoti, Z. Liu, in *Nanostructures for Cancer Therapy*, (Eds: A. Ficai, A. M. Grum), Elsevier, Amsterdam **2017**, pp. 261–283.
[45] A. Garcia, M. Marquez, T. Cai, R. Rosario, Z. Hu, D. Gust, M. Hayes, S. A. Vail, C.-D. Park, *Langmuir* **2007**, *23*, 224.
[46] S. Guragain, B. P. Bastakoti, M. Ito, S. Yusa, K. Nakashima, *Soft Matter* **2012**, *8*, 9628.
[47] H. Zhang, J. Li, H. Cui, H. Li, F. Yang, *Chem. Eng. J.* **2015**, *259*, 814.
[48] L. Wang, M. Liu, C. Gao, L. Ma, D. Cui, *React. Funct. Polym.* **2010**, *70*, 159.
[49] C. Dagallier, H. Dietsch, P. Schurtenberger, F. Scheffold, *Soft Matter* **2010**, *6*, 2174.
[50] G. Uğur, J. Chang, S. Xiang, L. Lin, J. Lu, *Adv. Mater.* **2012**, *24*, 2685.
[51] C. Weber, R. Hoogenboom, U. S. Schubert, *Prog. Polym. Sci.* **2012**, *37*, 686.
[52] C. de las H Alarcón, S. Pennadam, C. Alexander, *Chem. Soc. Rev.* **2005**, *34*, 276.
[53] E. G. Kelley, J. N. L. Albert, M. O. Sullivan, T. H. Epps, III, *Chem. Soc. Rev.* **2013**, *42*, 7057.
[54] A. Halperin, M. Kröge, F. M. Winnik, *Angew. Chem., Int. Ed.* **2015**, *54*, 15342.
[55] M. Taylor, P. Tomlins, T. Sahota, *Gels* **2017**, *3*, 4.
[56] I. Aibara, J. Chikazawa, T. Uwada, S. Hashimoto, *J. Phys. Chem. C* **2017**, *121*, 22496.
[57] M. Kano, E. Kokufuta, *Langmuir* **2009**, *25*, 8649.
[58] T. E. de Oliveira, C. M. Marques, P. A. Netz, *Phys. Chem. Chem. Phys.* **2018**, *20*, 10100.
[59] L. Tang, L. Wang, X. Yang, Y. Feng, Y. Li, W. Feng, *Prog. Mater. Sci.* **2021**, *115*, 100702.
[60] H. Hatakeyama, A. Kikuchi, M. Yamato, T. Okano, *Biomaterials* **2006**, *27*, 5069.
[61] J. Tobis, Y. Thomann, J. C. Tiller, *Polymer* **2010**, *51*, 35.
[62] E. Uğuzdoğan, O. S. Kabasakal, *Colloids Surf., A* **2010**, *368*, 129.
[63] P. Kujawa, V. Aseyev, H. Tenhu, F. M. Winnik, *Macromolecules* **2006**, *39*, 7686.
[64] J. Zhao, J. Shan, G. Van Assche, H. Tenhu, B. Van Mele, *Macromolecules* **2009**, *42*, 5317.
[65] I. Bischofberger, V. Trappe, *Sci. Rep.* **2015**, *5*, 15520.
[66] Y. Shiraishi, S. Sumiya, K. Manabe, T. Hirai, *ACS Appl. Mater. Interfaces.* **2011**, *3*, 4649.
[67] S. Uchiyama, Y. Matsumura, A. P. de Silva, K. Iwai, *Anal. Chem.* **2003**, *75*, 5926.
[68] T. Tsuji, S. Yoshida, A. Yoshida, S. Uchiyama, *Anal. Chem.* **2013**, *85*, 9815.
[69] L. Yin, C. He, C. Huang, W. Zhu, X. Wang, Y. Xu, X. Qian, *Chem. Commun.* **2012**, *48*, 4486.
[70] J. Hu, C. Li, Y. Cui, S. Liu, *Macromol. Rapid Commun.* **2011**, *32*, 610.
[71] Z. Guo, W. Zhu, Y. Xiong, H. Tian, *Macromolecules* **2009**, *42*, 1448.
[72] S. Yao, A. M. Jones, J. Du, R. K. Jackson, J. O. Massing, D. P. Kennedy, N. E. Bencivenga, R. P. Planalp, S. C. Burdette, W. R. Seitz, *Analyst* **2012**, *137*, 4734.
[73] A. Matsumoto, S. Ikeda, A. Harada, K. Kataoka, *Biomacromolecules* **2003**, *4*, 1410.
[74] Y. Zhang, Y. Guan, S. Zhou, *Biomacromolecules* **2006**, *7*, 3196.
[75] Z. H. Farooqi, W. Wu, S. Zhou, M. Siddiq, *Macromol. Chem. Phys.* **2011**, *212*, 1510.
[76] T. Hoare, R. Pelton, *Macromolecules* **2007**, *40*, 670.
[77] D. Wang, T. Liu, J. Yin, S. Liu, *Macromolecules* **2011**, *44*, 2282.
[78] Z. Tang, Y. Guan, Y. Zhang, *Polym. Chem.* **2014**, *5*, 1782.
[79] Z. H. Farooqi, A. Khan, M. Siddiq, *Polym. Int.* **2011**, *60*, 1481.

[80] V. Lapeyre, I. Gosse, S. Chevreux, V. Ravaine, *Biomacromolecules* **2006**, *7*, 3356.
[81] Z. Liu, F. Luo, X.-J. Ju, R. Xie, Y.-M. Sun, W. Wang, L.-Y. Chu, *J. Mater. Chem. A.* **2013**, *1*, 9659.
[82] H.-Y. Peng, W. Wang, F. Gao, S. Lin, L.-Y. Liu, X.-Q. Pu, Z. Liu, X.-J. Ju, R. Xie, L.-Y. Chu, *J. Mater. Chem. C.* **2018**, *6*, 11356.
[83] A.-L. Chen, H.-R. Yu, X.-J. Ju, R. Xie, W. Wang, L.-Y. Chu, *RSC Adv.* **2014**, *4*, 26030.
[84] D. Büning, F. Ennen-Roth, S. V. Walter, T. Hennecke, M. Ulbricht, *Polym. Chem.* **2018**, *9*, 3600.
[85] J. Yin, C. Li, D. Wang, S. Liu, *J. Phys. Chem. B* **2010**, *114*, 12213.
[86] L. Tan, J. Liu, W. Zhou, J. Wei, Z. Peng, *Mater. Sci. Eng. C.* **2014**, *45*, 524.
[87] Z. Wang, Z. Yang, T. Gao, J. He, L. Gong, Y. Lu, Y. Xiong, W. Xu, *Anal. Methods* **2015**, *7*, 2738.
[88] X. Wan, T. Liu, S. Liu, *Langmuir* **2011**, *27*, 4082.
[89] Q. Wang, H. Wang, Q. Chen, Y. Guan, Y. Zhang, *ACS Appl. Polym. Mater.* **2020**, *2*, 3966.
[90] J. Hu, C. Li, S. Liu, *Langmuir* **2010**, *26*, 724.
[91] M. Matsuguchi, K. Takaoka, H. Kai, *Sens. Actuators, B* **2015**, *208*, 106.
[92] J.-K. Chen, J.-Y. Li, *Sens. Actuators, B* **2010**, *150*, 314.
[93] Z. Gong, D. Tang, X. Zhang, J. Ma, Y. Mao, *Appl. Surf. Sci.* **2014**, *316*, 194.
[94] L.-N. Chen, C.-C. Kuo, Y.-C. Chiu, W.-C. Chen, *RSC Adv.* **2014**, *4*, 45345.
[95] J.-T. Wang, Y.-C. Chiu, H.-S. Sun, K. Yoshida, Y. Chen, T. Satoh, T. Kakuchi, W.-C. Chen, *Polym. Chem.* **2015**, *6*, 2327.
[96] H.-J. Lin, C.-Y. Chen, *J. Mater. Sci.* **2016**, *51*, 1620.
[97] L.-N. Chen, N.-K. Weng, W.-C. Wu, W.-C. Chen, *Mater. Chem. Phys.* **2015**, *163*, 63.
[98] W.-C. Wu, H.-J. Lai, *J. Polym. Res.* **2016**, *23*, 223.
[99] D. Ran, Y. Wang, X. Jia, C. Nie, *Anal. Chim. Acta.* **2012**, *723*, 45.
[100] N. Adrus, M. Ulbricht, *Polymer* **2012**, *53*, 4359.
[101] F. Liu, S. Huang, F. Xue, Y. Wang, Z. Meng, M. Xue, *Biosens. Bioelectron.* **2012**, *32*, 273.
[102] T. Ye, S. Yan, Y. Hu, L. Ding, W. Wu, *Polym. Chem.* **2014**, *5*, 186.
[103] J.-T. Zhang, N. Smith, S. A. Asher, *Anal. Chem.* **2012**, *84*, 6416.
[104] Y. Liu, Y. Zhang, Y. Guan, *Chem. Commun.* **2009**, 1867.
[105] M. Honda, K. Kataoka, T. Seki, Y. Takeoka, *Langmuir* **2009**, *25*, 8349.
[106] J. Shin, S. G. Han, W. Lee, *Sens. Actuators, B* **2012**, *168*, 20.
[107] C. D. Sorrell, M. J. Serpe, *Anal. Bioanal. Chem.* **2012**, *402*, 2385.
[108] M. R. Islam, M. J. Serpe, *Anal. Bioanal. Chem.* **2014**, *406*, 4777.
[109] M. R. Islam, M. J. Serpe, *Anal. Chim. Acta* **2014**, *843*, 83.
[110] K. C. C. Johnson, F. Mendez, M. J. Serpe, *Anal. Chim. Acta* **2012**, *739*, 83.
[111] M. R. Islam, K. C. C. Johnson, M. J. Serpe, *Anal. Chim. Acta.* **2013**, *792*, 110.
[112] M. R. Islam, M. J. Serpe, *APL Mater.* **2013**, *1*, 052108.
[113] M. R. Islam, M. J. Serpe, *Biosens. Bioelectron.* **2013**, *49*, 133.
[114] M. R. Islam, M. J. Serpe, *Chem. Commun.* **2013**, *49*, 2646.
[115] D. Parasuraman, M. J. Serpe, *ACS Appl. Mater. Interfaces* **2011**, *3*, 4714.
[116] D. Parasuraman, M. J. Serpe, *ACS Appl. Mater. Interfaces* **2011**, *3*, 2732.
[117] Q. M. Zhang, D. Berg, S. M. Mugo, M. J. Serpe, *Chem. Commun.* **2015**, *51*, 9726.
[118] G. Zhang, N. Yang, Y. Ni, J. Shen, W. Zhao, X. Huang, *Sens. Actuators, B* **2011**, *158*, 130.
[119] C. H. Park, H. Yang, J. Lee, H.-H. Cho, D. Kim, D. C. Lee, B. J. Kim, *Chem. Mater.* **2015**, *27*, 5288.
[120] M. Mueller, M. Tebbe, D. V. Andreeva, M. Karg, R. A. Alvarez Puebla, N. Pazos Perez, A. Fery, *Langmuir* **2012**, *28*, 9168.
[121] Q. Zhou, G. Meng, P. Zheng, S. Cushing, N. Wu, Q. Huang, C. Zhu, Z. Zhang, Z. Wang, *Sci. Rep.* **2015**, *5*, 12865.
[122] H. Gehan, L. Fillaud, M. M. Chehimi, J. Aubard, A. Hohenau, N. Felidj, C. Mangeney, *ACS Nano* **2010**, *4*, 6491.
[123] J. Zhou, K. Mishra, V. Bhagat, A. Joy, M. L. Becker, *Polym. Chem.* **2015**, *6*, 2813.
[124] W. Wu, T. Zhou, J. Shen, S. Zhou, *Chem. Commun.* **2009**, 4390.
[125] W. Wu, T. Zhou, M. Aiello, S. Zhou, *Biosens. Bioelectron.* **2010**, *25*, 2603.
[126] H. Wang, J. Yi, D. Velado, Y. Yu, S. Zhou, *ACS Appl. Mater. Interfaces* **2015**, *7*, 15735.
[127] E. M. Lucchetta, J. H. Lee, L. A. Fu, N. H. Patel, R. F. Ismagilov, *Nature* **2005**, *434*, 1134.
[128] V. M. Lauschke, C. D. Tsiairis, P. François, A. Aulehla, *Nature* **2013**, *493*, 101.
[129] A. C. Kimmelman, E. White, *Cell Metab.* **2017**, *25*, 1037.
[130] A. Schroeder, D. A. Heller, M. M. Winslow, J. E. Dahlman, G. W. Pratt, R. Langer, T. Jacks, D. G. Anderson, *Nat. Rev. Cancer* **2012**, *12*, 39.
[131] F. Vitzthum, F. Behrens, N. L. Anderson, J. H. Shaw, *J. Proteome Res.* **2005**, *4*, 1086.
[132] B. B. Lowell, B. M. Spiegelman, *Nature* **2000**, *404*, 652.
[133] G. M. Story, A. M. Peier, A. J. Reeve, S. R. Eid, J. Mosbacher, T. R. Hricik, T. J. Earley, A. C. Hergarden, D. A. Andersson, S. W. Hwang, P. McIntyre, T. Jegla, S. Bevan, A. Patapoutian, *Cell* **2003**, *112*, 819.
[134] T. Voets, G. Droogmans, U. Wissenbach, A. Janssens, V. Flockerzi, B. Nilius, *Nature* **2004**, *430*, 748.
[135] F. C. Baker, F. Siboza, A. Fuller, *Temperature* **2020**, *7*, 226.
[136] S. Hu, H. Wu, X. Liang, C. Xiao, Q. Zhao, Y. Cao, X. Han, *Chemosphere* **2022**, *287*, 131987.
[137] V. S. Struchkov, R. H. Kurmaev, D. M. Iakunov, I. A. Lubimov, *IOP Conf. Ser.: Mater. Sci. Eng.* **2019**, *534*, 012018.
[138] M. Gardner, A. Candee, J. Kramlich, R. Koppang, *Development of a process control sensor for the glass industry*, U. S. Department of Energy, Idaho Falls, ID, **1991**.
[139] A. Mallik, S. D. Gupta, in 2009 Int. Conf. on Computer and Automation Engineering, IEEE, Piscataway, NJ **2009**, pp. 287-292.
[140] A. Bakker, J. H. Huijsing, *IEEE J. Solid-State Circuits* **1996**, *31*, 933.
[141] Y. Huang, T. Guo, Z. Tian, B. Yu, M. Ding, X. Li, B.-O. Guan, *ACS Appl. Mater. Interfaces* **2017**, *9*, 9024.
[142] J. H. Oh, S. Y. Hong, H. Park, S. W. Jin, Y. R. Jeong, S. Y. Oh, J. Yun, H. Lee, J. W. Kim, J. S. Ha, *ACS Appl. Mater. Interfaces* **2018**, *10*, 7263.
[143] C. Rullyani, M. Singh, S.-H. Li, C.-F. Sung, H.-C. Lin, C.-W. Chu, *Org. Electron.* **2020**, *85*, 105818.
[144] K. Saha, S. S. Agasti, C. Kim, X. Li, V. M. Rotello, *Chem. Rev.* **2012**, *112*, 2739.
[145] S. Maji, B. Cesur, Z. Zhang, B. G. De Geest, R. Hoogenboom, *Polym. Chem.* **2016**, *7*, 1705.
[146] S. Wu, L. Lei, Y. Xia, S. Oliver, X. Chen, C. Boyer, Z. Nie, S. Shi, *Polym. Chem.* **2021**, *12*, 6903.
[147] Y. Liu, X. Dai, S. Mallawaarachchi, H. Hapuarachchi, Q. Shi, D. Dong, S. H. Thang, M. Premaratne, W. Cheng, *J. Mater. Chem. C* **2017**, *5*, 10926.
[148] S. Mallawaarachchi, Y. Liu, S. H. Thang, W. Cheng, M. Premaratne, *Phys. Chem. Chem. Phys.* **2019**, *21*, 24808.
[149] A. Choe, J. Yeom, R. Shanker, M. P. Kim, S. Kang, H. Ko, *NPG Asia Mater.* **2018**, *10*, 912.
[150] S. Feng, Q. Li, S. Wang, B. Wang, Y. Hou, T. Zhang, *ACS Appl. Mater. Interfaces* **2019**, *11*, 21049.
[151] W. Liu, X. Zhang, G. Wei, Z. Su, *Sensors* **2018**, *18*, 3162.
[152] Z. Wang, H. Zhou, W. Chen, Q. Li, B. Yan, X. Jin, A. Ma, H. Liu, W. Zhao, *ACS Appl. Mater. Interfaces* **2018**, *10*, 14045.
[153] T. Zhan, H. Xie, J. Mao, S. Wang, Y. Hu, Z. Guo, *ChemistrySelect* **2021**, *6*, 4229.
[154] F.-W. Wang, C.-W. Hsu, C.-C. Hsieh, *ACS Appl. Mater. Interfaces* **2019**, *11*, 8591.

[155] T. Zhang, G.-Q. Liu, W.-H. Leong, C.-F. Liu, M.-H. Kwok, T. Ngai, R.-B. Liu, Q. Li, *Nat. Commun.* **2018**, *9*, 3188.
[156] M. Umar, D. Son, S. Arif, M. Kim, S. Kim, *ACS Appl. Mater. Interfaces* **2020**, *12*, 55231.
[157] H. Kye, Y. Koh, Y. Kim, S. Han, H. Lee, W. Lee, *Sensors* **2017**, *17*, 1398.
[158] M. Barbieri, F. Cellini, I. Cacciotti, S. D. Peterson, M. Porfiri, *J. Mater. Sci.* **2017**, *52*, 12506.
[159] F. Cellini, S. D. Peterson, M. Porfiri, *Int. J. Smart Nano Mater.* **2017**, *8*, 232.
[160] S. Uchiyama, T. Tsuji, K. Kawamoto, K. Okano, E. Fukatsu, T. Noro, K. Ikado, S. Yamada, Y. Shibata, T. Hayashi, N. Inada, M. Kato, H. Koizumi, H. Tokuyama, *Angew. Chem., Int. Ed.* **2018**, *57*, 5413.
[161] B.-Y. Chen, Y.-C. Lung, C.-C. Kuo, F.-C. Liang, T.-L. Tsai, D.-H. Jiang, T. Satoh, R.-J. Jeng, *Polymers* **2018**, *10*, 1259.
[162] J. Qiao, Y.-H. Hwang, D.-P. Kim, L. Qi, *Anal. Chem.* **2020**, *92*, 8579.
[163] H. Zhang, J. Jiang, P. Gao, T. Yang, K. Y. Zhang, Z. Chen, S. Liu, W. Huang, Q. Zhao, *ACS Appl. Mater. Interfaces.* **2018**, *10*, 17542.
[164] J. A. Sobrinho, G. A. Brito Júnior, I. O. Mazali, F. A. Sigoli, *New J. Chem.* **2020**, *44*, 8068.
[165] D. Gong, T. Cao, S.-C. Han, X. Zhu, A. Iqbal, W. Liu, W. Qin, H. Guo, *Sens. Actuators, B* **2017**, *252*, 577.
[166] S. H. Lee, H. T. Bui, T. P. Vales, S. Cho, H.-J. Kim, *Dyes Pigm.* **2017**, *145*, 216.
[167] F. Kong, M. Lin, T. Qiu, *Polymer* **2018**, *151*, 117.
[168] S. Uchiyama, K. Takehira, T. Yoshihara, S. Tobita, T. Ohwada, *Org. Lett.* **2006**, *8*, 5869.
[169] S. Uchiyama, P. Remón, U. Pischel, K. Kawamoto, C. Gota, *Photochem. Photobiol. Sci.* **2016**, *15*, 1239.
[170] S. L. Percival, S. McCarty, J. A. Hunt, E. J. Woods, *Wound Repair Regener.* **2014**, *22*, 174.
[171] G. Kocak, C. Tuncer, V. Bütün, *Polym. Chem.* **2017**, *8*, 144.
[172] G. Gerlach, M. Guenther, J. Sorber, G. Suchaneck, K.-F. Arndt, A. Richter, *Sens. Actuators, B* **2005**, *111-112*, 555.
[173] G. Gerlach, M. Guenther, G. Suchaneck, J. Sorber, K. Arndt, A. Richter, *Macromol. Symp.* **2004**, *210*, 403.
[174] W. Wu, T. Zhou, M. Aiello, S. Zhou, *Chem. Mater.* **2009**, *21*, 4905.
[175] S. Uchiyama, Y. Makino, *Chem. Commun.* **2009**, 2646.
[176] C. Yang, Y. Tian, C. Chen, A. K.-Y. Jen, W. Chen, *Macromol. Rapid Commun.* **2007**, *28*, 894.
[177] Y. Kim, D. Kim, G. Jang, J. Kim, T. S. Lee, *Sens. Actuators, B* **2015**, *207*, 623.
[178] G. Liu, W. Zhou, J. Zhang, P. Zhao, *J. Polym. Sci., Part A: Polym. Chem.* **2012**, *50*, 2219.
[179] H. Zhou, F. Liu, X. Wang, H. Yan, J. Song, Q. Ye, B. Z. Tang, J. Xu, *J. Mater. Chem. C* **2015**, *3*, 5490.
[180] Y. Shen, M. Kuang, Z. Shen, J. Nieberle, H. Duan, H. Frey, *Angew. Chem.* **2008**, *120*, 2259.
[181] J. Lü, Y. Fu, D. Wang, C. Lü, *Sens. Actuators, B* **2018**, *254*, 996.
[182] D. W. Boening, *Chemosphere* **2000**, *40*, 1335.
[183] T. W. Clarkson, L. Magos, G. J. Myers, *N. Engl. J. Med.* **2003**, *349*, 1731.
[184] J. LaDou, *Int. J. Hyg. Environ. Health* **2006**, *209*, 211.
[185] D. Rosner, G. Markowitz, *Am. J. Ind. Med.* **2007**, *50*, 740.
[186] R. L. Boeckx, *Anal. Chem.* **1986**, *58*, 274A.
[187] G. K. Kinuthia, V. Ngure, D. Beti, R. Lugalia, A. Wangila, L. Kamau, *Sci. Rep.* **2020**, *10*, 8434.
[188] I. Cesarino, É. T. G. Cavalheiro, C. M. A. Brett, *Electroanalysis* **2010**, *22*, 61.
[189] S. Caroli, *Talanta* **1999**, *50*, 327.
[190] M. E. Mahmoud, I. M. M. Kenawy, M. A. H. Hafez, R. R. Lashein, *Desalination* **2010**, *250*, 62.
[191] I. Narin, M. Soylak, L. Elçi, M. Doğan, *Talanta* **2000**, *52*, 1041.
[192] I. K. Tonlé, S. Letaief, E. Ngameni, A. Walcarius, C. Detellier, *Electroanalysis* **2011**, *23*, 245.
[193] Q. Dai, H. Liu, C. Gao, W. Li, C. Zhu, C. Lin, Y. Tan, Z. Yuan, Y. Jiang, *New J. Chem.* **2018**, *42*, 613.
[194] Q. Dai, C. Gao, Y. Liu, H. Liu, B. Xiao, C. Chen, J. Chen, Z. Yuan, Y. Jiang, *Tetrahedron* **2018**, *74*, 6459.
[195] C. Wang, J. Fu, K. Yao, K. Xue, K. Xu, X. Pang, *Spectrochim. Acta, Part A* **2018**, *199*, 403.
[196] X.-J. Jiang, Y. Fu, L.-H. Xu, H.-L. Lu, S.-Q. Zang, M.-S. Tang, T. C. W. Mak, *Sens., Actuators B* **2014**, *202*, 388.
[197] M. Deng, Y. Wang, G. Men, H. Shang, S. Jiang, *Sens., Actuators B* **2016**, *234*, 609.
[198] F.-C. Liang, Y.-L. Luo, C.-C. Kuo, B.-Y. Chen, C.-J. Cho, F.-J. Lin, Y.-Y. Yu, R. Borsali, *Polymers* **2017**, *9*, 136.
[199] S. Zhu, F. Zhao, M. Deng, T. Zhang, C. Lü, *Dyes Pigm.* **2019**, *168*, 369.
[200] S. Lin, W. Wang, X.-J. Ju, R. Xie, Z. Liu, H.-R. Yu, C. Zhang, L.-Y. Chu, *Proc. Natl. Acad. Sci. USA* **2016**, *113*, 2023.
[201] P.-J. Yan, F. He, W. Wang, S.-Y. Zhang, L. Zhang, M. Li, Z. Liu, X.-J. Ju, R. Xie, L.-Y. Chu, *ACS Appl. Mater. Interfaces* **2018**, *10*, 36425.
[202] Y.-Q. Liu, X.-J. Ju, X.-Q. Pu, S. Wen, W.-Y. Liu, Z. Liu, W. Wang, R. Xie, L.-Y. Chu, *J. Hazard. Mater.* **2021**, *404*, 124157.
[203] Y. Wang, Z. Liu, H. Peng, F. He, L. Zhang, Y. Faraj, W. Wang, X. Ju, R. Xie, L. Chu, *ChemPhysChem* **2018**, *19*, 2025.
[204] Y. Wang, Z. Liu, F. Luo, H.-Y. Peng, S.-G. Zhang, R. Xie, X.-J. Ju, W. Wang, Y. Faraj, L.-Y. Chu, *J. Membr. Sci.* **2019**, *575*, 28.
[205] W.-Y. Liu, X.-J. Ju, Y. Faraj, F. He, H.-Y. Peng, Y.-Q. Liu, Z. Liu, W. Wang, R. Xie, L.-Y. Chu, *J. Membr. Sci.* **2020**, *613*, 118523.
[206] F. Wang, R. P. Planalp, W. R. Seitz, *Polymers* **2019**, *11*, 1935.
[207] J. Qiao, H. Ding, Q. Liu, R. Zhang, L. Qi, *Anal. Chem.* **2017**, *89*, 2080.
[208] P. Q. Nhien, P.-H. Wu, C.-H. Wu, J. I. Wu, B. T. B. Hue, B.-W. Du, F.-H. Ko, C.-C. Weng, Y.-K. Li, H.-C. Lin, *Sens. Actuators, B* **2021**, *344*, 130241.
[209] J. Han, Y. Cai, Y. Wang, X. Dai, L. Wang, C. Li, B. An, L. Ni, *New J. Chem.* **2018**, *42*, 12853.
[210] A. Puri, M. Kumar, *Indian J. Occup. Environ. Med.* **2012**, *16*, 40.
[211] X. Shen, X. Yang, C. Su, J. Yang, L. Zhang, B. Liu, S. Gao, F. Gai, Z. Shao, G. Gao, *J. Mater. Chem. C* **2018**, *6*, 2088.
[212] K. Ljung, M. Vahter, *Environ. Health Perspect.* **2007**, *115*, 1533.
[213] Z. Zhu, J. Xue, B. Wen, W. Ji, B. Du, J. Nie, *Sens. Actuators, B* **2019**, *291*, 441.
[214] H. M. Yang, J. Y. Teoh, G. H. Yim, Y. Park, Y. G. Kim, J. Kim, D. Yoo, *ACS Appl. Mater. Interfaces.* **2020**, *12*, 5413.
[215] Z. Zhang, S. Maji, A. B. da F Antunes, R. De Rycke, Q. Zhang, R. Hoogenboom, B. G. De Geest, *Chem. Mater.* **2013**, *25*, 4297.
[216] W. Kunz, J. Henle, B. W. Ninham, *Curr. Opin. Colloid Interface Sci.* **2004**, *9*, 19.
[217] B. Kang, H. Tang, Z. Zhao, S. Song, *ACS Omega* **2020**, *5*, 6229.
[218] S. Yusa, K. Fukuda, T. Yamamoto, Y. Iwasaki, A. Watanabe, K. Akiyoshi, Y. Morishima, *Langmuir* **2007**, *23*, 12842.
[219] Z. Zhang, S. Maji, A. B. da Fonseca Antunes, R. De Rycke, R. Hoogenboom, B. G. De Geest, *Angew. Chem.* **2016**, *128*, 7202.
[220] B. A. Humphreys, E. C. Johnson, E. J. Wanless, G. B. Webber, *Langmuir* **2019**, *35*, 10818.
[221] W. S. P. Carvalho, C. Lee, Y. Zhang, A. Czarnecki, M. J. Serpe, *J. Colloid Interface Sci.* **2021**, *585*, 195.
[222] S. M. Mugo, J. A. Dhanjai, *IEEE Sens. J.* **2020**, *20*, 5741.
[223] J. Doorn, T. Storteboom, A. Mulder, W. de Jong, B. Rottier, I. Kema, *Ann. Clin. Biochem.: Int. J. Lab. Med.* **2015**, *52*, 421.
[224] Y. Tian, L. Du, P. Zhu, Y. Chen, W. Chen, C. Wu, P. Wang, *Biosens. Bioelectron.* **2021**, *176*, 112899.
[225] O. Abuzalat, D. Wong, S. S. Park, S. Kim, *Nanoscale* **2020**, *12*, 13523.
[226] B. H. Monien, N. Bergau, J. G. F. Hogervorst, T. S. Nawrot, I. Trefflich, C. Weikert, K. Abraham, *Mol. Nutr. Food Res.* **2021**, *65*, 2100584.

[227] X. Ma, W. Liao, H. Zhou, Y. Tong, F. Yan, H. Tang, J. Liu, *J. Mater. Chem. B* **2020**, *8*, 10630.
[228] R. M. Myerson, *Med. Clin. North Am.* **1973**, *57*, 925.
[229] Y. Lin, S. Tanaka, *Appl. Microbiol. Biotechnol.* **2006**, *69*, 627.
[230] X.-Y. Zou, F. Luo, R. Xie, L.-P. Zhang, X.-J. Ju, W. Wang, Z. Liu, L.-Y. Chu, *Anal. Methods* **2016**, *8*, 4028.
[231] H.-Y. Peng, W. Wang, F.-H. Gao, S. Lin, X.-J. Ju, R. Xie, Z. Liu, Y. Faraj, L.-Y. Chu, *Ind. Eng. Chem. Res.* **2019**, *58*, 17833.
[232] Y. Zhou, C. Chen, J. Zhao, J. Fei, Y. Ding, Y. Cai, *Electrochim. Acta* **2016**, *192*, 158.
[233] P. Zhao, M. Ni, C. Chen, C. Wang, P. Yang, X. Wang, C. Li, Y. Xie, J. Fei, *Electroanalysis* **2020**, *32*, 1354.
[234] H. M. N. Ahmad, G. Dutta, J. Csoros, B. Si, R. Yang, J. M. Halpern, W. R. Seitz, E. Song, *ACS Appl. Polym. Mater.* **2021**, *3*, 329.
[235] A. Babu, G. Sivakumar, M. Anandan, P. Adhya, T. Akash, T. Mondal, V. Nutalapati, S. Maji, *Eur. Polym. J.* **2023**, *200*, 112527.
[236] F. Gonon, M. Buda, R. Cespuglio, M. Jouvet, J.-F. Pujol, *Nature* **1980**, *286*, 902.
[237] K. A. Keefe, M. J. Zigmond, E. D. Abercrombie, *J. Neural Transm.* **1993**, *91*, 223.
[238] J. J. Clark, S. G. Sandberg, M. J. Wanat, J. O. Gan, E. A. Horne, A. S. Hart, C. A. Akers, J. G. Parker, I. Willuhn, V. Martinez, S. B. Evans, N. Stella, P. E. M. Phillips, *Nat. Methods* **2010**, *7*, 126.
[239] K. Jiang, Y. Wang, G. Thakur, Y. Kotsuchibashi, S. Naicker, R. Narain, T. Thundat, *ACS Appl. Mater. Interfaces* **2017**, *9*, 15225.
[240] J. Wang, X. Zhang, K. Shi, Q. Zhang, *Front. Chem.* **2021**, *3*, https://doi.org/10.3389/fchem.2021.580025.
[241] Y. Zhang, W. S. P. Carvalho, C. Fang, M. J. Serpe, *Sens. Actuators, B* **2019**, *290*, 520.
[242] O. Guselnikova, P. Postnikov, Y. Kalachyova, Z. Kolska, M. Libansky, J. Zima, V. Svorcik, O. Lyutakov, *ChemNanoMat* **2017**, *3*, 135.
[243] F. Cellini, L. Block, J. Li, S. Khapli, S. D. Peterson, M. Porfiri, *Sens. Actuators, B* **2016**, *234*, 510.
[244] Y. Jiang, N. Wang, S. Zhuo, Q. He, Z. Ma, M. Liu, D. Zhang, *J. Appl. Polym. Sci.* **2021**, *138*, https://doi.org/10.1002/app.50023.
[245] M. Matsuguchi, A. Tada, *Sens. Actuators, B* **2017**, *251*, 821.
[246] M. Matsuguchi, S. Fujii, *Sensors* **2018**, *18*, 3283.
[247] J. Sun, J. Ge, W. Liu, M. Lan, H. Zhang, P. Wang, Y. Wang, Z. Niu, *Nanoscale* **2014**, *6*, 255.
[248] A. W. Bell, D. E. Bauman, *J. Mammary Gland Biol. Neoplasia* **1997**, *2*, 265.
[249] J. C. Bae, E. J. Rhee, W. Y. Lee, S. E. Park, C. Y. Park, K. W. Oh, S. W. Park, S. W. Kim, *Diabetes Care* **2011**, *34*, 727.
[250] V. Ganapathy, M. Thangaraju, P. D. Prasad, *Pharmacol. Ther.* **2009**, *121*, 29.
[251] J. Huang, M. Li, P. Zhang, P. Zhang, L. Ding, *Sens. Actuators, B* **2016**, *237*, 24.
[252] H. Lin, M. Li, L. Ding, J. Huang, *Appl. Biochem. Biotechnol.* **2019**, *187*, 1569.
[253] T. Ye, X. Bai, X. Jiang, Q. Wu, S. Chen, A. Qu, J. Huang, J. Shen, W. Wu, *Polym. Chem.* **2016**, *7*, 2847.
[254] F. Li, C. Wang, W. Guo, *Adv. Funct. Mater.* **2018**, *28*, https://doi.org/10.1002/adfm.201705876.
[255] F. Chen, Q. Cao, C. Dong, B. Shao, W. Zhai, X. Ma, B. Wei, *Ultrason. Sonochem.* **2018**, *49*, 190.
[256] G. Vancoillie, R. Hoogenboom, *Polym. Chem.* **2016**, *7*, 5484.
[257] S. Jia, Z. Tang, Y. Guan, Y. Zhang, *ACS Appl. Mater. Interfaces* **2018**, *10*, 14254.
[258] Z. Tang, Y. Guan, Y. Zhang, *Polym. Chem.* **2018**, *9*, 1012.
[259] Z. Tang, S. Jia, L. Yao, Y. Guan, Y. Zhang, *Langmuir* **2018**, *34*, 8288.
[260] M. Peng, S. Yuan, X. Shi, X. Lu, *J. Appl. Polym. Sci.* **2019**, *136*, 6.
[261] X. Li, X. Li, X. Shi, M. Peng, X. Lu, *Eur. Polym. J.* **2019**, *120*, 109230.
[262] Y. Zhang, K. Liu, Y. Guan, Y. Zhang, *RSC Adv.* **2012**, *2*, 4768.
[263] J. Fan, X. Jiang, Y. Hu, Y. Si, L. Ding, W. Wu, *Biomater. Sci.* **2013**, *1*, 421.
[264] J. Qiao, H. Wu, H. Wei, L. Mao, T. Wang, L. Qi, *Anal. Chem.* **2020**, *92*, 4445.
[265] M. Yang, C. Ma, S. Ding, Y. Zhu, G. Shi, A. Zhu, *Anal. Chem.* **2019**, *91*, 14029.
[266] M. Wei, X. Li, M. J. Serpe, *ACS Appl. Polym. Mater.* **2019**, *1*, 519.
[267] P.-F. Li, R. Dietz, R. von Harsdorf, *Circulation* **1997**, *96*, 3602.
[268] Q. M. Zhang, D. Berg, J. Duan, S. M. Mugo, M. J. Serpe, *ACS Appl. Mater. Interfaces.* **2016**, *8*, 27264.
[269] T. Shu, Q. Shen, Y. Wan, W. Zhang, L. Su, X. Zhang, M. J. Serpe, *RSC Adv.* **2018**, *8*, 15567.
[270] Y. Zhou, J. Cao, J. Zhao, Y. Xie, J. Fei, Y. Cai, *Microchim. Acta* **2016**, *183*, 2501.
[271] K. Manivannan, C.-C. Cheng, J.-K. Chen, *Electroanalysis* **2017**, *29*, 1443.
[272] Y. Wang, H. Zhong, X. Li, X. Zhang, Z. Cheng, Z. Zhang, Y. Zhang, P. Chen, L. Zhang, L. Ding, J. Wang, *J. Electroanal. Chem.* **2019**, *851*, 113410.
[273] Z. Chen, Z. Hua, L. Xu, Y. Huang, M. Zhao, Y. Li, *J. Mol. Recognit.* **2008**, *21*, 71.
[274] M. Fang, K. Zhuo, Y. Chen, Y. Zhao, G. Bai, J. Wang, *Anal. Bioanal. Chem.* **2019**, *411*, 5799.
[275] X. Jia, X. Li, C. Lv, S. Wang, W. Dong, *J. Mater. Sci.* **2020**, *55*, 11572.
[276] H. R. Culver, I. Sharma, M. E. Wechsler, E. V. Anslyn, N. A. Peppas, *Analyst* **2017**, *142*, 3183.
[277] H. R. Culver, M. E. Wechsler, N. A. Peppas, *ACS Nano* **2018**, *12*, 9342.
[278] X. Dong, Y. Ma, C. Hou, B. Zhang, H. Zhang, Q. Zhang, *Polym. Int.* **2019**, *68*, 955.
[279] Y. Zhao, Y. Chen, M. Fang, Y. Tian, G. Bai, K. Zhuo, *Anal. Bioanal. Chem.* **2020**, *412*, 5811.
[280] C. Sun, L. Pan, L. Zhang, J. Huang, D. Yao, C.-Z. Wang, Y. Zhang, N. Jiang, L. Chen, C. Yuan, *Analyst* **2019**, *144*, 6760.
[281] E. Turan, G. Özçetin, T. Caykara, *Macromol. Biosci.* **2009**, *9*, 421.
[282] D. Çimen, E. Akbulut, G. Demirel, T. Caykara, *React. Funct. Polym.* **2009**, *69*, 655.
[283] K. Yoshimatsu, H. Koide, Y. Hoshino, K. J. Shea, *Nat. Protoc.* **2015**, *10*, 595.
[284] Y. Jiang, M. G. Colazo, M. J. Serpe, *Anal. Bioanal. Chem.* **2018**, *410*, 4397.
[285] Y. Jiang, M. G. Colazo, M. J. Serpe, *Colloid Polym. Sci.* **2016**, *294*, 1733.
[286] W. Zhang, M. Wei, W. S. P. Carvalho, M. J. Serpe, *Anal. Chim. Acta* **2018**, *999*, 139.
[287] H.-W. Yang, J.-K. Chen, C.-C. Cheng, S.-W. Kuo, *Appl. Surf. Sci.* **2013**, *271*, 60.
[288] C. Yang, Y. Tian, A. K.-Y. Jen, W. Chen, *J. Polym. Sci., Part A: Polym. Chem.* **2006**, *44*, 5495.
[289] J.-K. Chen, J.-Y. Li, *J. Colloid Interface Sci.* **2011**, *358*, 454.
[290] J.-K. Chen, J.-Y. Li, *Appl. Phys. Lett.* **2010**, *97*, 6.
[291] Y.-Z. Liu, K. Manivannan, A.-W. Lee, Y.-J. Huang, P.-L. Wei, J.-K. Chen, *RSC Adv.* **2017**, *7*, 22777.
[292] K. B. Goh, H. Li, K. Y. Lam, *Sens. Actuators, B* **2018**, *268*, 465.
[293] Y. Wei, Z. Liu, F. Luo, L. Zhang, W. Wang, X. Ju, R. Xie, L. Chu, *Macromol. Chem. Phys.* **2017**, *218*, https://doi.org/10.1002/macp.201700216.
[294] K. Chen, R. He, X. Luo, P. Qin, L. Tan, Y. Tang, Z. Yang, *Biosens. Bioelectron.* **2017**, *94*, 609.
[295] B. Mutharani, P. Ranganathan, S.-M. Chen, *J. Taiwan Inst. Chem. Eng.* **2019**, *96*, 599.
[296] B. Mutharani, P. Ranganathan, S.-M. Chen, *Sens. Actuators, B* **2020**, *304*, 127361.

[297] B. Mutharani, P. Ranganathan, S.-M. Chen, T.-W. Chen, M. A. Ali, A. H. Mahmoud, *Ultrason. Sonochem.* **2020**, *64*, 105008.
[298] B. Mutharani, T.-W. Chen, S.-M. Chen, X. Liu, *Sens. Actuators, B* **2020**, *316*, 128103.
[299] P. Zhao, M. Ni, C. Chen, Z. Zhou, X. Li, C. Li, Y. Xie, J. Fei, *Nanoscale* **2019**, *11*, 7394.
[300] L. Wang, Y. Zhang, W. Zhang, T. Ren, F. Wang, H. Yang, *J. Raman Spectrosc.* **2017**, *48*, 243.
[301] J.-J. Zhao, W. Wang, F. Wang, Y. Zhao, Q.-W. Cai, R. Xie, X.-J. Ju, Z. Liu, Y. Faraj, L.-Y. Chu, *Ind. Eng. Chem. Res.* **2020**, *59*, 10469.
[302] M. S. Khan, S. K. Misra, K. Dighe, Z. Wang, A. S. Schwartz-Duval, D. Sar, D. Pan, *Biosens. Bioelectron.* **2018**, *110*, 132.
[303] T. Swift, M. Katsikogianni, R. Hoskins, P. Teratarantorn, I. Douglas, S. MacNeil, S. Rimmer, *Acta Biomater.* **2019**, *87*, 197.
[304] B. Hu, D.-W. Sun, H. Pu, Q. Wei, *Talanta* **2020**, *218*, 121188.
[305] B. Mutharani, P. Ranganathan, S.-M. Chen, S. K. D. Vishnu, *Sens. Actuators, B* **2020**, *304*, 127232.
[306] B. Mutharani, P. Ranganathan, S.-M. Chen, C. Karuppiah, *Microchim. Acta* **2019**, *186*, 167.
[307] B. Mutharani, P. Ranganathan, S.-M. Chen, R. S. Kannan, *Ultrason. Sonochem.* **2019**, *56*, 200.
[308] J. Sun, F. Zhou, H. Hu, N. Li, M. Xia, L. Wang, X. Wang, G. Wang, *Anal. Chem.* **2020**, *92*, 6136.
[309] I. Ali, L. Chen, Y. Huang, L. Song, X. Lu, B. Liu, L. Zhang, J. Zhang, L. Hou, T. Chen, *Langmuir* **2018**, *34*, 4908.
[310] M. Nakamitsu, H. Imai, Y. Oaki, *ACS Sens.* **2020**, *5*, 133.
[311] I. Thivaios, V. Koukoumtzis, J. K. Kallitsis, G. Bokias, *Sens. Actuators, B* **2016**, *233*, 127.

Anubhab Das was born and raised in Kakdwip, West Bengal, India. He received his B.Sc. in Chemistry (2017) from Dinabandhu Andrews College, Kolkata in West Bengal. He completed his Master's in Chemistry (2019) from Scottish Church College, Kolkata in West Bengal. He is currently pursuing his Ph.D. under the guidance of Dr. Samarendra Maji from SRM Institute of Science and Technology, Kattankulathur Campus, Chennai, Tamil Nadu. His research has focused on the development of novel smart polymeric materials that may be utilized to identify nitrogenous contaminants in agricultural samples.

Anashwara Babu was born and raised in Ernakulam district in Kerala. She received her B.Sc. degree in Chemistry (2018) from Union Christian College, Aluva affiliated with Mahatma Gandhi University, Kottayam in Kerala, and did her Master's in Chemistry (2020) from Maharajas College, Ernakulam (Autonomous) in Kerala. She is currently pursuing her Ph.D. under the supervision of Dr. Samarendra Maji from SRM Institute of Science and Technology, Kattankulathur Campus, Chennai, Tamil Nadu. Her research interest lies in synthetic polymer chemistry, and currently, she is working on the development of antifouling and antimicrobial polymeric interfaces for teeth, bones, and artificial implants.

Sourav Chakraborty completed his B.Sc. degree in Chemistry from Scottish Church College, Kolkata, India. He did his M.Sc. from Ramakrishna Mission Residential College, Narendrapur, India. He completed his M.Tech. from IIT Kharagpur, India. He joined in the group of Prof. Brigitte Voit at IPFDresden, Germany, as a DAAD fellow for his M.Tech project work. On 2015 he achieved his Ph.D. degree from Technical University of Dresden, Germany, where he worked in the field of miniemulsion polymerization. Presently, he is a faculty member of Scottish Church College, Kolkata and has been working there for last 6 years.

Joachim F. R. Van Guyse received his M.Sc. in Chemistry at Ghent University in 2014. In 2019, he obtained his Ph.D. degree under the supervision of Richard Hoogenboom. Later that year, he joined the group of Kazunori Kataoka at the Innovation Center of NanoMedicine (ICONM) in Kawasaki, Japan. In 2020, he was awarded a post-doctoral fellowship from the Japan Society for the Promotion of Science (JSPS) for the development of polymer-micelle carriers for mRNA delivery. In 2022, he was appointed as an assistant professor at Leiden University, where his research focuses on the development of polymers for the delivery of biotherapeutics.

Richard Hoogenboom is full professor at Ghent University heading the supramolecular chemistry (SC) group that focuses on poly(2-oxazoline)s, supramolecular materials and responsive polymers. He obtained his Ph.D. degree from Eindhoven University of Technology under supervision of Prof. Ulrich S. Schubert and performed postdoctoral research with Prof. Martin Möller (RWTH Aachen) and Prof. Roeland Nolte (Radboud University Nijmegen). He is editor-in-chief for European Polymer Journal and associate editor for Australian Journal of Chemistry. Since January 2018, Prof. Hoogenboom is also cofounder of Avroxa BV that commercializes poly(2-oxazoline)s as Ultroxa.

Samarendra Maji obtained his M.Sc. degree in Chemistry from BHU, Varanasi, in 2004. He obtained his M.Tech. (2006) and Ph.D. (2010) from IIT, Kharagpur, India. He performed postdoctoral research with Prof. Andreas Greiner & Prof. Seema Agarwal (Philipps University Marburg, Germany) and Prof. Richard Hoogenboom (Ghent University, Belgium). Currently, he is working as research associate professor, in the Department of Chemistry, SRMIST, Kattankulathur. His major research interests are synthesis of smart polymers via CRP's (RAFT/MADIX) & polymeric–inorganic hybrid nanomaterials. He is the recipient of prestigious AvH Fellowship of Germany (2010) and FWO Pegasus Marie Curie Fellowship of Belgium (2012).